Katja Nevalainen

Melt-Compounded Composites of Inorganic Nanofiller and Atomic-Layer-Deposition-Coated Polymer Powder

Tampere 2013

Katja Nevalainen

Melt-Compounded Composites of Inorganic Nanofiller and Atomic-Layer-Deposition-Coated Polymer Powder

Thesis for the degree of Doctor of Science in Technology to be presented with due permission for public examination and criticism in Konetalo Building, Auditorium K1702, at Tampere University of Technology, on the 5th of April 2013, at 12 noon.

Abstract

Much research is being done to develop material combinations of polymer nanocomposites with tailored properties. Industry has been slow to adopt this technology mainly because several challenges such as good nanofiller dispersion and sufficient interfacial interaction between filler and matrix must be overcome to develop nanocomposites with truly enhanced properties. In this work, the effect of three different melt-compounding approaches to form thermoplastic nanocomposites was explored. The purpose was to study the effect of the processing method on nanofiller dispersion and the properties of a variety of nanofilled matrixes. First, the focus was drawn on composites formed from readily available commercial fillers and on processing techniques common to conventional plastics, but later composite materials tailored by atomic-layer-deposition (ALD) technology were studied.

Direct melt-compouding of polycarbonate nanoclay composites showed a mixture of exfoliated, intercalated, and confined morphology. Also large clay agglomerates were found. Samples showed increased Young's modulus and tensile yield strength when compared to unfilled polycarbonate, but their ductility was significantly affected in tensile loading. A transition from ductile to brittle deformation occurred at clay loadings higher than 3 wt.%. The results also showed that nanoclay surface modification plays an important role, e.g., in terms of Young's modulus enhancement. On the other hand, a two-step masterbatch dilution approach of polypropylene composites filled with 4 wt.% of micro-calcium carbonate, nano-calcium carbonate, nano-titanium dioxide, nanoclay, and multi-walled carbon nanotubes suggested no or only minor improvements in Young's modulus and tensile yield strength but considerably improved fire behavior compared to its unfilled, coupling-agent-modified counterpart. Improved fire properties were obtained though both individually dispersed fillers and large filler agglomerates were observed. The highest reduction in peak heat release and the lowest burning rate were obtained for a coupling-agent-modified polypropylene filled with multi-walled carbon nanotubes. This was attributed to the matrix's high filler volume content, but also other factors such as the composite's lower oxygen permeability and higher thermal stability over other studied polypropylene composites contributed to the cone calorimeter results.

ALD-thin film coating of micron-sized polymer powder and subsequent melt-compounding yielded individually dispersed ribbon- or plate-like metal oxide nanofillers. However, this composite formation approach was somewhat sensitive to ALD process precursor remnants, by-products, and/or successive thermal treatments. The results indicated that if the polymer had poor chemical resistance and if a significant amount of ALD processing chemicals were left on ALD-coated particles, the polymer's molecular weight and melt viscosity decreased abruptly. However, this was observed only in titanium dioxide-filled polyamide but not in the other studied materials such as aluminium-oxide or aluminium-doped-zinc-oxide filled polyamide and polystyrene nanocomposites. Even if ALD-created nanofillers with a high aspect ratio were well dispersed throughout the polymer matrix, the final mechanical properties of the studied materials were only modestly enhanced. One explanation for this is the low nanofiller content (< 1.5 wt.%) measured in the composites. The ALD-tailored nanocomposite formation approach is still considered attractive, and incorporating ALD-created nanofillers in a polymer matrix is expected to improve the composite properties, when (i) polymer molecular weight degradation is avoided, (ii) the nanofiller content is kept high, (iii) the created thin film is strong, and (iv) the load transfer between matrix and filler is efficient.

Though the manufacture of composites with well dispersed nanofillers and good filler interaction with the polymer at a reasonable cost remains challenging, this work provides processing guidelines for further development of nanocomposite materials for practical applications.

Acknowledgements

List of publications

This thesis is based on original experimental work presented in detail in the following six publications, which in the text are referred to as *publications I-VI.* Additionally, some unpublished data are presented and discussed.

I Nevalainen, K., Vuorinen, J., Villman, V., Suihkonen, R., Järvelä, P., Sundelin, J. & Lepistö, T. 2009. Characterization of twin-screw-extruder-compounded polycarbonate nanoclay composites. *Polymer Engineering and Science* 49, pp. 631-640.

II Nevalainen, K., Auvinen, S., Orell, O., Eteläaho, P., Suihkonen, R., Vuorinen, J. & Järvelä, P. 2013. Characterization of melt-compounded and masterbatch-diluted polypropylene composites filled with several fillers. *Polymer Composites*, in press.

III Nevalainen, K., Hintze, C., Suihkonen, R., Sundelin, J., Eteläaho, P., Vuorinen, J., Järvelä, P. & Isomäki, N. 2008. Thermal and rheological behaviour comparison of melt-compounded nanocomposites of atomic-layer-deposition-coated polyamide particles and commercial nanofillers. *Journal of Nanostructured Polymers and Nanocomposites* 4, pp. 128-138.

IV Nevalainen, K., Suihkonen, R., Eteläaho, P., Vuorinen, J., Järvelä, P., Isomäki, N., Hintze, C. & Leskelä, M. 2009. Mechanical and tribological property comparison of melt-compounded nanocomposites of atomic-layer-deposition-coated polyamide particles and commercial nanofillers. *Journal of Vacuum Science and Technology A: Vacuum, Surfaces, and Films* 27, pp. 929-936.

V Nevalainen, K., Isomäki, N., Honkanen, M., Suihkonen, R., McNally, T., Harkin-Jones, E., Syrjälä, S., Vuorinen, J. & Järvelä, P. 2012. Melt-compounded nanocomposites of titanium dioxide atomic-layer-deposition-coated polyamide and polystyrene powders. *Polymers for Advanced Technologies* 23, pp. 357-366.

VI Nevalainen, K., Isomäki, N., Honkanen, M., Suihkonen, R. & Vuorinen, J. 2012. Nanocomposites via melt-compounded ALD-coated powder. *Proceedings of the 32nd SAMPE Europe International Technical Conference & Forum 2011 (SEICO 11)* on New Material Characteristics to Cover New Application Needs, Paris, France, March 28-29, 2011. New York, Curran Associates, Inc. pp. 417-424.

Author's contribution

I   The author shared with the co-authors and the laboratory research team the experimental work. She interpreted the results, and wrote the manuscript as corresponding author. J. Sundelin was responsible for the microscopical and X-ray diffraction studies and contributed to their reporting. V. Villman helped with friction and wear tests. All the authors commented on the experimental part, and read and approved the manuscript.

II   The author processed and characterized the material or supervised the work, interpreted the results, and wrote the manuscript as corresponding author. O. Orell helped with fire testing. M. Honkanen made the microscopical studies and S. Auvinen was responsible for the barrier studies. All the authors commented on the experimental part, and read and approved the manuscript.

III The author processed and characterized the material or supervised the work, interpreted the results, and wrote the manuscript as corresponding author. N. Isomäki was responsible for ALD-coating process and contributed the sections on ALD thin film processing. C. Hintze helped with sample manufacturing. J. Sundelin and S. Syrjälä were responsible for the microscopical and rheological studies, respectively. Both contributed to results analysis. All the authors commented on the experimental part, and read and approved the manuscript.

IV   The author processed and characterized the material or supervised the work, interpreted the results, and wrote the manuscript as corresponding author. N. Isomäki was responsible for ALD-coating process and contributed the sections on ALD thin film processing. C. Hintze and R. Suihkonen helped with sample manufacturing and mechanical testing. J. Sundelin made the microscopical studies, whereas R. Beek from CSM instruments performed the nano scratch tests. Both contributed to results analysis. M. Leskelä contributed to the literature-review-based discussions dealing with properties, impurity content, and stability of the ALD-created titanium dioxide films. All the authors commented on the experimental part, and read and approved the manuscript.

V   The author processed and characterized the material or supervised the work, interpreted the results, and wrote the manuscript as corresponding author. N. Isomäki was responsible for ALD-coating process and contributed the sections on ALD thin film processing. M. Honkanen and T. McNally were responsible for microscopical and gel permeation chromatography studies, respectively. R. Suihkonen and T. Salmi helped with flexural strength equations. S. Syrjälä was responsible for and contributed to the sections on rheological tests and analysis of the materials. All the authors commented on the experimental part, and read and approved the manuscript.

VI   The author processed and characterized the material or supervised the work, interpreted the results, and wrote the manuscript as corresponding author. N. Isomäki was responsible for ALD-coating process and contributed the sections on ALD thin film processing. M. Honkanen was responsible for the microscopical studies. All the authors commented on the experimental part, and read and approved the manuscript.

TABLE OF CONTENTS

Symbols and abbreviations

Ø	Diameter
ALD	Atomic layer deposition, also called atomic layer epitaxy (ALE)
Al_2O_3	Aluminium oxide, also called alumina
BSE	Backscattered electron
$CaCO_3$	Calcium carbonate
Cl	Clorine
d_{001}	Interlayer spacing
DEZ	Diethylzinc, with the molecular formula $Zn(CH_2CH_3)_2$
DSC	Differential scanning calorimetry
EDS	Energy dispersive spectrometer
Fe_2O_3	Iron oxide
GPC	Gel permeation chromatography
HCl	Hydrochloric acid
H_2O	Water
HRR	Heat release rate
MFR	Melt-mass flow rate, also called the melt flow index (MFI)
M_n	Number average molecular weight
M_w	Weight average molecular weight
MWCNT	Multi-walled carbon nanotubes
MWD	Molecular weight distribution
N_2	Nitrogen
PA	Polyamide, also called nylon
PC	Polycarbonate
PE-HD	High density polyethylene
PE-LD	Low density polyethylene
PHRR	Peak heat release rate
PMMA	Polymethyl methacrylate
PP	Polypropylene
PPgMA	Maleic anhydride-modified polypropylene
PS	Polystyrene
SEM	Scanning electron microscopy
SiO_2	Silicon dioxide, also called silica
TEM	Transmission electron microscopy
T_g	Glass transition temperature
TGA	Thermogravimetric analysis
$TiCl_4$	Titanium tetrachloride
TiO_2	Titanium dioxide, also called titania
TMA	Trimethylaluminium, with the molecular formula $Al(CH_3)_3$
vol.%	Volume percent
wt.%	Weight percent
XRD	X-ray diffraction
ZnO	Zinc oxide
ZnO:Al	Aluminum-doped zinc oxide, also called AZO

1 Introduction

In the past few decades, the main approach to develop polymeric materials, and thus new applications, has been physical property modification of existing materials by compounding with fillers or blending with other polymers. Traditionally, the filler used has been a material of micron-sized particle such as talc, glass, or calcium carbonate, which has lowered costs by being less expensive than the other ingredients in the polymer-based product. As the relative cost of polymers dropped, attention shifted to possible improvements of polymer properties. Today, micron-sized particles and fibres are used in polymers for several reasons, e.g., to increase stiffness and strength, add color and conductivity to the compound (Jancar 1999, Rothon 2003, Wypych 2010).

Polymer nanocomposites represent a promising class of materials that contain polymers incorporated with inorganic fillers having at least one dimension in the range of 1-100 nm (Paul & Robeson 2008). Well dispersed nanofillers lead to a very large interfacial area per volume between nanoparticles and the host polymer and thus increase the number of filler-polymer matrix interactions compared to micron-sized filled polymer. Nanocomposites have been shown to possess properties substantially different from those of a larger-dimensional filler material of the same composition. In fact, much research is being done to develop effective material combinations, and both scientific and industrial communities are paying a great deal of attention to nanocomposites and to studying a wide range of polymers from thermoplastics and thermosets to elastomers filled with, e.g., nanoclays, carbon nanotubes, and nano-calcium carbonates (Alexandre & Dubois 2000, Ray & Okamoto 2003, Rumiana 2007, Paul & Robeson 2008, Gupta et al. 2010).

Inorganic nanofillers are incorporated in a thermoplastic matrix by the following three main methods: in-situ polymerization, solution intercalation, and melt-compounding. In-situ polymerization has been claimed as the most efficient for producing a nanocomposite with high filler dispersion and enhanced properties. For industrial applications, the most convenient and preferred method is melt-compounding, because it is a simple, low-cost and environmentally friendly (i.e., no solvents needed) technique and, moreover, compatible with existing processing infrastructures, offering thus significant industrial and economic advantages (Alexandre & Dubois 2000, Ray & Okamoto 2003, Rothon 2003, Pavlidou & Papaspyrides 2008).

For a reinforcing effect in conventional composites, much filler (typically 30-60 wt.%) is used, which increases the weight of the final product by about 20-30%. In contrast, nanocomposite properties over unfilled polymer or conventional composites usually improve already with about 5 wt.% nanofiller additions or even less. Several studies have shown that such low filler content offers advantages such as easier processing, lighter weight, and better surface appearance. In addition, these nanocomposites can exhibit, e.g., equal or improved mechanical performance, better barrier properties, improved thermal resistance, and enhanced flame retardancy (Kojima et al. 1993, Ray & Okamoto 2003, Jordan et al. 2005, Laachachi et al. 2005, Dumont et al. 2007, Rumiana 2007, Pavlidou & Papaspyrides 2008). Polymer nanocomposites offer great potential for developing advanced materials. In fact, commercial products are already available that make use of nano-sized fillers such as automotive parts, sporting goods, and packaging materials. Yet despite their vast potential for commercial application, polymer nanocomposites are making only slow inroads into industry, and their full impact may well lie some years ahead (Paul & Robeson 2008, Gupta et al. 2010).

Many challenges must be overcome before the potential of polymer nanocomposite materials can be fully realized. It is not yet easy to produce high-quality nanocomposites commercially and at a viable price and at the same time control nanofillers' physical properties such as particle size distribution, purity, and the thermal stability of their surface modification. The slow progress in commercializing nanocomposites is mainly due to their limited performance resulting from poor bonding between filler and matrix and from nanofillers' tendency to agglomerate. For optimum properties, homogeneous nanofiller dispersion in the polymer matrix is often thought to be a basic requirement. But even after several attempts to produce a fine and uniform nanofiller dispersion within the polymer together with adequate adhesion between matrix and nanofiller, nanocomposite manufacture is considered a major challenge and very time- and energy-intensive (Ray & Okamoto 2003, Yoon et al. 2003a, Rothon 2003, Rault et al. 2009, Gupta et al. 2010). In addition, there is growing anxiety about the health and environmental effects of nanofillers. Many thermoplastic nanocomposite materials have been produced by feeding powder nanofillers and polymer into an extruder for melt-compounding. Especially airborne nanoparticles released during such manufacture constitute a health risk, because they are easily inhaled into the body (Tsai et el. 2008, NIOSH 2009, Wypych 2010).

In developing thermoplastic nanocomposites, it is important to be knowledgeable about the effect of different processing approaches on nanofiller dispersion and composite performance. Special attention should be paid to new approaches to improve the processing techniques common to conventional plastics, because the shear force during melt-compounding may not be strong enough to overcome nanofillers' strong tendency to agglomerate. Such a study would prove useful, provide further knowledge, and possibly help develop nanocomposite materials for future practical applications. Using a commercial masterbatch in polymer nanocomposite production would be a better choice than conventional direct melt-compounding, because the former offers, e.g., enhanced nanofiller dispersion and fewer healthy risks than using powder nanofillers in the incorporation process (Zhu & Xanthos 2004, Prashantha et al. 2009). Another promising, though less studied, choice in nanotechnology is atomic layer deposition (ALD). By ALD it is possible to create very thin nanofiller layers directly on polymer particles before melt-compounding even at relatively low temperatures. Subsequent melt-compounding of such ALD-coated polymer particles is seen as an attractive method for producing metal oxide nanocomposites (Liang et al. 2007, Spencer et al. 2007, Liang et al. 2008, Liang 2008), as it ensures good nanofiller dispersion (Spencer et al. 2007, Liang et al. 2007) and improves barrier properties (Liang et al. 2008) and may also reduce work-related risks from handling powder nanofillers. However, since only a few scientific studies have been published on this method, its functionality and ability to improve, e.g., the mechanical properties of the final product are not well explored. Consequently, a study on this topic would expand the current knowledge of exploiting ALD for polymer nanocomposite manufacture.

This thesis work focused on the possibility of improving nanofiller dispersion and hence the properties of melt-compounded thermoplastic composites by selecting a suitable processing approach. Focus was first drawn to composites filled with readily available commercial fillers to assess the performance of composites prepared using processing techniques already adopted in the plastics industry (*publications I-II*), but later nanocomposite materials tailored by ALD technology were studied (*publications III-VI*).

2 Melt-compounded thermoplastic nanocomposites

2.1 Melt-compounding

Melt-compounding is the most convenient and preferred approach to incorporate micro- and nanofillers in a thermoplastic matrix in high-volume applications. In principle, polymer and filler in this process are heated to the polymer's melting or softening point, and the two are mixed in a mixing head or in an extruder (White 1991, Ray & Okamoto 2003, Gupta et al. 2010).

Powder form commercial nanofillers used in polymer nanocomposites are supplied as agglomerates, in which two or more particles joined to form a bigger particle. In melt-compounding, the target is to turn these agglomerates to singly dispersed nanofillers, in which the polymer surrounds each individual particle. However, this is difficult to realize in practise, because melt-compounding may not provide sufficient shear force for it. As the particle size of the filler decreases, the particle's surface area and tendency to agglomerate increase. Moreover, the filler is often incompatible with the polymer, because fillers are usually hydrophilic, whereas the polymers used (such as polyolefins) are predominantly hydrophobic. It is possible, however, to inhibit nanofiller agglomeration and improve adhesion to the polymer by modifying the filler surface, as is done with conventional micron-sized fillers. Coating agents such as silanes, stearic acid, and fatty acids are used to lower the surface energy of nano-sized fillers such as calcium carbonate, silicon dioxide, or titanium dioxide (Rothon 2003, Ahn et al. 2004, Osman et al. 2004, Avella et al. 2006, Gupta et al. 2010, Wypych 2010). On the other hand, nanoclay surfaces are usually modified by exchanging the metal cations in layered particles for more hydrophobic organic ions such as alkyl ammonium or phosphonium ions. The target is to reduce the nanoclay's surface energy but also to increase the distance between the silicate layers to facilitate the access of polymer chains between them. Especially nanoclay surface modifications are, however, susceptible to thermal degradation under the melt-compounding conditions of several thermoplastic polymers due to their low thermal resistance. If the filler's surface chemistry is degraded, the advantage to improve the compatibility and adhesion between filler and polymer is lost. Furthermore, the increase gained in the silicate interlayer distance is reduced (Pluart et al. 2003, Ray & Okamoto 2003, Gelfer et al. 2004, Pavlidou & Papaspyrides 2008).

To improve the compatibility of filler and matrix, it is also possible to chemically modify a thermoplastic polymer or add a third component, i.e., a coupling agent, such as a maleic anhydride derivate and an amino acid, to the composite system. In polyolefin-based nanoclay filler composite, maleic-anhydride-modified polypropylene (PPgMA) is often applied (Hasegawa et al. 2000, Modesti et al. 2005, Eteläaho et al. 2009a). Other important factors affecting filler dispersion in the polymer matrix include (i) melt-compounding (direct melt-compounding, masterbatch dilution), (ii) a melt-compounding device (batch mixer, single-screw extruder, twin-screw extruder), (iii) processing parameters (screw speed and configuration, compounding temperature, residence time), (iv) raw material properties (morphology, molecular weight, molecular weight distribution, functional groups, polarity, viscosity), and (v) the applied recipe (filler content, coupling agent content) (Alexandre & Dubois 2000, Ray & Okamoto 2003, Chavarria 2007, Pavlidou & Papaspyrides 2008, Gupta et al. 2010).

Alexandre & Dubois (2000), among others, have introduced potential morphologies of polymer composites containing plate-type nanofillers such as nanoclay. The morphologies are generalized as phase-separated, intercalated, and exfoliated, as shown in Fig. 1. In phase-separated or conventional microcomposites, nanoclay filler exists in agglomerates with no polymer inserted between the silicate layers. Intercalated and exfoliated morphologies are typically regarded as

nanocomposites, because in both cases, each 1-nm thick silicate layer is in contact with the polymer. This provides a large interface essential for improving composite properties. However, it is often stated that only a highly exfoliated nanocomposite system with strong adhesion between nanoclay and matrix will show the best properties, such as improved mechanical and barrier performance compared to an unfilled matrix (Alexandre & Dubois 2000).
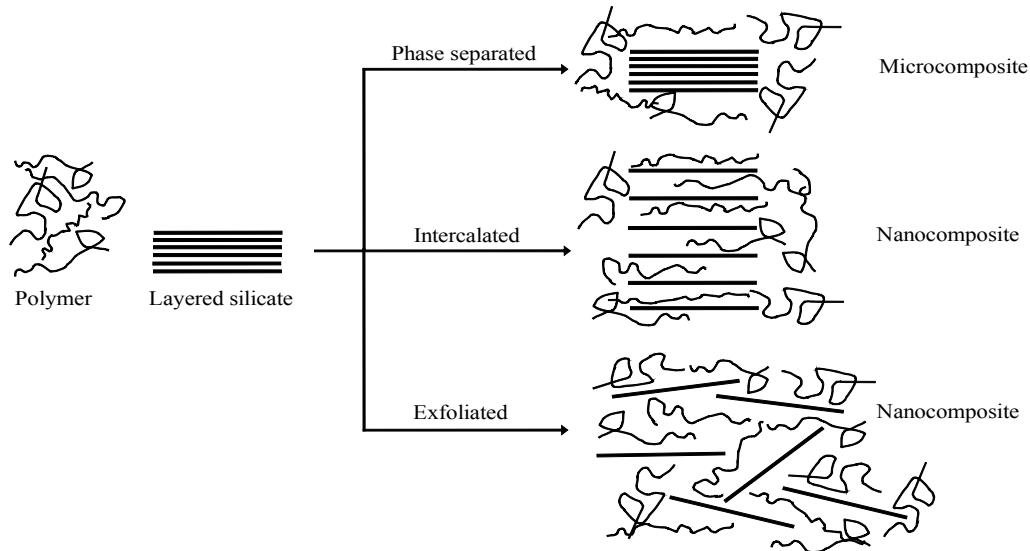
Fig. 1: Schematics of the three main types of layered silicates (nanoclays) in a polymer matrix.

A classification such as large nanofiller cluster, small nanofiller cluster, and individually dispersed nanofiller is used to describe a nanocomposite morphology that contains fillers other than the plate type. In case of tubular nanofillers, the term bundle is often employed.

2.2 Twin-screw extrusion

Several different melt-compounding devices are used to form polymer nanocomposites. Generally, the twin-screw extruder is considered a more effective device to produce thermoplastic polymer composites than single-screw extruders or batch-type mixers. Twin-screw extruders are usually classified by the direction of screw rotation—co-rotating and counter-rotating—and by the degree of screw intermesh—non-intermeshing (tangential), partially, or fully intermeshing (Fig. 2a; White 1991, Wang 2000, Dennis et al. 2001, Gianelli et al. 2004, Vermogen et al. 2005). In studies by Dennis et al. (2001) on nanoclay-filled polyamide composites, the counter-rotating, non-intermeshing twin-screw extruder yielded the best delamination and nanoclay dispersion over the other three systems, single-screw, co-rotating intermeshing, and counter-rotating intermeshing extruder designs. However, they studied only some experimental conditions, and thus both co-rotating and counter-rotating intermeshing extruder types are believed to yield high nanofiller dispersion with an optimized screw configuration (Dennis et al. 2001). In fact, later studies by Mehrabzadeh & Kamal (2004) on nanoclay-filled polyamide showed mostly exfoliated structure when a co-rotating intermeshing (with mixing and kneading elements) twin-screw extruder was used. Furthermore, using linear low-density polyethylene filled with graphite nanoplatelets, Kim et al. (2009) showed that the counter-rotation setting gave better results than the co-rotating version when a small-scale table-top twin-screw extruder was used.
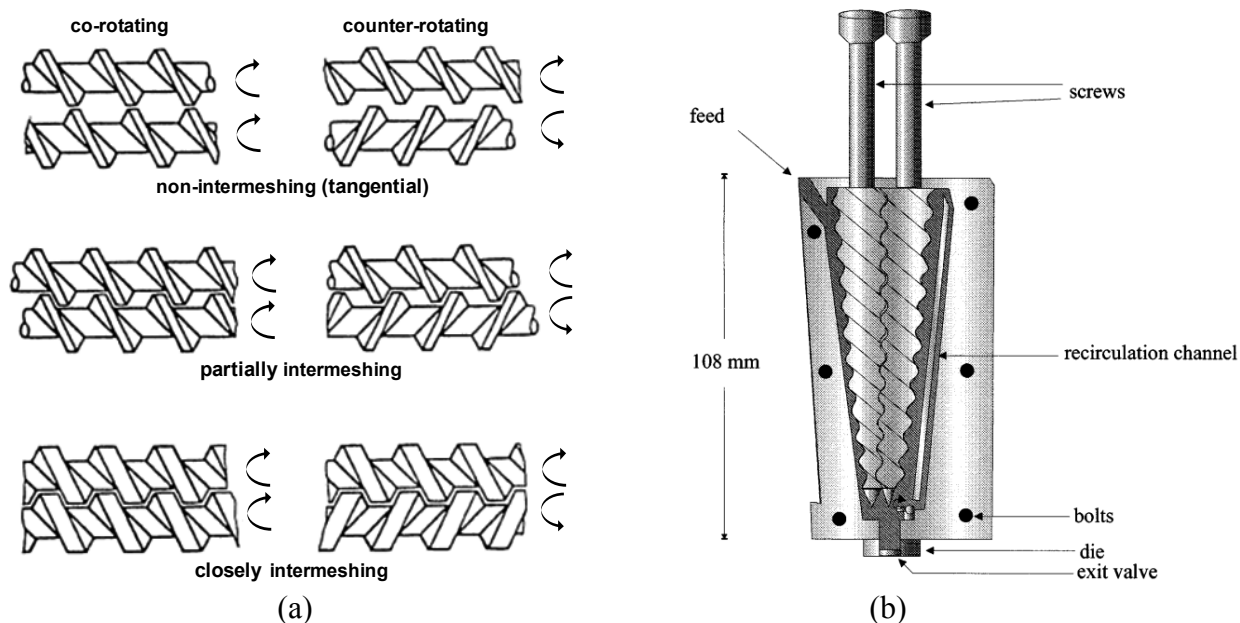
Fig. 2: Typical (a) classification of twin-screw extruders according to their various degrees of intermeshing and (b) cross-sectional view of a microcompounder with a batch mode and a conical twin-screw design. The former modified and reprinted from Wang (2000) with permission from Smithers Rapra; the latter reprinted from Marić & Macosko (2001), Copyright (2001), with permission from Wiley.

Because of the size and scale of many commercial twin-screw extruders (process output ranging typically from a few to several thousand kilograms per hour), small table-top extruders or other batch mixers (process output typically 0.5 kilograms per hour or less) are preferable for studying new material combinations. This is a convenient method especially with a limited or expensive supply of raw material or when only preliminary results are sought for fast and at a low cost. One example of a small-scale extruder is the microcompounder (often called also minicompounder or miniextruder), shown in Fig. 2b. Many microcompounders have a batch mode and a conical screw design to provide sufficient mixing. The residence or dwell time is typically well controlled due to the possibility of closed material circulation. In addition, the split barrel design of such microcompounders enables simple cleaning of the processing equipment, thus reducing sample contamination between experiments. However, in contrast to microcompounders, which have mainly fixed assembly, conventional twin-screw extruders have a modular assembly, which can be varied in its diameter/length ratio of the screw, screw profile itself, and feeding position. Furthermore, because of their weak compounding and low shear force, microcompounders often produce a lower degree of filler dispersion and nanocomposite property enhancements than conventional twin-screw extruders (Chavarria et al. 2007, Furlan et al. 2011). Samples prepared with a microcompounder, however, have been shown to follow a similar material property trend as those observed with a conventional twin-screw extruder, as Chavarria et al. (2007) have demonstrated for nanoclay filled polyamide.

Although considerable effort has been invested in nanocomposite melt-compounding technology, most publications, with a few exceptions, still concentrate on resultant product properties and give only a few details on how to set up processing equipment or configure an extruder. It remains a challenge to determine the best extrusion process and thus to maximize nanofiller dispersion. For example, various screw configurations, which help control residence time and shear intensity, affect nanocomposite morphology (Dennis et al. 2001, Vermogen et al. 2005, Gupta et al. 2010, Furlan et al. 2011). On the other hand, effects of melt-compounding

5

conditions, especially on nanoclay dispersion and composite performance, have been studied by several researchers, but no extensive summaries of optimal processing conditions exist in the literature. Generally, an increase in screw speed leads to better nanofiller dispersion, if the residence time is sufficiently long. A long residence time enables penetration of the polymer chains and/or the coupling agent between the filler particles thus enhancing nanofiller dispersion and allowing more time for the possible coupling agent to establish strong bonding between matrix and filler. Clearly, too long a residence time, when, e.g., a low screw speed and feeding rates are used, increases processing costs and accelerates the degradation of thermally sensitive materials. The effect of the processing temperature is another important parameter. As temperature increases, the polymer chain's mobility increases and viscosity drops, resulting in less mechanical force being applied to nanofillers. When a high-melt viscosity polymer is used, a low processing temperature and/or high screw speed yield generally high mixing shear intensity, which effectively breaks nanofiller agglomerates into smaller units (Dennis et al. 2001, Yoon et al. 2003a, Mehrabzadeh & Kamal 2004, Modesti et al. 2005, Kim et al. 2008, Gupta et al. 2010). However, a very high shear intensity brought on by an aggressive screw shear may not be the method to produce optimal nanocomposite properties (Dennis et al. 2001, Furlan et al. 2011). Consequently, it is difficult to find a balance between temperature, residence time, and shear intensity. Each composite system must be specifically studied to optimize nanofiller dispersion in terms of chemical compatibility and melt-compounding conditions.

One attractive though somewhat less studied nanocomposite manufacturing method than direct nanofiller incorporation in twin-screw extruders is the two-step masterbatch dilution approach. Here, in the first step, a polymer concentrate with a high nanofiller content is typically manufactured and then diluted in the second step with the same host polymer. In addition to the fact that a high nanofiller content in masterbatches, resulting in high melt viscosity, leads to high shear stresses during melt-mixing, the masterbatch approach produces typically better nanofiller dispersion due to longer residence time in the twin-screw extruder. For industrial purposes too, using a commercial masterbatch to produce polymer nanocomposites would be a good choice, because it minimizes employee contact with powder form fillers (Zhu & Xanthos 2004, Gianelli et al. 2004, Eteläaho 2009b, Prashantha et al. 2009). The disadvantages of the masterbatch approach include increased material or processing costs and possible thermal degradation of organic materials.

2.3 Nanocomposite properties

A major reason for adding micron-sized or nano-sized inorganic fillers to polymers is to improve their mechanical performance. Generally, when a rigid filler is added to a soft polymer matrix, filled systems show increased Young's modulus and tensile strength especially if sufficient filler dispersion and adhesion is achieved between filler and polymer matrix (Sumita et al. 1983, Kojima et al. 1993, Fornes et al. 2001, Rothon 2003, Wang et al. 2006, Chavarria et al. 2007, Suin et al. 2013). In nanocomposites, these property improvements are achieved with a considerably lower filler content than that in conventional microcomposites without sacrificing polymer processability or adding excessive weight. Furthermore, when the same filler weight content is used, nanocomposites may possess higher Young's modulus and tensile yield strength than conventional composites, as Sumita et al. (1983) showed in their studies on polypropylene (PP) films (Fig. 3) filled with silicon dioxide (SiO_2) particles. Nanocomposites differ from conventional composite materials in terms of their exceptionally high surface-to-volume ratio in the dispersed phase and/or their high aspect ratio when good nanofiller dispersion is achieved. Because the polymer surrounding the filler is often affected near the filler, the incorporated filler

may alter the local chemistry, polymer chain mobility, polymer chain conformation, the degree of polymer chain ordering, or crystallinity. If this interaction zone (also called interface) is, e.g., 1 nm thick on a composite containing micron-sized fillers, it would amount to about 0.3% of the total composite volume. However, a 1-nm thick interaction zone on nanoparticles may be as much as 30% of the total composite volume. In theory, polymer nanocomposites are expected to improve material properties to an extraordinary degree (Wu et al. 2002, Roton 2003).
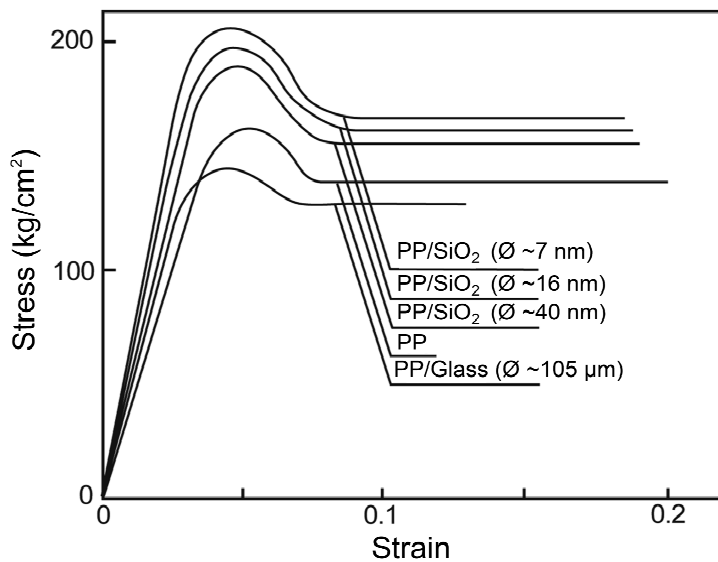
Fig. 3: Effect of filler particle size on stress-strain curve of 10 wt.% filled PP composite films melt-compounded in a two-roll mill. The tensile test was run at 30°C at a strain rate of 20 mm/min. Modified and reprinted from Sumita et al. (1983), Copyright (1983), with permission from Springer.

In thermoplastic nanocomposites, most research has been carried out on systems containing nanoclays or carbon nanotubes, though also several other nano-sized fillers such as calcium carbonate, titanium dioxide, and aluminium oxide have been studied (Chan et al. 2002, Avella et al. 2006, Laachachi et al. 2005, Paul & Robeson 2008, Prashantha et al. 2009). Selection of nanoparticles often depends on what thermal, mechanical, and electrical properties nanocomposites should have. While there is a significant amount of data available, results on nano-sized filler effects on, e.g., mechanical properties have not been consistent. One reason for this discrepancy derives from varying levels of nanofiller dispersion and adhesion between the polymer and fillers due to different filler surface treatments and sample processing methods. Improvements in polymer properties due to nanofiller addition vary also from polymer to polymer and change according to used filler, filler particle geometrical shape, particle size, and filler content (Dennis et al. 2001, Wu et al. 2002, Jordan et al. 2005, Modesti et al. 2005, Prashantha et al. 2009, Baniasadi et al. 2010)

Even granting exceptions, most studies show that Young's modulus increases with increasing nanofiller content regardless of adhesion and filler dispersion. Such property improvement is typically accompanied by a decrease in the elongation at break and toughness (Sumita et al. 1983, Wu et al. 2002, Chan et al. 2002, Yoon et al. 2003a, Hsieh et al. 2004, Bikiaris et al. 2008). A drop in impact strength and a rise in yield strength have also been observed in many nanofilled systems (Yoon et al. 2003a, Baniasadi et al. 2010) but contradictional results also exist (Alexandre & Dubois, 2000, McNally et al. 2003, Modesti et al. 2005, Furlan et al. 2011). Jordan et al. (2005) concluded about composites with good interaction between filler and matrix

that yield strength tends to increase with increasing filler content and decreasing particle size. In contrast, adding poorly interacting nanoparticles to the matrix often lowers the yield strength (Jordan et al. 2005).

Whereas reinforcements with nanocomposites have been the main interest, several other properties have been improved such as better barrier properties, improved thermal resistance, and enhanced flame retardancy, in comparison to conventional microcomposites (Ray & Okamoto 2003, Jordan et al. 2005, Laachachi et al. 2005, Pavlidou & Papaspyrides 2008). It is believed that adding inorganic fillers to the polymer matrix enhances its barrier properties, because fillers are considered impenetrable by gas molecules. A filled polymer matrix is expected to possess enhanced barrier properties by forcing gas molecules to follow a more tortuous path as they diffuse through the material, which slows down the diffusion. Especially, layered silicates are considered effective in improving the gas barrier properties of polymers, due to a large aspect ratio and maximal path length, which the gas is forced to follow (Ray & Okamoto 2003, Dumont et al. 2007, Bikiaris et al. 2008). Clearly, application of spherical and tubular particles is expected to produce a shorter path than plate-like particles, though such an application also affects gas diffusion through the material. Bikiaras et al. (2008) and Carvalho et al. (2010), e.g., observed about a 20% oxygen barrier enhancement after adding 2.5 wt.% multi-walled carbon nanotube fillers in polypropylene and 3 wt.% nanoclay in low density polyethylene, respectively. Even higher improvement level have been obtained if a plate-type nanofiller is well dispersed and aligned parallel to the film surface, whereas with poor dispersion almost no improvement may take place or filler permeability may even increase.

Both micron- and nano-sized inorganic fillers can also be used to improve fire retardant properties with a subtle increase in composite thermal stability. Laachachi et al.'s (2005) heat release rate (HRR) curves for titanium-dioxide (TiO_2) and iron-oxide-(Fe_2O_3)-filled polymethyl methacrylate (PMMA), shown in Fig. 4, agree reasonable well with Paul & Robeson's (2008) generalized HRR curves for nanofiber- or platelet-modified polymers in the cone calorimetry test. The HRR curve's position, shape, and intensity vary from one nanocomposite system to another, but HRR drops with no significant change in the overall heat release (area under the curve). The often observed short ignition time due to nanofiller incorporation to the polymer has been generally attributed to a rapidly heating thin layer near the sample surface. Filler migration to the surface and/or loss of the first few hundred nanometers of polymer typically results in filler accumulation on the sample surface. This char, among other things, protects the bulk material from outside heat and slows down the diffusion of oxygen into the material as well as generation of volatile gases in the burning area, thereby decreasing the rate of mass loss in the burning polymer. Inspection of char residues after a cone calorimeter test has also suggested that incomplete filler surface coverage and char rupture during burning leads to poor flammability resistance. This is often related to low nanofiller content, low aspect ratio, poor nanofiller dispersion, and/or agglomeration during combustion (Ray & Okamoto 2003, Laoutid et al. 2009, Gupta et al. 2010, Paul & Robeson 2008).
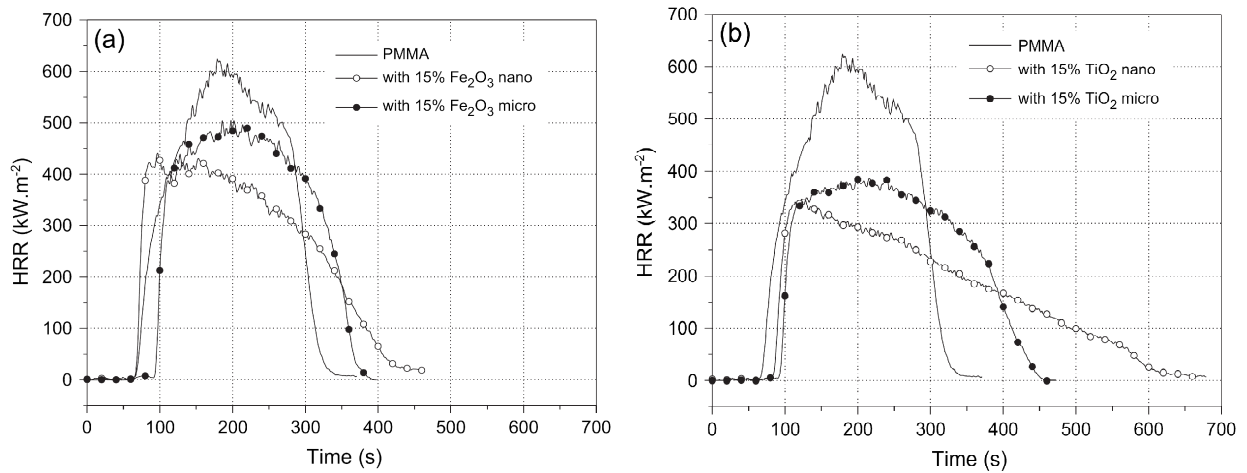
Fig. 4: Effect of filler particle size on the heat release rate (HRR) for (a) PMMA/Fe$_2$O$_3$ composites and (b) PMMA/TiO$_2$ composites prepared by melt-compounding with a laboratory batch mixer. Fillers were well distributed in PMMA, though some agglomerates (typically < 0.2 μm, some also in the micrometric range) were also found. Reprinted from Laachachi et al. (2005), Copyright (2005), with permission from Elsevier.

If nanofillers are used simultaneously with conventional flame retardants, the result may be synergistic effects that reduce the total amount of filler necessary. Synergism has also been observed between nanofiller and conventional reinforcing fibers in mechanical property enhancements, e.g., by Hopmann et al. (2012), who observed increased Young's modulus in polypropylene matrix with combined use of nanoclay and short glass fibre, especially when a coupling agent was used.

3 Atomic-layer-deposition-tailored melt-compounding

3.1 Atomic layer deposition (ALD)

ALD technology is a chemical gas phase thin film deposition method operating in a vacuum. Traditionally, ALD has been used to manufacture thin film electroluminescent flat-panel displays, but later ALD thin films have found other applications including microelectronics, solar cells, and protective coatings. Materials deposited by ALD are mostly oxides, nitrides and metals, but it is possible to deposit a whole range of other materials as well (Ritala & Leskelä 2002, Puurunen 2005).

The ALD process consists of an alternating series of self-limiting chemical reactions between gas phase precursors and the substrate. In a typical ALD process (Fig. 5), precursors (reactants A and B) are pulsed into the reactor alternately one at a time. During the first pulse (Step 1a), the precursor gas reacts only with the substrate surface, and a (sub)monolayer is formed attached to the substrate via covalent bonding. The precursor cannot react with other similar precursor molecules. After the first pulse, excess precursors and gaseous reaction by-products are removed by purging with an inert gas such as nitrogen (Step 1b). Then a second precursor is pulsed to form chemical bonds with the previously deposited monolayer. After all the reactive groups have been consumed, no more reactions take place, and the surface becomes covered again with a (sub)monolayer, but now of the second precursor (Step 2a). In the last step of the ALD cycle, unreacted precursor molecules and possible reaction by-products are purged from the chamber (Step 2b). This cycle is then repeated as many times as necessary to obtain the desired film thickness (Ritala & Leskelä 2002, Puurunen 2005, Pore 2010, Miikkulainen et al. 2013).
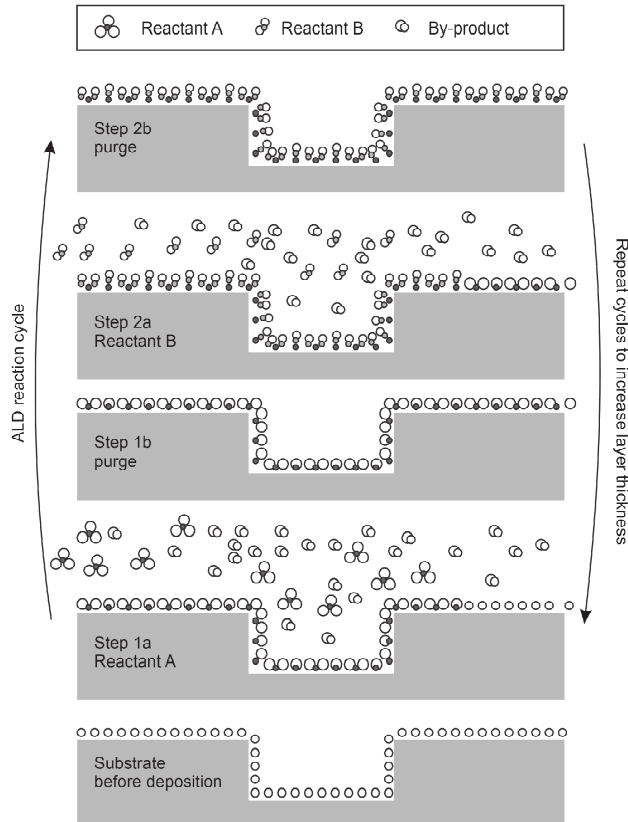
Fig. 5: Schematics of one ALD coating cycle. Reprinted from Miikkulainen (2013), Copyright (2013), with permission from the American Institute of Physics.

The duration of an ALD cycle depends on, e.g., the reactor used, substrate geometry, reaction kinetics, and processing temperature. In optimized conditions, cycle times as short as one second are possible, but in research scale reactors several seconds are typically required for one ALD cycle. Furthermore, if a low deposition temperature is used and the substrate has a high surface area, cycle time of several minutes is required. Clearly, if the pulse times for introducing precursors into the ALD reactor chamber are too short, precursors may not be able to form a saturated layer on the substrate surface with the result that the thin film grows at a slow rate. Sufficiently long purge times between precursor pulses are important to remove all excess precursor material and possible reaction by-products from the reaction chamber before the next precursor is introduced (Ritala & Leskelä 2002, Puurunen 2005, Bosund 2007, Pore 2010).

The deposition temperature is a factor that must be well controlled, because it affects the ALD-thin film growth rate and quality. If the processing temperature is too low, the following two may follow: (i) growth may be excessive if the precursors condense on the substrate surface, often accumulating impurities in the created film, (ii) growth may slow down when the precursor molecules are chemically inactive or unreactive with the substrate, and are removed from the ALD chamber in the purging stage. If processing temperatures are too high, the precursor may decompose and react dissimilarly from the original molecules, resulting in unstable film growth, or desorb from the substrate surface, resulting in reduced growth (Ritala & Leskelä 2002, Bosund 2007).

3.2 ALD-tailored melt-compounding

In this work, ALD-tailored melt-compounding refers to ALD coating of micron-sized polymer powder and subsequent melt-compounding. This method helps to promote nanofiller dispersion in the polymer matrix. The desired filler content is easily controlled by adjusting the size of the used polymer particle and the thickness of the ALD thin film on polymer particles. In melt-compounding process, particles are heated and compacted, and their thin-film shells are broken. The shell remnants disperse to form a nanocomposite with individually dispersed inorganic nanofillers (Liang et al. 2007, Spencer et al. 2007, Liang et al. 2008, Liang 2008). This nanocomposite formation not only promotes thorough mixing of the polymer and nanofiller, but also minimizes the required residence time in the energy intensive melt-compounding step.

The advantages of ALD over other thin-film deposition techniques (e.g., physical vapor deposition) include good uniformity, thickness control due to the self-limiting property, and better step coverage. Furthermore, several thin films such as aluminium oxide, titanium dioxide, and zinc oxide can be deposited at relatively low temperatures (<150°C), thereby reducing, if not altogether eliminating, thermal damage of temperature-sensitive polymers (Ritala & Leskelä 2002, Wilson et al. 2003). However, the challenge in ALD-coating of polymers such as polyethylene, polypropylene and polystyrene is that they do not have chemically active functional groups such as hydroxyl (–OH), carbonyl oxygen (–C=O), or amine (–NH$_2$) groups, which are necessary to initiate growth of an inorganic film (Liang et al. 2008, Wilson et al. 2008). According to the model proposed by Wilson et al. (2008) in Fig. 6, initial nucleation may, however, occur via absorption and diffusion of the first ALD precursor onto the surface and the near surface regions of the polymer and a subsequent reaction with a second precursor. The first ALD thin film clusters form at or near the surface of the polymer particles with the pores on the polymer surfaces becoming smaller and gradually closing with subsequent ALD-coating cycles. An ALD thin film will finally merge to form a continuous layer on the polymer substrate. Such

ALD films are thought to lead to a physically rather than chemically bonded interface between ALD thin film and polymer (Spencer et al. 2007, Liang 2008, Wilson et al. 2008).
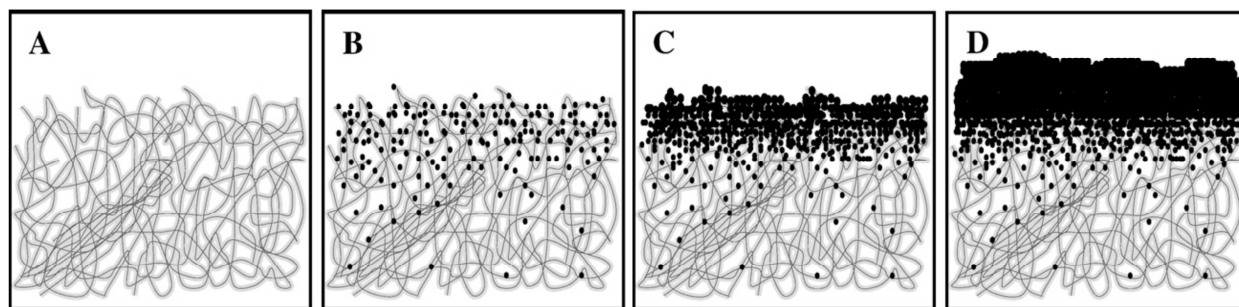
Fig. 6: Proposed growth mechanism of an aluminium oxide (Al_2O_3) ALD thin film on a polymer substrate where (a) is polymer before deposition, (b) first Al_2O_3 nucleation clusters on the surface and near-surface regions of the polymer, (c) the Al_2O_3 thin film merges and a continuous Al_2O_3 ALD film on the polymer begins to form, and (d) Al_2O_3 grows linearly on the polymer surface. Reprinted from Wilson et al. (2008), Copyright (2007), with permission from Elsevier.

Another critical issue in applying ALD technology to nanocomposite manufacture is cost. ALD is considered a slow (deposition rates typically < 0.1 nm/cycle) and expensive method requiring complicated deposition instrumentation and thus often unsuitable for high-volume manufacture of commercial products (Ritala & Leskelä 2002, Pore 2010). To help ALD-tailored polymer nanocomposite formation become main stream, a scalable, cost-effective ALD reactor solution must be developed. Intensive work has been done with good results, e.g., on compensating for the modest thin film growth rate in the ALD process with more efficient and scalable fluidized bed reactors (King et al. 2007). According to Liang (2008), integrating a fluidized bed reactor with an existing polymer production process would allow manufacture of ALD-coated polymer particles at reasonable investment costs. Another fascinating solution is the development of the current batch type process into a continuous substrate coating process, as introduced by Heller et al. (2008) in their patent application of a method for roll-to-roll atomic layer deposition on continuously fed objects. In fact, research equipment is already available for continuous ALD, supplied by Beneq Oy, Finland. Functional solutions may thus be available for tackling future ALD-coating challenges. As a first step to cost-effective commercialization of ALD-tailored polymer nanocomposites, one solution is to use ALD-coated polymer particles—because of their readily verifiable functionality—as additives in the polymer matrix (Nevalainen et al. 2008).

3.3 Nanocomposite properties

The application of ALD to thermoplastic nanocomposite fabrication is very attractive in terms of improved nanofiller dispersion, but only a few scientific studies exist on ALD-coating of micron-sized polymer powders and especially on the properties of melt-compounded ALD-tailored nanocomposites. But though knowledge here is limited, the results are encouraging. For example, ALD has been successfully used in a fluidized bed reactor at a reaction temperature of 80°C or below to deposit, e.g., thin aluminium oxide (Al_2O_3) and titanium dioxide (TiO_2) films on micron-sized polymer particles. The studied polymer particles included low density polyethylene (PE-LD), high density polyethylene (PE-HD), and polymethyl methacrylate (PMMA), but also other polymers have been studied (Spencer et al. 2007, Liang et al. 2008, Liang 2008, King et al. 2007, Wilson et al. 2008). In addition, successful ALD-coatings have been made on several polymer films by, e.g., Kääriäinen et al. (2011).

To our knowledge, only one research group has reported on melt-compounded ALD-tailored nanocomposites. Well-dispersed polymer nanocomposites were obtained by melt-compounding Al_2O_3 ALD-coated PE-HD particles (Fig. 7; Spencer et al. 2007, Liang et al. 2008). The nanocomposite showed improved barrier properties against helium gas (Liang et al. 2008), and its diffusion coefficient and permeability decrease was about 15% of 4.8 wt.% Al_2O_3 PE-HD composite prepared from ALD-coated polymer particles (Ø ≈ 60 μm). Compared to an unfilled matrix, about a 50% diffusion coefficient reduction was obtained for 18 wt.% Al_2O_3 PE-HD composite films prepared from ALD-coated polymer particles (Ø ≈ 16 μm). However, increased permeability was detected because of voids formed at or near the interface of polymer and aluminium oxide (Fig. 7b). This reduction could not be avoided despite efforts to improve the film's barrier properties with silane treatment of the ALD-coated polymer particles prior to melt-compounding (Liang 2008).
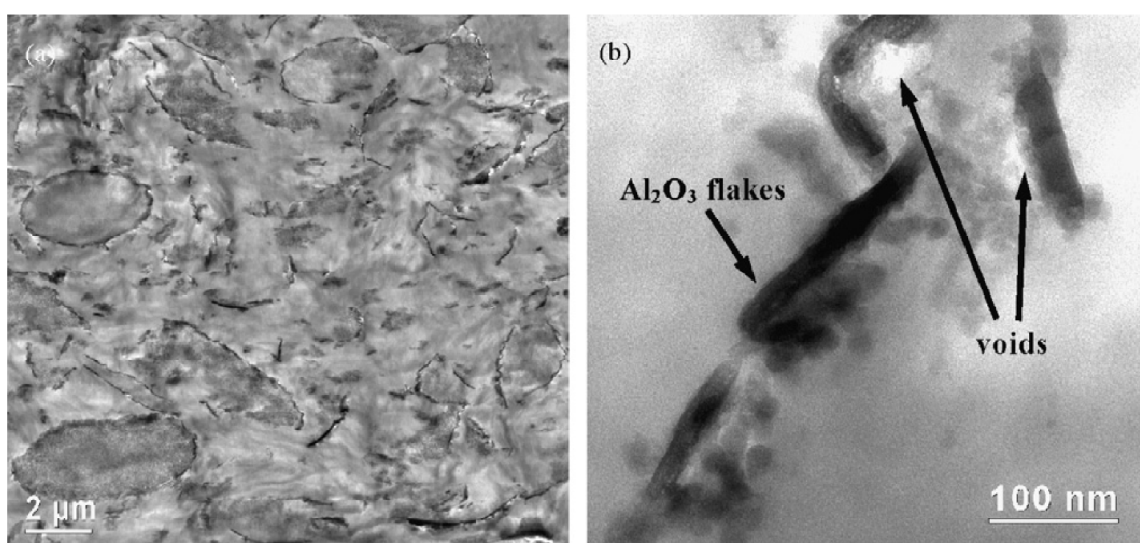
Fig. 7: Transmission electron microscopy image of an ALD-tailored Al_2O_3 PE-HD composite prepared by melt-compounding using table-top sized extruder, where (a) is low magnification and (b) high magnification. Filler content was 12 wt.% and PE-HD particle diameter 16 μm. Reprinted from Liang et al. (2008), Copyright (2008), with permission from Elsevier.

These preliminary studies show that ALD can be used to coat polymer particles with conformal metal-oxide thin film coatings of varying thickness. ALD-created metal oxide fillers incorporated in polymer offer benefits over their commercial spherical counterparts especially due to their significantly higher aspect ratio and reduced risks with handling powder nanofillers. Advantages over, e.g., surface-modified nanoclay include high chemical and thermal stability. According Liang (2008), the ALD-tailored nanocomposite formation technique helps improve at least nanocomposites' barrier properties and may even bring in other advanced features such as considerably enhanced mechanical properties.

4 Aims of the study

The objective in the experimental part was to study the effect of the processing route on the properties of nanofilled thermoplastic composites. The research questions of this study were as follows:

- What kind of nanofiller dispersion and composite properties are obtained through direct melt-compounding and masterbatch melt-compounding? (*publications I- II*)
- Can application of ALD-tailored nanocomposite formation yield better dispersion than conventional direct melt-compounding? (*publications III- VI*)
- What kind of property changes are achieved with ALD-tailored composites when nanofiller content and type are altered? (*publications V-VI*)

Several melt-compounded thermoplastic composites of inorganic fillers and ALD-coated polymer particles with varying filler contents were manufactured, and selected properties such as filler dispersion, mechanical strength, fire resistance, and melt-flow properties were studied. For *publications I-II*, materials were chosen so that property changes could be compared with previously reported results and material performance could be assessed. *Publications III-VI*, on the other hand, sought to provide further insight into the application of ALD technology to nanocomposite formation and to identify possible advantages and challenges in implementing ALD technology. Fig. 8 shows the experimental route and summarized outputs of the publications comprising this dissertation.

Publication I   Publication II   **Publications III-VI and some unpublished data**

PC matrix	PP/PPgMA matrix		PA matrix	PA & PS matrixes

Filled with nanoclay / *Filled with micro-CaCO₃, nano-CaCO₃, nano-TiO₂, nanoclay or MWCNT*

1st Trial — PA powder coated with TiO₂ ALD thin film

Pilot-scale twin-screw extruder

Table-top twin-screw extruder   Atomic layer deposition

Direct melt-compounding / **Masterbatch formation and dilution step**

Direct melt-compounding / **ALD-tailored melt-compounding**

2nd Trial — PA and PS powder coated with TiO₂, Al₂O₃ or ZnO:Al ALD thin film

Pilot-scale injection molding machine and/or cast film line

Table-top injection molding machine

XRD, SEM, TEM, TGA, DSC, Tensile test, Impact test

Ash content test, Optical microscope, TEM, TGA, O₂TR, Tensile test, Cone calorimeter

Ash content test, Rotational rheometer, TGA, DSC, GPC, TEM, Melt-flow length in a mould, Tensile test, Flexural test

Computed filler content — Ash content test, SEM, TEM, MFR

The dispersion and mechanical properties of composites when nanofiller weight percentage is altered. The dispersion and fire performance of composites when filler type is varied.

Comparison of direct and ALD-tailored melt-compounding in terms of composite dispersion, melt-flow, and mechanical properties. The dispersion and mechanical performance of composites when ALD-created nanofiller type and content is varied.

Success of ALD thin film coating and its effects on material's melt-flow properties

The effect of processing route on melt-compounded composites of inorganic nanofillers and ALD-coated polymer powder

Fig. 8: Outline of experiments and main aims of this study consisting of *publications I-VI* and some unpublished data (abbreviations explained in section 5).

5 Experimental

5.1 Studied materials

Four different polymer matrixes, seven commercial fillers, and three tailor-made nanofillers were used in this study (Tables 1-2). The target filler contents for commercial filler grades varied from 1 wt.% to 5 wt.%. For ALD-tailored nanocomposites, the filler content was altered by altering the metal-oxide film thickness on polymer powder and/or polymer particle size. Target ALD-created nanofiller contents were computed to be less than 1.5 wt.% to maintain a reasonable processing time for ALD-coating. Prior to melt-processing, all composite materials in this chapter were dried at an elevated temperature (typically 70-80°C) for several hours.

For direct melt-compounding studies (*publication I*), commercial bisphenol-A polycarbonate (Makrolon 3103 MAS157, now renamed as Makrolon ET3113) was used as matrix. Two nanoclays were selected, Nanomer I.34TCN and Nanomer I.30P, composed of montmorillonite modified with organic modifiers (Table 2). For a two-step process in which concentrate masterbatch is first created and then diluted (*publication II*), on the other hand, a polypropylene-ethylene random copolymer (PP RD204CF) was used as matrix. For melt-compounding, five different fillers, namely micro-calcium carbonate (micro-$CaCO_3$), nano-calcium carbonate (nano-$CaCO_3$), nano-titanium dioxide (nano-TiO_2), nanoclay, and multi-walled carbon nanotubes (MWCNT) were selected (Table 2). To promote adhesion between filler and PP matrix and to assist proper filler dispersion, maleic anhydride modified PP (PPgMA) was used.

For nanocomposite materials tailored by ALD technology, polyamide 12 (PA 2200) and polystyrene (PS 80/03) powder with an average particle diameter of 60 and 80 μm, respectively, as reported by the supplier, were used (*publications III-VI*). Nanometer-scale thin films of titanium dioxide (TiO_2), aluminium oxide (Al_2O_3), and aluminum-doped zinc oxide (ZnO:Al, also called AZO) were deposited on both PA and PS particles in a flow-type reactor P400 (Beneq Oy, Finland). Polymer powder (ca. 100 g/coating cycle) was placed on a filter-covered plate (Ø 200 mm), mounted in an ALD chamber (Fig. 9). For comparison, two commercial TiO_2 fillers (unmodified P25 and surface modified T805, see Table 2) were used to form conventional direct melt-compounded nano-TiO_2 filled PA composites (*publications III-IV*).

Fig. 9: Schematics of an ALD-reactor chamber used for thin film coating of polymer powder (modified from *publication III*).

Table 1: Used polymer matrixes and coupling agent and their selected properties (*publications I-VI* and some unpublished results).

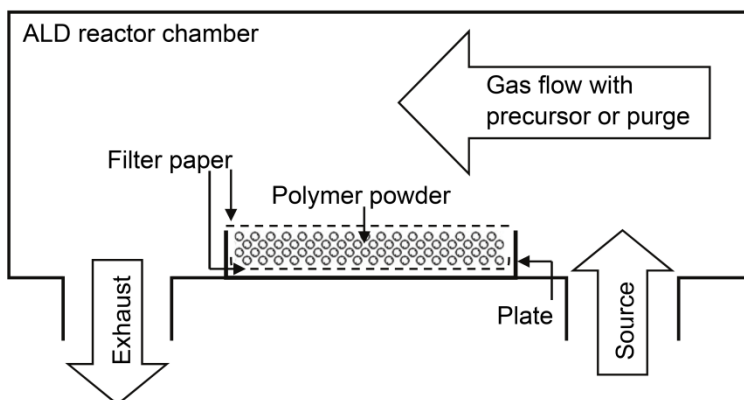| Polymer	Trade name	Supplier	Melt-mass flow rate (g/10 min)		M_w (kg/mol)	M_w/M_n	Density (g/cm^3)	Additional information	Publication
PC	Makrolon 3103 MAS157	Bayer AG [a,b]	6.5	(300°C, 1.2 kg)	51	1.6	1.2	bisphenol-A PC, extrusion grade	I
PP	PP RD204CF	Borealis AG [a,b]	8	(230°C, 2.16 kg)	310	3.4	0.9	random copolymer, film grade	II
PA	Eosint P PA 2200	EOS GmbH [c]	2-3	(191°C, 2.16 kg)	34	3.6	1.0	powder for laser sintering	III-VI, unpublished
PS	PS 80/03	EOS GmbH [c,d]	4-5	(191°C, 2.16 kg)	129	3.5	1.1	powder for laser sintering	V-VI, unpublished
PPgMA	Scona TPPP 2112FA	Kometra GmbH [a]	2-7	(190°C, 2.16 kg)	217	2.9	0.9	contains ~ 1 wt.% maleic anhydride	II

[a] Presented material information provided by the supplier unless otherwise stated. M_w is weight average molecular weight and M_n is number average molecular weight.

[b] M_w and M_w/M_n approximations obtained from Tan et al. (2012) for PC and Gahleitner et al. (2005) for PP.

[c] Experimental data determined in-house. Melt-mass flow rate determined from powder form material, M_w, M_w/M_n, and density from injection molded samples (*publications V-VI* and some unpublished results). Molecular weight results for PA and PS are only approximate values and suitable for comparative studies between these two matrixes.

[d] EOS GmbH's commercial product PrimeCast 101 is made of the PS 80/03 and some additives.

Table 2: Used fillers and their selected properties (*publications I-VI* and some unpublished results).

Filler	Trade name	Supplier	Particle size[c] (nm)	Density (g/cm^3)	Additional information, surfactant content (wt.%) given in parentheses	Publication
nanoclay	Nanomer I.34TCN	Nanocor, Inc. [a]	$(16-22) \cdot 10^3$	2.1	octadecyl bis hydroxylethyl methyl ammonium modified (30-32 %)	I
nanoclay	Nanomer I.30P	Nanocor, Inc. [a]	$(15-20) \cdot 10^3$	2.1	octadecylamine modified (25-27%)	I, II
micro-CaCO$_3$	SuperPflex 100PCC	Mineral Technologies, Inc. [a]	700	2.7	stearic acid modified (1%)	II
nano-CaCO$_3$	Calofort SV E8870	Mineral Technologies, Inc. [a]	70	2.7	stearic acid modified (3%)	II
MWCNT	Baytubes C 150P	Bayer Material Science AG [a,b]	5-20	1.9	unmodified agglomerates	II
nano-TiO$_2$	Aeroxide TiO$_2$ T805	Degussa GmbH [a]	21	3.5	triethoxyoctylsilane modified (< 3%)	II, III
nano-TiO$_2$	Aeroxide TiO$_2$ P25	Degussa GmbH [a]	21	3.8	unmodified	III
ALD TiO$_2$	in-house manufactured	Beneq, Inc.	-	-	ALD-created thin film on polymer powder	III-VI
ALD Al$_2$O$_3$	in-house manufactured	Beneq, Inc.	-	-	ALD-created thin film on polymer powder	VI, unpublished
ALD ZnO:Al	in-house manufactured	Beneq, Inc.	-	-	ALD-created thin film on polymer powder	VI, unpublished

[a] Presented material information provided by the supplier unless otherwise stated.

[b] MWCNT density value includes impurities (< 5% residual metal catalyst) (Nadler et al. 2008).

[c] Mean dry particle size of nanoclays, average primary particle size of spherical fillers, and outer diameter range of MWCNT. MWCNT has 3-15 concentric tubes with a mean length of 0.48 µm. MWCNT agglomerate size is about 0.1-1 mm.

Our industrial partner was responsible for the ALD thin film deposition and for selecting the ALD precursors and processing parameters. The ALD-coating temperature was set at 40°C, 100°C, and 100°C for TiO_2, Al_2O_3, and ZnO:Al thin films, respectively. Growth rates of thin films (Table 3) at the selected temperatures were approximated from previous knowledge by the ALD reactor operator. Nitrogen (N_2) was used as carrier and purge gas for all prepared thin films. During deposition, the pressure setting in the reactor was typically 1 mbar. Significantly extended pulse times were used, especially during TiO_2 thin film coating, to ensure sufficient exposure of the powder surface to precursor gases.

Table 3: Used thin film precursors and ALD-deposition parameters (*publications III-VI* and some unpublished results).

ALD thin film	Metal and oxygen precursors[a]			Gas flow rate (slm)[b]	Deposition temp. (°C)	Expected growth rate (nm/cycle)[c]	Target ALD-film thickness (nm)[d]	Number of executed ALD-cycles[c]
TiO_2	$TiCl_4$	H_2O	-	unkn	40	0.05	5, 10, 25, 40	100, 200, 500, 800
Al_2O_3	TMA	H_2O	-	1	100	0.09	5, 10, 25, 40	57, 114, 285, 456
ZnO:Al	TMA	H_2O	DEZ	2	100	0.05	10, 25	333, 483

[a] Titanium tetrachloride ($TiCl_4$), water (H_2O), trimethylaluminum (TMA: $Al(CH_3)_3$), diethyl zinc (DEZ: $Zn(CH_2CH_3)_2$).
[b] The gas flow rate data (slm, standard liter per minute) for the TiO_2 thin film is unknown. It was not recorded during the thin film deposition and could not be traced back afterwards.
[c] ZnO:Al growth rate and cycle number takes account all subcycles including 30 H_2O/DEZ pulses, a H_2O/TMA pulse and 30 H_2O/DEZ pulses.
[d] Target thin film thickness is approximated nominal thickness of the ALD-created thin film, computed using expected growth rate and repeated ALD cycle number.

TiO_2 ALD films where grown using water vapor and titanium tetrachloride ($TiCl_4$) as precursors in sequences consisting of a 30-sec pulse of water vapor, followed by a 15-sec N_2 purge, then a 60-sec pulse of $TiCl_4$, and another 15-sec N_2 purge in an overall cycle of about 120 sec. The films were processed in two separate trials. In the first trial, PA powder was heated in a vacuum at 40°C for three hours and then coated with TiO_2 of an approximate nominal thickness of 10 and 40 nm (*publications III-IV*); in the second trial, both PA and PS powders were heated in a vacuum at 40°C for four hours and then coated with TiO_2 of an approximate nominal thickness of 5, 10, 25, and 40 nm (*publications V-VI*).

Al_2O_3 ALD films where grown using water vapor (H_2O) and trimethylaluminium (TMA) as precursors. The precursor pulsing sequence was 5 sec of water vapor, a 10-sec N_2 purge, 5 sec of TMA, and a 20-sec N_2 purge for an overall cycle of about 40 sec. For a ZnO:Al thin film, diethylzinc (DEZ) and trimethylaluminum (TMA) were used as zinc and aluminum precursors, respectively. The pulsing times for zinc oxide (ZnO) sublayer were 5 sec of water vapor, followed by a 6-sec N_2 purge, then 5 sec of DEZ, and another 10-sec N_2 purge. For the deposition of the ZnO:Al film, Al was doped into the ZnO film by introducing an Al precursor (TMA) into the reaction chamber as follows: after 30 cycles of H_2O/DEZ pulses, a cycle of H_2O/TMA and then 30 H_2O/DEZ pulses. The precursor pulsing sequence for H_2O/TMA was a 5-sec water vapor pulse, a 7-sec N_2 purge, a 5-sec TMA pulse, and a 10-sec N_2 purge. A full cycle thus consisted of 30 cycles of H_2O/DEZ pulses, a cycle of H_2O/TMA, and 30 H_2O/DEZ pulses took about 26 min. Before the deposition of the Al_2O_3 and ZnO:Al films, the polymer powder was heated in a vacuum at 100°C for four hours (*publication VI* and some unpublished results). For all studied thin films, ALD sequences were repeated as many times as necessary to deposit the target thin film thicknesses on the polymer powder (Table 3), yielding total processing times ranging roughly between 5 and 30 hours.

5.2 Sample processing

Pilot-scale laboratory extrusion and injection molding. PC and PP samples were melt-compounded in a co-rotating Brabender DSE 25 twin-screw extruder (screw diameter 25 mm, length/diameter ratio 44). A screw speed of 200 rpm for both polymers and processing temperatures of 280°C for PC and 170-185°C (from feeder to die) for PP were used (*publications I-II*). PC composites were compounded directly to desired filler contents (1, 3, and 5 wt.%), whereas PP compounds were manufactured by first preparing a masterbatch (8 wt.% filler, 3 wt.% PPgMA, 89 wt.% polymer) and then diluting it to 4 wt.% filler concentration. In all PP dilutions, the amount of PPgMA was kept constant (3 wt.%), i.e., PPgMA content was adjusted again in the dilution step. Unlike other composite samples, the PP/PPgMA/MWCNT masterbatch was processed twice with the extruder before the dilution step to improve otherwise poor dispersion. Subsequently, tensile, impact, or cone calorimeter specimens were injection-molded with a Krauss-Maffei KM50C2 injection molding machine, operating at a processing temperature of 290°C and a mold temperature of 70°C for PC; a processing temperature of 175-185°C (from feeder to die) and a mold temperature of 35°C was used for PP.

Pilot-scale laboratory cast film manufacture. For dispersion and barrier studies of PP composites (*publication II*), an approximately 90-µm thick cast film was prepared using a single-screw extruder Extrudex (screw diameter 30 mm, length/diameter 25) at processing temperatures of 180-195°C from feeder to die, respectively. The extruder was fitted with a 12-cm wide film extrusion die. The pulling device was equipped with an air knife for controlled film attachment to the chill roll immediately after the extrusion die.

Table-top laboratory extrusion and injection molding. ALD-tailored composites were melt-compounded in a co-rotating DSM Xplore 5-cm^3 microcompounder (a conical twin-screw extruder screw with a screw length of 90 mm), operating at 200 rpm with 2-min dwell time in *publications III-IV* and 100 rpm with 1-min dwell time in *publications V-VI*. For comparison, also direct melt-compounded nanocomposites where prepared (*publications III-IV*). PA and PS samples were melt-compounded at 220°C and 190°C, respectively. The specimens were injection-molded using a DSM Xplore 5-cm^3 micro injection molding machine. For the PA matrix, a processing temperature of 220°C and a mold temperature of 80°C were used; for PS, the temperatures were 190°C and 30°C, respectively.

5.3 Characterization techniques

X-ray diffraction (XRD). XRD patterns (*publication I*) were recorded using a Siemens D-500 diffractometer equipped with a Cu Kα radiation source (λ = 0.154 nm) and operating at 30 kV and 40 mA. XRD scanning was performed in a 2θ-range of 1.5°–8° at a scanning rate of 0.3 deg/min. The clay interlayer spacing (d_{001}) in the studied nanoclays and PC/nanoclay composites was determined from the peak (001) of the X-ray diffraction pattern using Bragg's law.

Transmission electron microscopy (TEM) and optical microscopy. Filler dispersion within the polymer and ALD-created film growth on polymer particles were examined by TEM using a JEOL model JEM 2010, operating at an accelerating voltage of 120 kV. TEM specimens were about 120 nm (*publications I, V,* and *VI*) or 60 nm (*publications III* and *IV*) thick and prepared by Leica Ultracut UCT at room temperature. All specimens were post-stained with uranyl acetate and lead citrate. The compositional data of ALD-created fillers was confirmed with an energy dispersive spectrometer (EDS) (*publications III-VI*). In addition, filler dispersion and PP film thickness was approximated using a Leica DM 2500M optical microscope (*publication II*).

Scanning electron microscopy (SEM). Specimen surfaces worn on a pin-on-disc (*publication I*) and ALD-coated polymer particles (*publications III-V*) were examined by SEM using Philips XL 30 apparatus, operating at an accelerating voltage of 10 kV. Compositional data was obtained with an energy dispersive spectrometer (EDS) Edax DX-4. Prior to SEM studies, specimens were coated with a thin carbon layer using a vacuum evaporator to avoid charging.

Thermogravimetric analyzer (TGA). The thermal stability of fillers and prepared PC and PP samples (*publications I-II*) and the inorganic material content of nanoclays (*publication I*) were studied by using a Perkin Elmer TGA6. In *publication I*, a heating rate of 20°C/min from 50 to 900°C in N_2 atmosphere was used, whereas in *publication II* a heating rate of 10°C/min recorded from 30°C to 900°C in both N_2 and air atmosphere were used.

Differential scanning calorimeter (DSC). The glass transition temperature and/or crystallinity of PC, PP, and PA samples (*publications I-III*) were tested using a Netzsch DSC 204 F1 at a scanning rate of 10°C/min under nitrogen. In *publications II-III* the heating-cooling cycle was recorded from room temperature or below to 200°C, and this cycle was then repeated. Before a cooling run, samples were held at 200°C for 3 or 5 minutes to erase their thermal and mechanical histories. Due to the hydroscopic nature of PA, PA samples were dried in a vacuum oven prior to experiment. The degree of the crystallinity was determined from the ratio of the heat of fusion of the specimen and the heat of fusion of 100% crystalline polymer for PA 12 209.2 J/g (McNally et al. 2003) and for PP 209 J/g (Housmans et al. 2009) where employed. The degree of crystallinity data were corrected for the presence of any inorganic material found in the polymer.

Tensile test. Tensile tests were run on PC, PP, and PA using a Messphysik (model Midi 10–20) and for PS using an Instron (model 8801) at room temperature. The test procedures used are described in Table 4. In *publication V*, e.g., Young's modulus was determined at a crosshead speed of 1 mm/min, whereas for the rest of the test (i.e., beyond 1% elongation) a crosshead speed of 50 mm/min was used for PA. For PP (*publication II*), two series of samples were tested. First, Young's modulus was determined at a crosshead speed of 1 mm/min. Second, to study tensile strength and elongation at break, a cross head speed of 50 mm/min was used until 50% elongation; for the rest of the test, a crosshead speed of 200 mm/min was used.

Table 4: Used tensile test equipment and testing procedure.

Matrix material	Sample type, strandard	Testing equipment	Procedure for testing rates	Publication
PC	Conventional dog-bone Type 1A, ISO 527-2	Messphysik	50 mm/min	I
PP	Film strip 20-mm wide cut in machine direction Type 2, EN ISO 527-3	Messphysik	*Young's modulus*: 1 mm/min < 1% elongation	II
			Tensile strength: 50 mm/min < 50% elongation	II
			200 mm/min > 50% elongation	II
PA	Small dog-bone Type 1BA, ISO 527-2	Messphysik	50 mm/min	IV
			1 mm/min < 1% elongation	V, unpublished
			50 mm/min > 1% elongation	V, unpublished
PS	Small dog-bone Type 1BA, ISO 527-2	Instron	1 mm/min	V, unpublished

Impact test and three-point flexural test. The notched Charpy impact strength was measured using a Ceast Resil 5.5 impact tester with a 2-J or 4-J hammer at room temperature as described in ISO 179 (*publications I and IV*). Three-point flexural tests (*publications V-VI*) were run using a Messphysik model Midi 10–20 with a crosshead speed of 1 mm/min, a span length of 32 mm,

and specimen dimensions of 2x4x40 mm^3. Specimen's cross-section was semi-circular with a 2-mm radius. Flexural stress values at yield on the tension side were used to compare the composite bending, here referred to as flexural strength, behavior (see *publication V*).

Oxygen transmission rate (O$_2$TR). Oxygen barrier test was performed on PP films (*publication II*) with a Mocon Ox-Tran 2/21 MH, as described in ASTM F1927-07 and ASTM D3985-05. The test conditions were 23°C and 50% relative humidity on both sides of the sample. The film was then exposed to a mixture of 10% oxygen and 90% nitrogen on one side and a mixture of 99% nitrogen and 1% hydrogen on the other side. The active test area was 5 cm^2, the rest being covered with a tight aluminium foil. Our films were considered homogenous, and thus the permeability was obtained by multiplying the oxygen permeance with the film thickness.

Cone calorimeter. Fire tests were conducted on PP samples (*publication II*) on a FTT Cone Calorimeter (Fire Testing Technology, UK). All samples were tested in triplicate under a 35 kW/m^2 heat flux according to ISO 5660. The distance between cone and specimen surface was 25 mm. The spark was continuous until the sample ignited. All samples with a surface area of 73 x 73 mm^2, a thickness of 6 mm, and identical masses of 28 ± 0.3 g were measured in the horizontal position and wrapped in thin aluminum foil (except for the irradiated sample surface). Tests were carried out without a frame and grid.

Melt-mass flow rate (MFR) and melt flow spiral test. The MFR of PA and PS samples (*publication V* and in some unpublished studies) was measured according to SFS ISO 1133 on a CEAST melt-flow indexer, model 6452/000, at 191°C under a static load of 2.16 kg. The melt-flow spiral test was run by injecting samples prepared with the microcompounder and micro injection molding machine into a spiral mold (see details in *publications V-VI)*.

Rotational rheometer. More detailed rheological measurements were performed by using a rotational rheometer (Anton Paar Physica MCR 301), and experiments were run in parallel-plate geometry (*publications III-IV*). In *publication III* the frequency sweep method was selected, and the frequency range was 0.1-550 rad/s at 200°C when hot-pressed PA disc samples, piled up to form specimens (Ø 25 mm, thickness 0.6 mm), were studied. The strain was selected as 1%. In *publication IV* steady shear experiments were run at two gap settings of 0.5 and 1 mm with shear rates ranging from 0.1 to 10 sec^{-1} for injection-molded, coin-shaped samples (Ø 25 mm, thickness 1.5 mm). These measurements were conducted at 200°C for PA and at 190°C for PS matrixes. All samples were dried in a (vacuum) oven for several hours before being tested under a continuous nitrogen purge.

Ash content test. To determine the inorganic filler content of the prepared composites, an ash content test was conducted (*publications II-VI*). Samples of 1-1.5 g were placed in an oven with the temperature raised gradually from 300 to 600°C over two hours. Typically, unfilled polymer contained some inorganic material, which was deducted from the composite's inorganic material to determine the amount of added filler in the polymer.

Gel permeation chromatography (GPC). Average molecular weights (M_w, M_n) and molecular weight distribution (MWD=M_w/M_n) were estimated using GPC (*publication V*). Chromatograms for PA were obtained using a refractive index detector equipped with a PL HFIPgel guard plus 2 x PL HFIPgel 300 x 7.7 mm, 9-μm columns and for PS using a light-scattering, differential-pressure, refractive index detector with a PLgel guard plus 2 x mixed bed-B 30 cm, 10-μm columns. Before GPC analysis, samples were dissolved in a solvent and filtered through a membrane. The solvent used for PA was 1,1,1,3,3,3-hexafluoro-2-propanol and for PS tetrahydrofuran (with antioxidant). For a detailed test procedure, see *publication V*.

6 Results and discussion

6.1 Effect of direct and masterbatch melt-compounding on PC or PP matrixes

6.1.1 Mechanical properties

Polycarbonate is a well-known engineering thermoplastic with relatively high molecular weight and high impact strength over a wide use temperature range. Applications of amorphous PC include automobile parts, audio discs, and helmet visors. For use in demanding applications PC has been tailored in many different ways, e.g., by addition of modifier, blending with other polymers or using hard surface coatings. The aim of such modification is often to decrease the polycarbonate's high melt viscosity or enhance its poor abrasion resistance. In principle, addition of well-dispersed nanofillers to PC could preserve the optical clarity of this amorphous polymer. PC nanocomposites would make an attractive study, especially if its good toughness could be retained accompanied with the promise of transparency, improved barrier, stiffness, and abrasion resistance (Yoon et al. 2003a, Hsieh et al. 2004, Suin et al. 2013).

To date, several attempts have been made to prepare PC/nanoclay composites by the melt-compounding approach for a desired set of properties (Lee & Han 2003, Yoon et al. 2003a, Hsieh, et al. 2004, Suin et al. 2013, Dhibar et al. 2012, Feng et al. 2012), yet this material combination is much less studied than, e.g., nanoclay-filled nylons or polyolefins. Furthermore, it has not been entirely established how different nanoclay surface coatings affect filler dispersion and mechanical properties, as recently stated by Feng et al. (2012). In this thesis, the effect of direct melt-compounded nanoclay fillers on the mechanical properties of PC and the extent of nanoclay dispersion were examined (*publication I*). Samples containing I.34TCN and I.30P nanoclays were studied and the mechanical properties of the prepared PC composites were compared (Fig. 10). These results were reported in terms of inorganic nanoclay content in the composite (determined by TGA) rather than the amount of surface modified nanoclay, since silicate was considered a reinforcing component. Our tensile test results (Fig. 10a-c) showed a considerable improvement in Young's modulus compared with that of unfilled PC, whereas more modest changes were detected in tensile strength (which is also yield strength in this case). The tensile strength of, e.g., I.34TCN composites increased with increasing inorganic nanoclay content from 0.5% to 12% compared to unfilled PC, illustrating good interaction between nanoclay particles and PC matrix. For the composite containing 5 wt.% I.34TCN filler, the increase in Young's modulus was 30%, whereas for the PC/I.30P composites the improvement was somewhat lower, i.e., less than 18% (Fig. 10a). Yoon et al. (2003a) obtained very similar property enhancement levels for their nanoclay filled polycarbonates. Generally, such increase in tensile strength and modulus in nanocomposites is explained in terms of the very large interacting area between the matrix and nanofiller, as discussed in section 2.3.
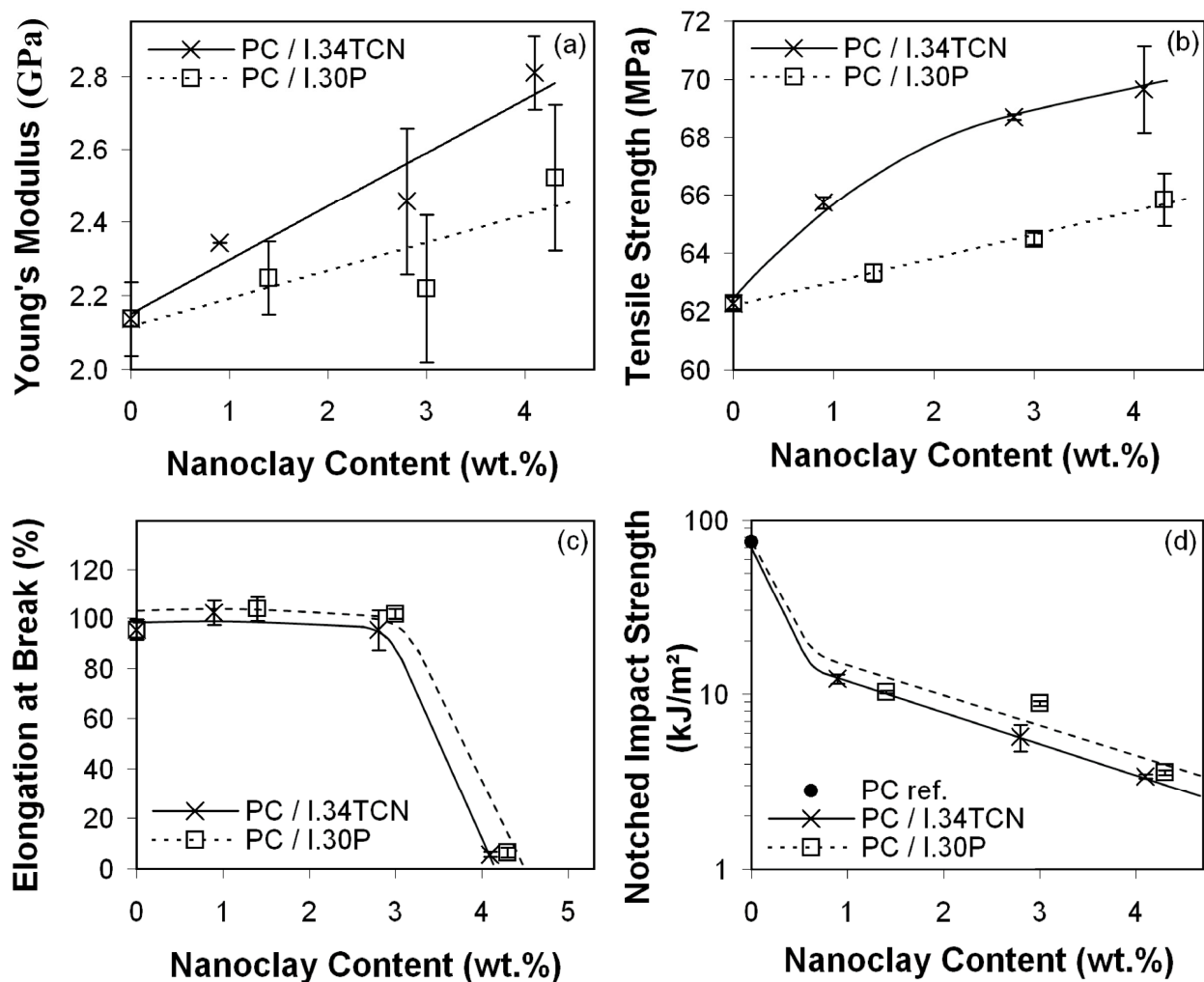
Fig. 10: Mechanical properties of direct melt-compounded I.30P and I.34TCN-nanoclay-filled PC composites as a function of inorganic nanoclay content, where (a) is Young's modulus, (b) tensile strength, i.e., yield strength in this case, (c) elongation at break, and (d) notched impact strength. Vertical bars show standard deviation values. The filled round marker in Fig. 10d illustrates the unfilled PC reference value provided by the material supplier, which was used when the expected behavior of the notched impact strength lines at very low filler content were drawn (*publication I*).

The ductility of the prepared PC composites was reduced especially at high filler loadings, as indicated by a significantly lower elongation at break and notched impact strength for both studied nanoclays (Fig. 10d). The notched impact strength decreased 70% as the nanoclay content increased from 1 to 5 wt.%, regardless of the used nanoclay surface modification. A 90% decrease in elongation at break was caused by a 5 wt.% nanoclay addition, a result similar to that obtained by Hieseh et al. (2004) for nanoclay-filled PC composites. They showed that at clay loadings higher than 3 wt.%, a change occurred in failure mode from ductile to brittle deformation in tensile testing. Such decrease in ductility may be due to exfoliated nanoclay platelets, which cause restraints and/or defect-like characteristics originating from large clay particles, which subsequently make the composite fail in a brittle manner in contrast to an unfilled polymer matrix (Yoon et al. 2003a). The mechanical properties of composites depend strongly not only on filler nano-dispersion (intercalation and exfoliation) but also on micro-dispersion in the polymer matrix. Thus to further understand our mechanical test results, we thought it crucial to study the structure of the prepared composites (see section 6.1.3).

6.1.2 Fire properties

Polyolefins (such as polypropylene and polyethylene) are the most widely used commodity plastics and are thus also an interesting option for nanocomposites. Semicrystalline PP is used, e.g., in packaging, ropes, and textile fibres due to its easy processability, low cost, and relatively good mechanical properties. However, to widen its application range in fields such as electronics, transportation, and decorating materials, PP must overcome some of its disadvantages such as low service temperature and high flammability. Flammability and the oxygen barrier properties of polyolefins have been enhanced by using layered silicates, whereas effects of spherical, tubular, and nonsilicate-layer based fillers have rarely been reported in the literature. The often increased flame retardancy properties obtained with nanofillers (and other halogen-free fire retardants) are rather polymer-specific, which means that while one nanofiller works well in one polymer, it may not work at all in another (Song et al. 2007, Rault et al. 2009, Baniasadi et al. 2010, Hull et al. 2011, Fina et al. 2012). Therefore, the effect of 4 wt.% micro-$CaCO_3$, nano-$CaCO_3$, nano-TiO_2, nanoclay, and MWCNT fillers was studied on the flammability properties of a PP matrix (*publication II*). Owing to the generally poor compatibility of PP with inorganic fillers, composites were prepared in a twin-screw extruder using the masterbatch dilution method and PPgMA as a coupling agent to enhance filler dispersion and polymer matrix-filler particle interaction.

The inorganic filler content showed that obtained filler contents in the PP matrix agreed well, within experimental error, with the target filler content ranging between 3.5 wt.% for nano-$CaCO_3$ and 4.4 wt.% for the MWCNT composite. The MWCNT content, however, is presumably somewhat higher than the results suggested, since part of unmodified MWCNT filler degrades already at ash content testing temperatures, as suggested by the TGA results introduced in *publication II*. The filler volume contents in the prepared PP composites were computed to be between 1.0 vol.% and 1.4 vol.% apart from the PP/PPgMA/MWCNT composite, where 2.1 vol.% was obtained. As for PC samples, mechanical test results were presented for PP composite films (*publication II*). However, in contrast to our PC studies, tensile test results showed that Young's modulus and yield strength remained essentially unchanged or increased up to 10% over the PPgMA-modified PP matrix. Due to unexpectedly small property changes, a concern arose about the success of filler dispersion and polymer-filler compatibility. Poor dispersion and low matrix-filler interaction are usually responsible for a small increment in Young's modulus and tensile strength of the composite over a unfilled polymer as, e.g., Baniasadi et al. (2010) observed for PP/nanoclay composites prepared by melt-compounding and in-situ polymerization. Also other authors (Wu et al. 2002, Rault et al. 2009) have shown similar results. Because of variation in the film thickness and possible changes in the film draw ratio due to adjusted winding unit parameters (see *publication II*), tensile test results give only a first approximation of the composite films' mechanical properties and are thus not given here in detail.

Only a few studies have focused on the effects of particle size and shape on polymer composite flammability and concentrated only on one filler-type at a time. Cipiriano et al. (2007) studied polystyrene composites filled with two MWCNTs having average aspect ratios (length to outer diameter) of 49 and 150 and showed that the latter reduced more efficiently the flammability of polystyrene. Laachachi et al. (2005), on the other hand, showed that nano-TiO_2 reduced the peak heat release rate (PHRR) of PMMA about 20% more than micro-TiO_2 (see Fig. 4). It was thus intriguing to study the effect of selected spherical, plate-, and tubular fillers on a PP matrix. The fire test results showed (Fig. 11) that addition of a somewhat lower-molecular-weight adhesion

promoter (PPgMA) increased the PHRR by 28% over neat PP. As for the prepared composites, the PHRR was reduced by incorporating fillers. Compared with PP/PPgMA, the PHRR of micro-$CaCO_3$, nano-$CaCO_3$, nano-TiO_2, and nanoclay composites dropped by 14, 21, 43, and 37%, respectively. The result suggests that spherical nano-TiO_2 yields to a reduction in PP flammability very similar to that in plate-like nanoclay. Filler dispersion studies could further explain our results, because, e.g., Fina et al. (2012) demonstrated that nanoclay dispersion has a significant effect on the PHHR of a melt-compounded nanofilled PP/PPgMA matrix. Their unmodified-nanoclay-filled PP had a conventional microcomposite structure and about 20% reduction in the PHHR, whereas their surface-modified clay formed an intercalated composite structure and had a PHHR reduction as high as 50% (Fina et al. 2012).
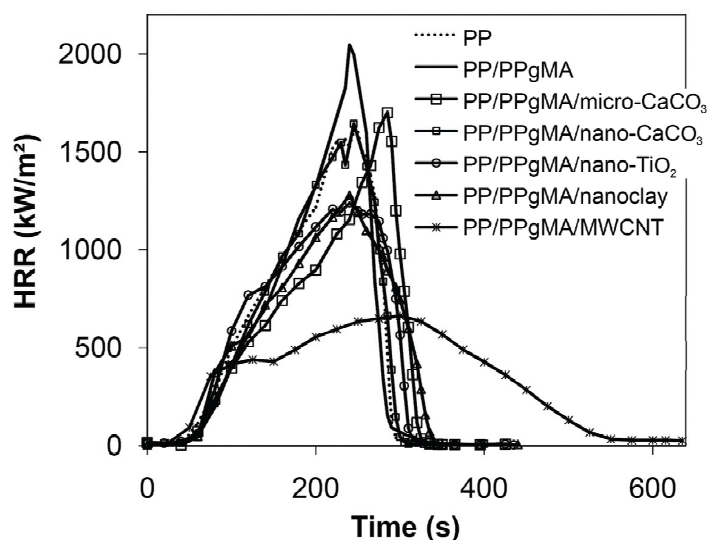

Fig. 11: Typical HRR curves obtained from cone calorimeter test for injection-molded unfilled PP and 4-wt.%-filled PP composite samples prepared using the masterbatch approach (*publication II*).

However, of all the studied composites, the PP/PPgMA/MWCNT sample showed the highest reduction in the PHRR, yielding a 67% lower PHHR than PP/PPgMA (Fig. 11). Though it had the shortest ignition time, it burned slowly with the longest flameout time. Furthermore, the PHRR appeared about 40 seconds later than in the PP/PPgMA sample, indicating a slower burning rate. Similar PP/MWCNT composite fire behavior was also reported by Rakhimkulov et al. (2010). The short ignition time of MWCNT-filled composites has been attributed to a rapidly heating thin layer near the sample surface, which increases the fuel production rate and decreases the time to ignition (Laoutid et al. 2009). Neat PP, e.g., heats deeper and thus takes longer to ignite (Kashiwagi et al. 2004). Our MWCNT composite fire results were supported by TGA analysis (*publication II*), showing how especially MWCNT inhibits the thermal decomposition of PP/PPgMA matrix. Furthermore, barrier measurements (*publication II*) revealed that the nanoclay- and MWCNT-filled composites had the highest oxygen barrier, which reduced the film's permeability by about 20% compared to PP/PPgMA, and because the fillers did not increase PP crystallinity, the drop in oxygen permeability was likely to have been caused by the filler. Fillers thus hinder the diffusion of oxygen in the material during a fire scenario.

After sample burning, PP and PP/PPgMA matrixes did not leave a residue, whereas the composite samples left behind a clear char (Fig. 12). The char residues of nanoclay and MWCNT composites were somewhat stronger and more continuous than those of TiO_2- and $CaCO_3$-filled PP. Yet their flocculated or island-type ash residue structure implies poor filler

dispersion. The fillers hardly increased char formation but rather replaced the flammable PP mass, since the total heat release for the composites dropped by only 1-3% compared to PP/PPgMA, and because the mass loss values were close to the intended filler content. Furthermore, smoke release during combustion increased for all studied composites (*publication II*).
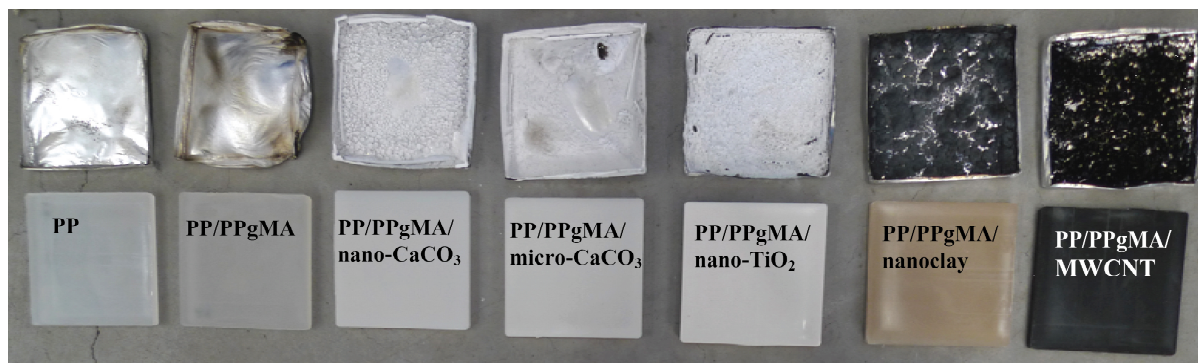

Fig. 12: Injection-molded unfilled PP and 4-wt.%-filled PP composite samples (73 mm x 73 mm, 6 mm thick) prepared using the masterbatch approach and their char residues after the cone calorimeter test (*publication II*).

Effective performance of MWCNT filled composite in fire, thermal and barrier tests could be attributed to its low oxygen permeability, high filler volume content, strong ash residue, and/or high thermal stability over the other fillers and composites. However, comparing absolute enhancements between the composites is challenging because of possible changes in the fire retardant mechanism and especially in filler dispersion.

6.1.3 Filler dispersion

The filler dispersion of prepared PC and PP composites was studied to understand the observed property changes and to estimate the effect of the chosen processing approach on the number and size of possible filler agglomerates. In the following discussions, the term dispersion is used only to illustrate nanocomposite structure. As observed in the presented TEM images in this work, nanofillers were well distributed, but some composites were insufficiently dispersed.

First, nanoclay dispersion in the PC matrix was studied by TEM, XRD, and SEM. Since no major differences were found in filler dispersions between I.30P and I.34TCN composites (*publication I*), this thesis focused especially on the latter. At first glance, the TEM images in Fig. 13 suggest that no agglomeration occurred in the I.34TCN-filled composites. The nanoclay seems well dispersed in the PC and in a similar fashion at each nanoclay concentration. Some nanoclay sheets where individually dispersed but most particles are dispersed in thin layers of silicate sheets (thickness varying between 20 nm and 50 nm) with some polymer insertion between the layers.
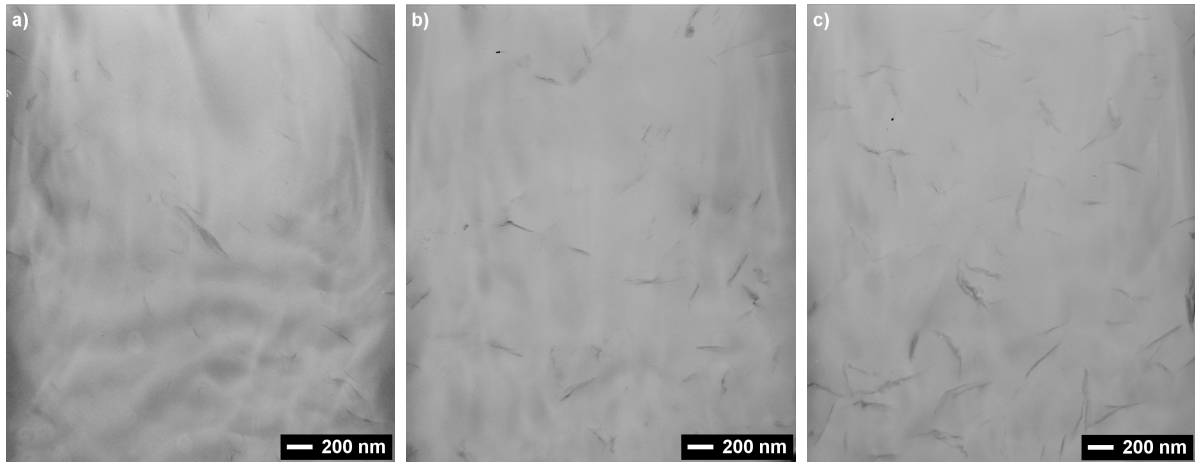
Fig. 13: Typical TEM images of (a) PC/1 wt.% I.34TCN, (b) PC/3 wt.% I.34TCN, (c) PC/5 wt.% I.34TCN direct-melt-compounded nanoclay-filled composites (*publication I*).

X-ray diffraction patterns along with interlayer spacing values d_{001} for clay powder and PC composites are shown in Fig. 14a. The intensity peaks reveal a low-intensity peak in PC/3 wt.% I.34TCN (d_{001} = 2.97 nm) and PC/5 wt.% I.34TCN (d_{001} = 2.94 nm) composites, suggesting that a portion of I.34TCN nanoclay was intercalated. A rather constant d_{001} value for a high intensity diffraction peak indicates that in PC/I.34TCN composites nanoclay dispersion appears similar at each nanoclay concentration (behavior also shown in the TEM images). Furthermore, the high intensity peak of PC/I.34TCN composites corresponds to about 1.45-nm interlayer spacing, suggesting that a significant proportion of the PC matrix did not intercalate into the nanoclay interlayer. In fact, the interlayer spacing appears confined, i.e., reduced from the I.34TCN initial interlayer spacing (d_{001} = 2.00 nm, Fig. 14), most likely a result of thermal degradation and/or desertion of the surfactant component of I.34TCN nanoclay during melt-processing, as suggested by other authors (Yoon et al. 2003a, Gelfer et al. 2004, Varghese & Karger-Kocsis 2004).

A SEM image of PC/I.34TCN composite surface worn on a pin-on-disc revealed micron-sized nanoclay agglomerates in the composites (Fig. 14b). From the SEM-EDS images of, we concluded that the 1 wt.% clay content contained 1-5 µm, 3 wt.% nanoclay 1-10 µm, and 5 wt.% nanoclay 1-30 µm sized agglomerates. Consequently, the PC composite structure contained exfoliated nanoclay platelets together with clay stacks of varying thickness and large clay agglomerates. The detected agglomerates were not seen in TEM images. Apparently, relatively scattered agglomerates are not necessary present in TEM specimens, which represent a very small specimen area. Agglomerates appeared to adhere well to the polymer, because no pull-outs were found in the matrix after the wear tests. This agrees with the enhanced tensile strength properties of prepared composites (Fig. 10b). Agglomerates may, however, decrease the benefit of nanoclay intercalation, especially its strength, because micro-particles often initiate failure due to stress concentration.
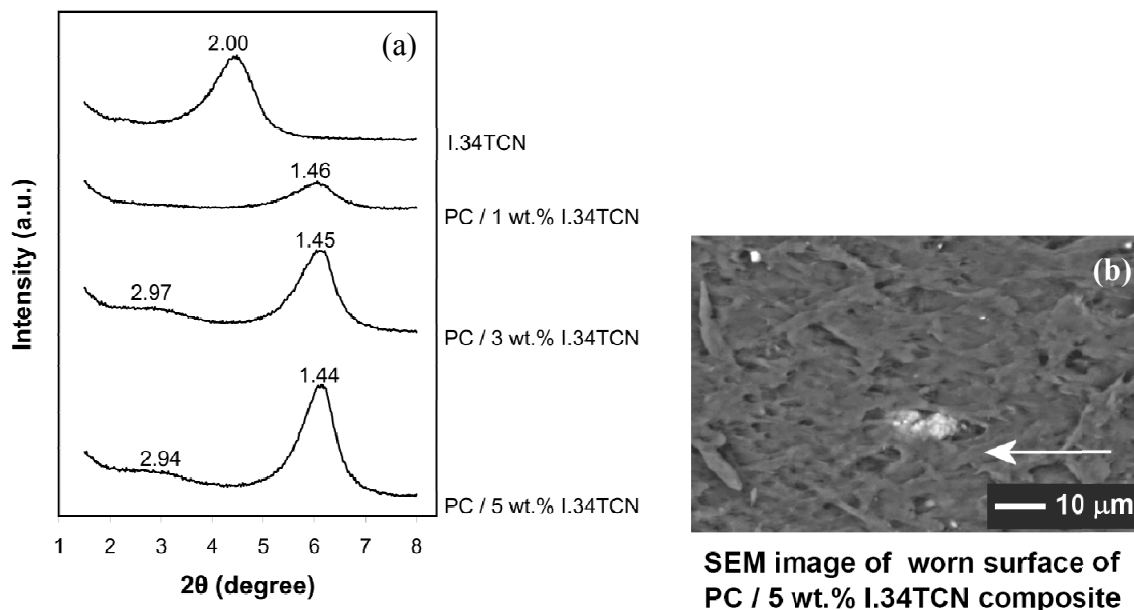
Fig. 14: Typical (a) XRD diffraction patterns along with interlayer spacing values of nanoclay (d_{001}) for I.34TCN nanoclay and I.34TCN filled PC composites, (b) SEM image of the worn surface of PC/5 wt.% I.34TCN composite (modified from *publication I*). In the latter, a wear condition of 1 MPa and 1 m/s was used in the pin-on-disc test. The arrow indicates the sliding direction. Samples were prepared using the direct melt-compounding approach.

Comparison of low magnification (~20 000x) TEM images of the studied I.34TCN and I.30P nanoclays in the PC matrix showed that the nano-scale dispersion of I.30P was generally better than that of I.34TCN (*publication I*). However, at high magnification (~100 000x, unpublished figures), the images showed that interlayer spacing in both composites was similar as also supported by the similar location of the XRD diffraction pattern peaks (see Fig. 3 in *publication I*). I.34TCN loses it thermal stability at lower temperatures than I.30P; thus some fraction of I.34TCN may have thermally degraded already at the processing temperatures used (~280°C) in this work, as suggested by its TGA results. Comparison of the derivate weight curves of the TGA data, however, showed that I.30P degraded at a faster rate than I.34TCN, suggesting complex behavior in the degree of reduction in interlayer spacing (*publication I*).

The studies by Feng et al. (2012) on several chemically modified nanoclays suggest that the mechanical properties of the PC/phosphate matrix are controlled by both morphology and nanoclay interaction within the matrix. In fact, composites containing I.34TCN nanoclay showed the best nanofiller dispersion and tensile strength properties over other studied surface modified commercial nanoclays, including I.44P, I.44PS, and I.31PS (Feng et al. 2012). Based on our dispersion and mechanical studies, we also assumed somewhat lower filler-matrix interaction and more micron-sized nanoclay agglomerates in the I.30P than the I.34TCN matrix, which then yielded, e.g., lower tensile strength values in the PC matrix. Enhanced mechanical properties of the PC/I.34TCN matrix were especially evident in Young's modulus test results (Fig. 10a). Of course, other factors such as changes in the polymer molecular weight may have played a role. Degradation of PC matrix was considered a concern, since the visual appearance of the injection-molded composite specimens changed from clear to light brown to dark brown as the filler content increased for both nanoclays (*publication I*). Such a color change in PC is attributed to a variety of chemical processes caused by thermal and oxidative degradation at elevated temperatures during melt processing. These reactions occur also in melt processing unfilled PC, turning it yellow over extended exposure at high temperatures. Color change in a sample is

generally affected by oxidation rather than decomposition, although both processes often occur simultaneously. In nanoclay-filled PC composites, part of the clay surface modification degraded during melt-compounding (as shown by TGA results for powder from nanoclay in *publication I*), and subsequently radical fragments formed during the degradation of filler's surface treatment promote polymer degradation. High filler content and good filler dispersion promote clay-induced chemical reactions and further reduce, e.g., polymer molecular weight. Such polymer degradation often lowers the polymer's mechanical strength, glass transition temperature, optical clarity, and changes its colour in the final composite (Yoon et al. 2003b, Fornes et al. 2003, Gelfer et al. 2004, Hsieh et al. 2004, Suin et al. 2013). We observed also a decrease in the glass transition temperature (T_g) from 150°C to 140°C for unfilled and 5-wt.% nanoclay-filled PC using DSC, respectively (*publication I*). This and observed sample color change indicated that in the presence of nanoclay, the molecular weight of PC may decrease and thus polymer chain mobility increase yielding lower T_g. However, the actual degree of the effects of polymer degradation on mechanical properties is difficult to estimate without more detailed study. For comparison, Suin et al. (2013) experiments on thermally stable phosphonium-modified nanoclay-filled PC, where PC degradation was minimized due to nanofiller addition, yielded mechanical property changes similar to those in our work but at lower filler contents (≤1 wt.%).

Dispersion in PP composites was studied by optical microscopy and TEM. The optical microscopy images of cross-section of the PP composite films (Fig. 15) revealed large filler agglomerates, even though several methods, such as using a coupling agent, high shear forces in the twin-screw extruder (due to a low processing temperature), and extended residence time (due to the two-step masterbatch dilution approach) were used to break down filler clusters. Micron-sized (Ø ≈ 1-50 μm) agglomerates were detected especially in composite films containing nanoclay and MWCNT, as shown in Figs. 15e and 15f, respectively.
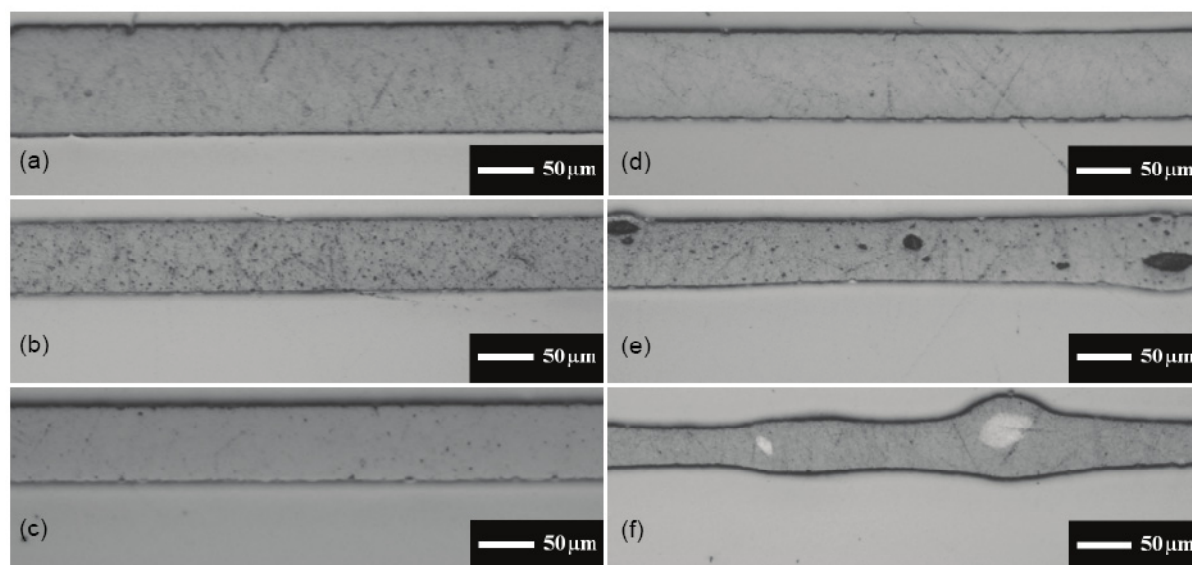
Fig. 15: Selected cross-section images of masterbatch-diluted (a) PP/PPgMA, (b) PP/PPgMA/micro-CaCO₃, (c) PP/PPgMA/nano-CaCO₃, (d) PP/PPgMA/nano-TiO₂, (e) PP/PPgMA/nanoclay, and (f) PP/PPgMA/MWCNT 4-wt.%-filled films characterized by optical microscopy. Also a more uniform filler dispersion was observed than shown in (e) and (f) (*publication II*).

TEM images were taken to further characterize the dispersion in PP composites. In micro-CaCO₃-filled TEM samples, the filler appeared detached from the PP matrix during TEM sample preparation. Because the hole size (0.3-0.7 μm) corresponded rather well to the micro-CaCO₃

particle size (Table 2), TEM images give a reasonable approximation of the filler dispersion. In Fig. 16, spherical fillers (micro-CaCO$_3$, nano-CaCO$_3$ and nano-TiO$_2$) are rather well dispersed overall as individual fillers or small agglomerates. In melt-compounding, nano-TiO$_2$ tended to form chain-like agglomerates (100-200 nm length), whereas nano-CaCO$_3$ particles formed filler clusters (100-200 nm diameter). Plate-like nanoclay filler sheets were difficult to separate in the PP matrix, as reported in several studies (Baniasadi et al. 2010, Szustakiewicz et al. 2011). A mixture of exfoliated, intercalated, and phase-separated (i.e., microcomposite) morphology was obtained, as shown in our optical microscopy and TEM images (Figs. 15-16). Typically, stacked nanoclay platelets were 300-800 nm and 100-200 nm in length and thickness (Fig. 16d), respectively. Optical microscopy and TEM results indicate that in melt-compounding nanoclays remained partly unchanged, consisting of rather thick stacks of parallel nanoclay sheets with no proper polymer insertion between the silicate layers. Nanotubes are also difficult to disperse in a PP matrix mainly due to their numerous carbon nanotube entanglements and strong van der Waals interactions that keep them tied together (Bikiaris et al. 2008, Gupta et al. 2010). Though a few large MWCNT bundles were found, also individual MWCNT tubes and small MWCNT agglomerates were observed (Fig. 16e). In conclusion, if we compare only the number of filler particle agglomerates we found and/or the largest agglomerate size of our composites in the optical microscopy and TEM images, we can arrange the samples in the following order: micro-CaCO$_3$ < nano-CaCO$_3$ < nano-TiO$_2$ < nanoclay, MWCNT.
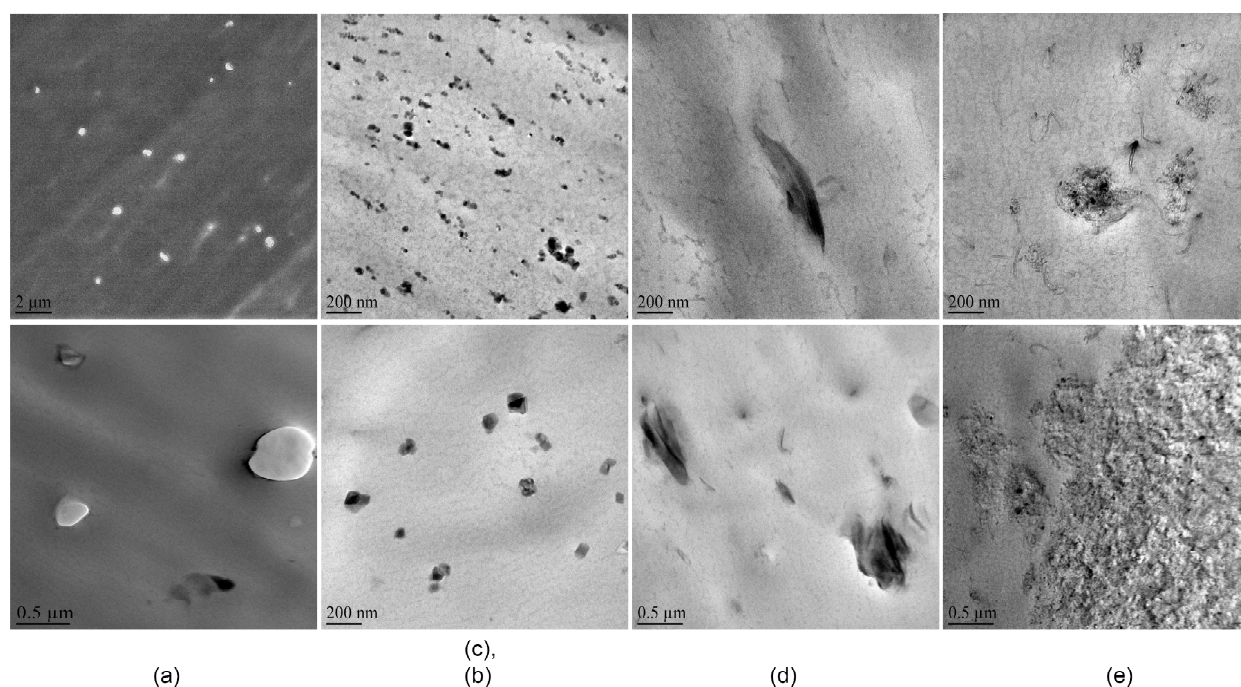
Fig. 16: Typical TEM images of masterbatch-diluted (a) PP/PPgMA/micro-CaCO$_3$, (b) PP/PPgMA/nano-CaCO$_3$, (c) PP/PPgMA/nano-TiO$_2$, (d) PP/PPgMA/nanoclay, and (e) PP/PPgMA/MWCNT 4-wt.%-filled injection-molded samples shown in low and high magnification, except for nano-CaCO$_3$ and nano-TiO$_2$ composites, which could not be clearly detected at low magnification (modified from *publication II*). In micro-CaCO$_3$-filled TEM samples, the filler detached from the PP, but because the hole size corresponded well to the micro-CaCO$_3$ particle size, the TEM images give a reasonable approximation of the dispersion.

The agglomerates and inadequate compatibility between filler and matrix are believed to contribute to the poor mechanical performance observed in our PP composite films. Even if poor dispersion and distribution typically entail also poor fire performance (Fina et al. 2012), there are

results to the contrary. For example, if a flocculated network layer uniformly covers the entire sample surface and does not rupture in burning, it effectively reduces the flammability of the matrix, as suggested by Rakhimkulov et al. (2010) with PP/MWCNT composites. Also our study showed the highest barrier and fire performance for MWCNT-filled PP composites of the fillers studied, even if large micron-sized filler agglomerates were found. TEM images (Fig. 16) suggest that MWCNT created a somewhat more effective barrier labyrinth of individual nanotubes and their agglomerates than the other fillers we studied. Oxygen barrier studies of the films presented in *publication II* support this conclusion, since MWCNT, followed by a nanoclay and nano-TiO$_2$-filled composite, yielded higher permeability reductions than CaCO$_3$-filled PP composites. Of the fillers studied, MWCNT thus turned out to be the most promising flame retardant additive in a PP/PPgMA matrix. However, due to an additional processing step, the PP matrix may be subjected to thermal oxidation during extended melt-processing, leading to macromolecule chain scission and decreased average molecular weight (Hinsken et al. 1991), which may also affect the fire, thermal and barrier behavior of a PP matrix.

In terms of the observed filler dispersion level in this study, processing nanofilled composites is considered difficult regardless of the selected manufacturing approach (direct or masterbatch melt-compounding). In fact, a direct-melt-compounded PC composite might have a somewhat better dispersion than a masterbatch-diluted PP composite, as suggested by a comparison of the TEM images of nanoclay filled composites (Fig. 13 and Fig. 16d). The mechanical properties supported this showing higher Young's modulus enhancement for the nanoclay-filled PC than PP film. In our work, for PC matrix containing 5 wt.% I.34TCN nanoclay the Young's modulus increase was 30% compared with that of unfilled PC. However, the result is sill somewhat modest when compared to, e.g., Kojima et al. (1993) studies on nanoclay-filled polyamide prepared by in-situ polymerization, whose Young's modulus increased by 68% with a less than 5-wt.% addition of nanoclay. Clearly, the selected processing approach plays a key role but also the differences in the polymer matrix properties such as crystallinity, polarity parameters, and melt flow characteristics explain our results. First, PP is a semicrystalline material and thus concentrates fillers in the noncrystalline phase, which often limits filler dispersion, e.g., by reducing nanoclay interlayer spacing (SFE 2007, Gupta et al. 2010). Second, PP is a nonpolar matrix; hence the compatibility of inherently polar fillers must be enhanced at least by using filler surface coatings and a coupling agent as well as extended residence time in melt-compounding, as was done in this work. Of course, better dispersion and nanofiller affinity to the PP matrix could be obtained by optimizing the chemical structures and processing parameters but still many examples show better results in polar polymers such as PC (Gupta et al. 2010). Third, the high melt viscosity of PC compared to many other matrixes may result in higher mechanical force being applied to fillers during melt-compounding.

Our results show that it is difficult to predict and control composite filler dispersion when conventional melt-compounding approach is used. Due to partially agglomerated fillers, we believe that the potential of nanofillers, especially with a high aspect ratio, has not been fully realized. Thus, new approaches must be explored to produce thermoplastic nanocomposites.

6.2 Effect of direct and ALD-tailored melt-compounding on the PA matrix

6.2.1 Thin-film-coated materials

Polyamides are semicrystalline engineering thermoplastics commonly used in textiles, automotives, and sportswear. They have generally good mechanical properties, are particularly

tough, and have excellent sliding and wear characteristics. Because polyamides contain polar amide groups (-CONH-), they have strong hydrogen-bonding interactions with, e.g., polar water vapor and inorganic nanofillers. Polyamides are, in fact, the oldest base material used to manufacture nanocomposites. Following the pioneering work of Toyota researchers, the first practical application of a nanoclay-filled nanocomposite was demonstrated in the automobile industry. Polyamide based nanocomposites have been used in several applications especially in motor vehicles because of their high strength and good thermal resistance (Jancar 1999, Ray & Okamoto 2003, Pavlidou & Papaspyrides 2008). PA was seen as an attractive material also in this work to prescreen the possibilities of ALD-tailored nanocomposite formation (*publications III-VI*) due to its material characteristics and easy availability to us in powder form. The objective in our preliminary studies (*publications III-IV*) was to compare polyamide nanocomposites prepared from ALD-coated PA particles and commercial nano-TiO_2 fillers (unmodified P25 and surface modified T805). In the first trial of thin film coated polymer powder, the target ALD-coating deposition thickness of TiO_2 films was 10 nm or 40 nm on the PA particle. Subsequently, ALD-coated powder was melt-compounded to form PA nanocomposites similarly to the conventional powder mixture of PA and nanofiller in a twin-screw microcompounder.

Prior to melt-compounding, ALD-coated PA powders were examined with a SEM. The results showed some variation in the PA particle size (Fig. 17a) with particle dimensions ranging from 20 μm to 90 μm. The success of ALD-created TiO_2 thin film formation on PA particles was estimated by means of backscattered electrons (BSE) in the SEM. According to this data (Fig. 17), the thickness of the TiO_2 coating on the particle surface seems to be linked to the brightness of the particle in the SEM images, i.e., the lighter the particle color, the higher the TiO_2 content. The result was confirmed with an EDS, which demonstrated that the darkest particles contained no titanium at all, whereas the brightest particles contained most titanium, yielding a titanium contents of 0–35 wt.% and 25–55 wt.% for 10-nm and 40-nm ALD-coated PA powder, respectively. The results suggest that the used ALD reactor and powder positioning in this work (see section 5) enabled precursor access and chemical reactions on only a part of the powder particles' available surface area. In contrast, other studies suggest that a more complex fluidized bed reactor creates smooth and uniform Al_2O_3 thin films on polymer powder when the number of ALD cycles is high enough (Spencer et al. 2007, Liang et al. 2007, Liang et al. 2008). Nevertheless, the uneven thin film was not considered critical, because in the subsequent extrusion step the high shear forces crushed the ALD-created TiO_2 shells of the PA particles.

EDS spectra (Fig. 17) also revealed that the ALD-created thin film contained a considerable amount of chlorine (0-14 wt.%), which was clearly a cause for concern in terms of, e.g., its degrading effect on the PA matrix during melt-compounding. Due to a high local TiO_2 content observed in the SEM-EDS results and an additional chemical residue found, it was intriguing to approximate the ALD-created filler content. The amount of inorganic filler in the prepared polymer composites was determined from theoretically calculated values of ideally thin-film-coated spherical PA particles (Ø 60 μm) and with an ash content test. If densities of 1.015 g/cm^3 for injection-molded PA and 3.5 g/cm^3 for TiO_2 were used, values of 0.3 wt.% and 1.4 wt.% for 10-nm and 40-nm ALD-coated PA, respectively, were calculated (*publication V*). The ash content test, however, suggested that the PA 10-nm TiO_2 ALD sample contained 1 wt.% of TiO_2 and the PA 40-nm TiO_2 ALD as much as 5 wt.% after the inorganic impurity content (1.5 wt.%) of unfilled PA was taken into account (*publication IV*). The conventional composites filled with P25 and T805 nano-TiO_2 filler, on the other hand, contained the intended filler content within the experimental error.
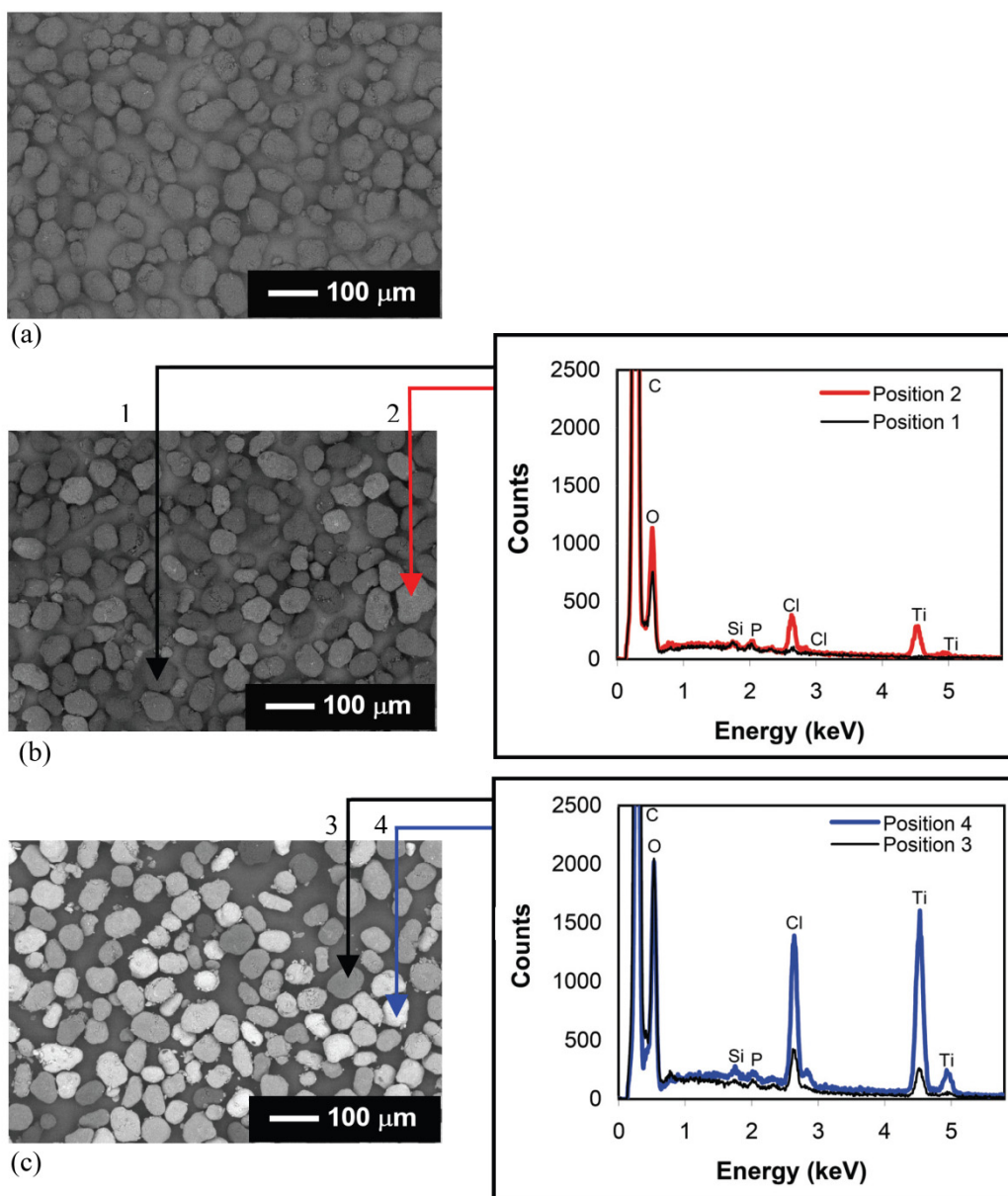
Fig. 17: SEM image and EDS spectra for (a) uncoated PA particles, (b) PA 10-nm TiO₂ ALD-coated particles, and (c) PA 40-nm TiO₂ ALD-coated particles from the first ALD-coating trial. The SEM specimens were coated with a thin carbon layer to avoid charging; therefore, carbon peaks were ignored in compositional analysis (*publication III*).

Apparently, in 40°C ALD-processing, the TiO₂ thin film grew at a faster rate than estimated. An increasing growth rate and the chlorine residue found may result, e.g., from undesired condensation or diffusion of unreacted precursors or by-products during the ALD process and lead to uncontrolled TiO₂ thin-film growth and thus complicate interpretation of the composite property test results. A higher Al₂O₃ film growth rate on a polymer particle substrate than on many other substrates has been explained by, e.g., the presence of hydrogen-bonded H₂O on the polymer surface. This H₂O can react with, e.g., TMA to deposit additional metal oxide on the powder (Spencer et al. 2007). Furthermore, polymer particles have more active sites on their surface exposed to gas phase reactants than the conventional plate- or film-shaped substrates (Liang et al. 2007). Other authors have also observed that ALD films are not always free of impurities, but that their impurity content is typically lower than that detected in our work. For example, Sammelselg et al. (1998) reported a chlorine residue of 0.3 wt.% for TiO₂ films grown

at 150 ºC from $TiCl_4$ and H_2O on inorganic substrates. Such an impurity content has been shown to decrease with increasing deposition temperature (Aarik et al. 1997, Sammelselg et al. 1998). Significantly elevated ALD-coating temperatures might, however, cause different challenges such as polymer melting and polymer degradation in ALD-coating process.

6.2.2 Melt-flow properties

The melt flow properties of the ALD-tailored and direct melt-compounded nano-TiO_2 composites were first examined during extrusion by monitoring the torsional resistance of the microcompounder screw. The data revealed significant differences in the processing behavior of the studied materials. The results (Fig. 18a) suggest that the screw torsional resistance, and hence melt viscosity, of PA ALD composites is considerably lower than that of a conventional nano-TiO_2- filled and unfilled PA matrix.
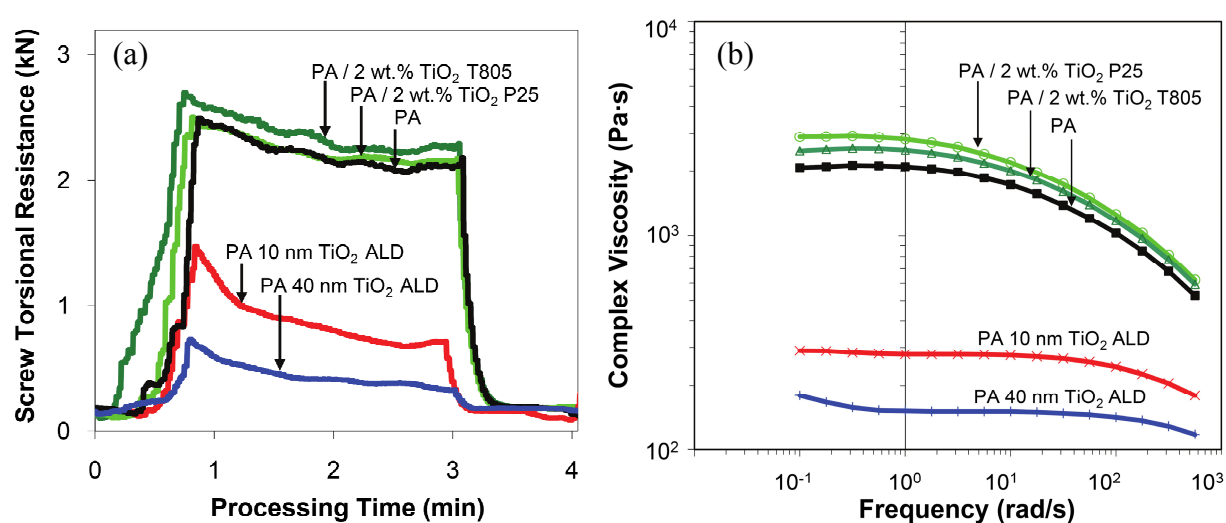

Fig. 18: Melt-flow behavior of selected PA samples (a) torsional resistance of the screw during melt-processing in a microcompounder, where the melt temperature was 220°C and compound dwell time in the screw was 2 min and (b) complex viscosity during a frequency sweep in a rotational rheometer with parallel-plate geometry at 200°C (modified from *publication III*). The data is based on samples prepared from the first ALD-coating trial.

These results were confirmed when rheological measurements (see Fig. 18b for complex viscosity during dynamic shear rheological tests) were carried out on the melt-compounded materials with a rotational rheometer. The complex viscosities of the ALD-tailored materials were much lower than those of the conventionally filled compounds or unfilled PA. Generally, when reinforced composites are formed, viscosity at low shear rates increases with filler concentration, whereas at high shear rates, shear thinning is often observed (Cho & Paul 2001, Rothon 2003, Pavlidou & Papaspyrides 2008). Because of the empirical Cox-Merz rule, the complex viscosity is equal to the steady shear viscosity over a range of frequencies and shear rates, also in this work, the conventional nano-TiO_2-filled composites showed higher complex viscosity values especially at low shear rates and stronger shear thinning at high shear rates than the unfilled PA (Fig. 18b). Apparently, individual nano-TiO_2 fillers and/or their clusters in a PA matrix tend to orient under a strong shear force, thus preventing the formation of polymer chain entanglements, which results in strong shear thinning behavior in nanofilled composites. Previous studies have also shown a significantly lower viscosity for, e.g., nanoclay-filled PA than for unfilled PA. Such low viscosity in the molten state has been related to three factors: (i)

slippage of polymer chains over nanoclay platelets during shear flow, (ii) partial entering of nanoclay surface-modifiers into the matrix, and/or (iii) molecular weight reduction due to the degradation of the matrix during melt-compounding (Cho & Paul 2001, McNally et al. 2003, Xu et al. 2008). Since no modifiers were used, the observed low viscosity for the ALD-tailored composites may have been due to slippage of the polymer chains over the filler particles or to a reduced molecular weight of the PA matrix. The latter was of particular concern because of considerable chlorine residues found in the ALD-created thin film coatings.

6.2.3 Thermal properties

Thermal properties such as the glass transition temperature (T_g) depend on molecular weight and the extend of the branching and crosslinking of the polymer matrix and on other factors such as polymer chemical structure and measurement conditions (Ehrenstein 2004). If it is assumed that apart from molecular weight these parameters are constant, then according to the equation proposed by Fox and Flory, T_g depends on the molecular weight of the polymer matrix so that a low molecular weight value result in a low T_g value (Kim et al. 2008). Consequently, comparison by DSC was seen as a fast way to approximate possible changes in the molecular weight of the specimens and further explain the unexpected rheological behavior of the composites. The results demonstrated that within experimental error the glass transition temperature, melting temperature, and the degree of crystallinity, of the host matrix did not change significantly due to addition of commercial TiO_2 or ALD-created TiO_2 even during three DSC heating cycles (*publication III*). The results by Zhang et al. (2006) on melt-compounded polyamide-66 filled with 1 vol.% of nano-TiO_2 filler (corresponding to about 3 wt.%) also showed no change in the degree of crystallinity or melting point of the host matrix. However, the glass transition temperature of the matrix was, in fact, increased by about 10°C which was suggested to be due to strong interactions between nanofillers and matrix (Zhang et al. 2006). Thus in *publications III-IV*, the degree of crystallinity and the degradation of the PA matrix were expected to have only a minor effect on changes in the rheological properties of PA ALD composites.

6.2.4 Filler dispersion

TEM observations of the direct melt-compounded nano-TiO_2-filled composites proved that TiO_2 disperses well in a PA matrix. The TiO_2 particles had a slight tendency to cluster, but the agglomerates remained typically below 100 nm for both surface modified T805 and unmodified P25 TiO_2 fillers (*publications III-IV*). Thus only the TEM image of the T805-filled composite is presented here in Fig. 19a. The morphology of the ALD-tailored composites clearly differed from that of conventional nano-TiO_2-filled composites (Fig. 19b-c). The ALD-created TiO_2 appeared as ribbons, their thickness and length varying between 10-50 and 100-1500 nm, respectively, depending on, e.g., the ALD-coating thickness and TiO_2 shell breaking mechanisms during melt-compounding. The PA 40-nm ALD specimen's TiO_2 ribbons, which were as long as 5 μm, were observed by SEM of broken tensile bar samples (*publication IV*).
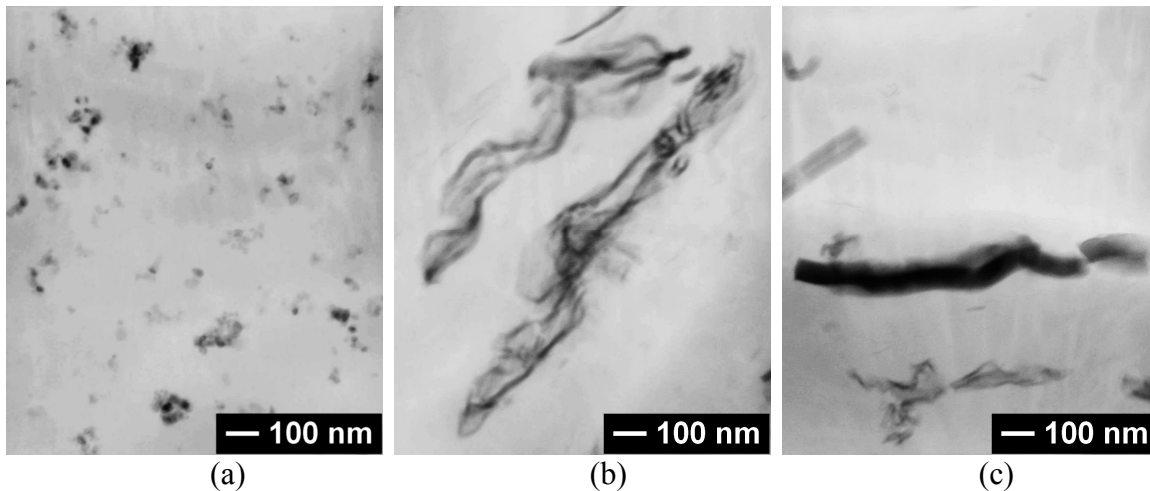
Fig. 19: TEM images of (a) PA/2 wt.% TiO$_2$ T805, (c) PA 10 nm TiO$_2$ ALD-tailored, and (d) PA 40 nm TiO$_2$ ALD-tailored composite samples from the first ALD-coating trial (*publication III).*

6.2.5 Mechanical properties

The tensile test results showed that ALD-tailored composites had a significantly higher Young's modulus than the unfilled and the conventionally nano-TiO$_2$-filled polyamide matrix even if high standard deviation values were observed. For the ALD-tailored composites, the increase was as high as 70–100%, whereas for the P25- and T805-filled PA composites, the improvement was not significant and varied greatly as a function of filler content. The tensile strength (in this case also yield strength) for the studied composites increased slightly (2-10%), except for the PA 40-nm TiO$_2$ ALD sample. The transition from ductile to brittle behavior occurred especially in the ALD-tailored composites. Notched impact strength experiments supported this, suggesting that the impact strength of the ALD-tailored composites decreased significantly compared to the unfilled PA matrix, whereas conventionally melt-compounded composites showed no significant change. A very different fracture mechanism was indicated for the ALD-tailored materials, when their tensile bar fracture surfaces were observed. Ductile deformation occurred with unfilled PA, resulting in tensile bar thinning and a neat fracture surface, but with ALD composites, a large void was created in the tensile bar either during the fracture or more likely already during injection-molding (*publication IV*).

In conclusion of our preliminary studies, intensive research is required to minimize the chlorine residues from ALD-coating chemicals and to study the effects of chlorine on a polymer matrix. Also the reasons for very different tensile test results and the fracture mechanism of ALD-tailored composite materials compared to conventional composites should be carefully examined. Nevertheless, the results so far are encouraging since melt-compounded, ALD TiO$_2$ thin-film-coated PA powder possesses unique properties over conventionally filled nano-TiO$_2$ composites, including easy melt-processability as implied by their significantly lower viscosity and good dispersion, accompanied with a unique TiO$_2$ ribbon structure unlike that in spherical clusters formed from commercial nano-TiO$_2$ particles. Furthermore, the increase in Young's modulus in ALD-tailored TiO$_2$ nanocomposite was significant when compared to, e.g., our studies on nanofilled PC and PP matrixes (*publications I-II*). Sarwar et al. (2007) also showed only a 30 % increase in Young's modulus upon addition of 5-wt.% spherical nano-TiO$_2$ to a PA processed via the sol-gel process. Hassinger & Burkhart (2012) suggested an even lower increase (ca. 10%) in Young's modulus due to incorporation of 2 vol.% (corresponding to about 7 wt.%) of spherical nano-TiO$_2$ via melt-compounding.

6.3 Effect of ALD-tailored melt-compounding on PA and PS matrixes

6.3.1 Thin-film-coated materials

The work presented here expands our preliminary studies on ALD-tailored melt-compounding and explores the use of different ALD-created metal oxide thin films. Nanometer-scale thin films of TiO_2, Al_2O_3, and ZnO:Al with an approximate nominal thickness varying between 5 nm to 40 nm were laid on both polyamide and polystyrene particles. PS powder was chosen as another intriguing matrix due to its easy availability to us in powder form and very different characteristics from those of a PA matrix. Even though no significant changes were found in the overall degree of crystallinity in ALD-tailored TiO_2 PA nanocomposites compared to unfilled PA (see section 6.2.3), the rate of crystallization, crystal size, and morphology in the composite matrix may have changed as observed previously in nanoclay-filled nanocomposites (Jordan et al. 2005, Pavlidoua & Papaspyrides 2008). Because of the amorphous characteristics of PS, the effect of ALD-created nanofillers on polymer morphology is minimized. Additionally, due to its brittleness, polystyrene is sensitive to defect sites induced by agglomerate or the interfacial debonding of nanofillers (Gao et al. 2009). Consequently, the effects of ALD-created nanofiller dispersion and interfacial interactions on the mechanical properties of this nonpolar composite matrix could be estimated and compared with a semicrystalline and polar PA matrix.

The target was to assess the success of ALD-particle coating and examine changes in the melt flow behavior, morphology, and mechanical properties of ALD-tailored nanocomposites (*publications V-VI* and some unpublished results). We also sought to understand the reasons behind the marked decrease in viscosity and the increase in stiffness and brittleness observed in our previous work *(publications III-IV)* on ALD-tailored PA TiO_2 nanocomposites.

The success of ALD coating was evaluated in terms of nanofiller content and ALD thin-film growth. The ALD-created inorganic nanofiller content was estimated by both computing and measuring the inorganic filler content. The amount of inorganic filler in the prepared polymer composites was determined from theoretically calculated values of ideally thin-film-coated spherical PA (Ø 60 μm) and PS particles (Ø 80 μm). Measured densities of 1.015 g/cm^3 and 1.048 g/cm^3 for injection-molded PA and PS, respectively, were used (*publication V*), whereas assumed densities of 3.5 g/cm^3, 3.99 g/cm^3, and 5.6 g/cm^3 were used for ALD-created TiO_2, Al_2O_3, and ZnO, respectively (Jensen et al. 2002, Wypych 2010). True density values of ALD-created oxide layers depend, among other things, on deposition temperature. Generally, the density is low at low deposition temperatures (Gorner et al. 2003, Choi et al. 2012). Furthermore, since with ZnO:Al, also the wt.% ratio of the composition ingredients have an effect, for rough comparison only the density value for ZnO was used. Fig. 20 shows ALD-created nanofiller content ranges from 0.03 wt.% to 1.2 wt.%, depending on the created ALD-thin film, target ALD-film thickness, and substrate. These values are typically lower than the computed wt.% contents for the studied ALD-thin films. In the PS matrix (Fig. 20b, Table 6), the inorganic filler content increased linearly as a function of the desired ALD coating thickness. Especially the TiO_2 ALD-film results agree surprisingly well with the theoretically calculated trend of ideally thin-film-coated spherical PS particles, whereas the Al_2O_3 and ZnO:Al filler contents show significantly lower values.
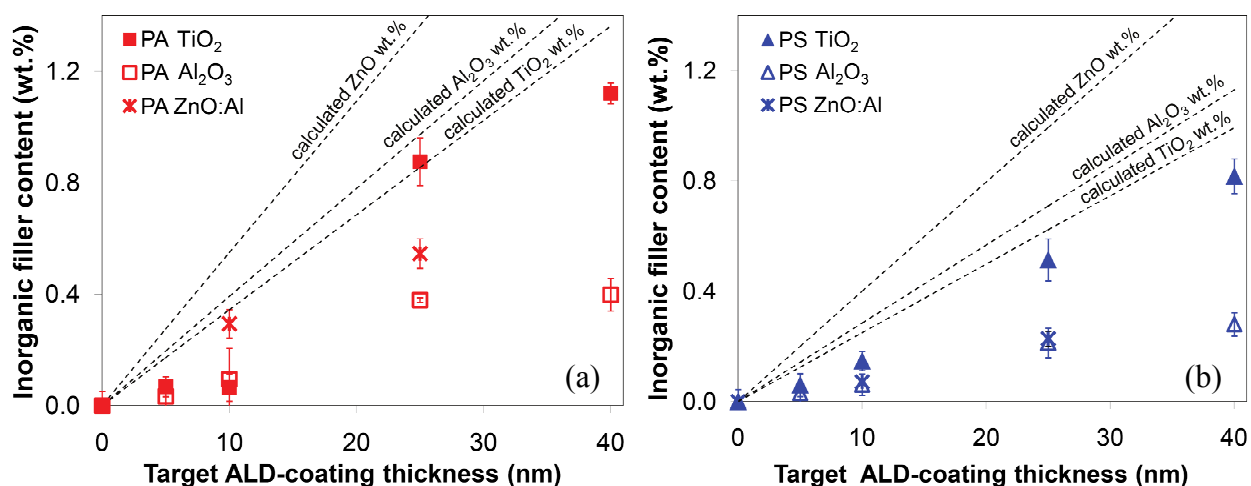
Fig. 20: Measured inorganic nanofiller content with a theoretically calculated trend of an ideally thin-film coated spherical particle as a function of a target ALD-coating thickness of TiO_2, Al_2O_3 and ZnO:Al- (or ZnO-) coated (a) PA particles and (b) PS particles (modified from *publication V* with some unpublished results and data from *publication VI*). Vertical bars show standard deviation values. The data is based on samples prepared from the second ALD-coating trial.

Because the PA particles were small, we expected the nanofiller contents of the ALD-coated PA to be higher than that of the ALD-coated PS. However, according to the results (Fig. 20a, Table 6), the ALD thin-film growth on PA particles did not provide a linear increase in filler content, and yielded a lower filler content than expected. In our preliminary studies (section 6.2), the TiO_2 content of the sample PA 40-nm ALD was as high as 5.3 wt.%, whereas now similar process settings yielded only 1.1 wt.% of TiO_2. The observed filler contents for Al_2O_3 and ZnO:Al on PA powder were even lower than the TiO_2 content. The filler content results show how challenging it is to control ALD-coating thickness on polymer particles. The growth rate of an ALD-thin film varied considerably due to, e.g., process parameters, used precursors, competing film growth processes (e.g., precursor condensation), and slow reaction rates at low temperatures. Furthermore, some batch-to-batch variation is possible due to the varying thickness of the powder layer applied in the ALD chamber (Fig. 9) or other changes in ALD-deposition process.

To confirm the results on filler content and to further characterize the morphology of the created thin films, a cross-sectional TEM image of selected ALD-coated powder particles was taken (Figs. 21-22). Unexpected detachment and damage in the epoxy-cast PA particles and uneven thin film ruled out evaluation of the ALD coating thickness. Although a TiO_2 ALD coating layer could not be detected on a collapsed PA particle, compositional analysis showed a discontinuous TiO_2 thin film at the interface of the epoxy matrix after PA particle detachment (Fig. 22a-d). Several attempts were also made to characterize the Al_2O_3 and ZnO:Al thin films on PA powder, but without success. With Al_2O_3, some traces of thin film were found on both epoxy and the collapsed PA particle, as suggested by the EDS. ZnO:Al thin films were difficult to detect, and only small traces of them could be found on PA particles.
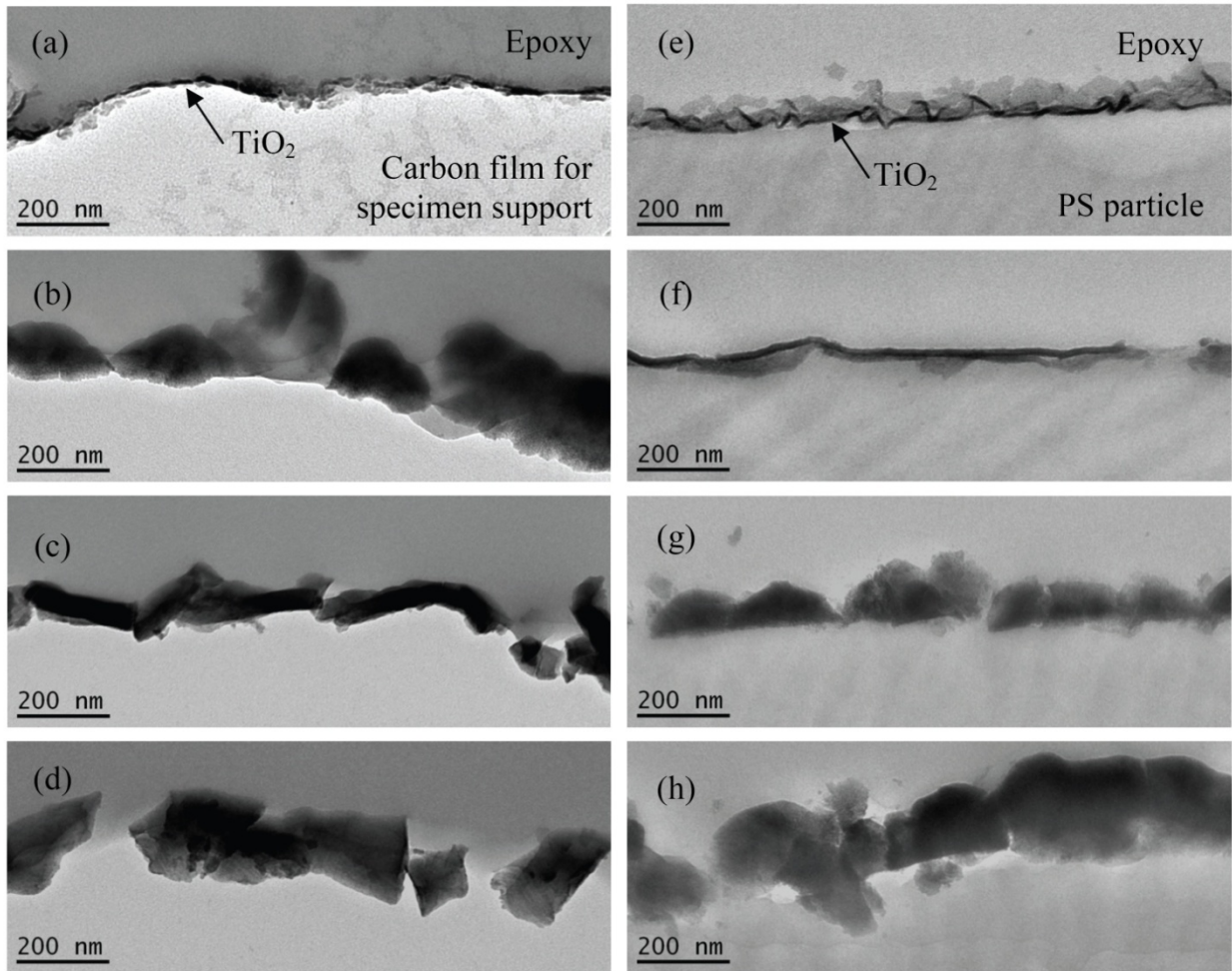
Fig. 21: Typical cross-sectional TEM image of (a) 5-nm, (b) 10-nm, (c) 25-nm, and (d) 40-nm ALD-created TiO_2 film on an epoxy matrix detached from a PA particle and of (e) 5-nm, (f) 10-nm, (g) 25-nm, and (h) 40-nm ALD-created TiO_2 film on a PS particle. Large uncoated areas were also found (*publication V*). The images are based on samples prepared from a second ALD-coating trial.

The cross-sectional TEM images of the TiO_2, Al_2O_3, and ZnO:Al ALD-coated PS particles (Figs. 21e-f and 22) indicate that all particles were firmly attached to the epoxy and that film thickness increased in a controlled manner, as ash content test results suggested. Even if the ALD-coating was uneven and somewhat damaged, the TiO_2 film, e.g., thickened from 5 to over 100 nm, as a function of the target coating thickness. In general, the thin film was more uniform on PS particles than on PA particles, yet uncoated areas could be detected.
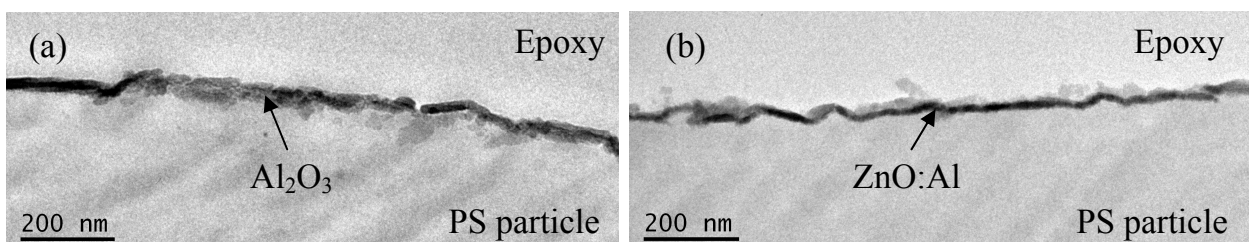
Fig. 22: Typical cross-sectional TEM image of 25-nm ALD-created (a) Al_2O_3 film and (b) ZnO:Al film on a PS particle. In the latter, Al could not be detected in compositional analysis. Some uncoated areas were also found (unpublished results). The images are based on samples prepared from the second ALD-coating trial.

38

6.3.2 Melt-flow properties

The MFR was measured to approximate the rheological properties of the polymer powders before melt-compounding. The PA powder showed (Fig. 23a) an MFR of 3 g/10 min for unfilled polymer but 200-400% higher values for ALD-tailored TiO_2 nanocomposites, as expected based on our previous studies (section 6.2.2). To study if the decrease in viscosity depended on the polymer matrix, we measured the MFR of the ALD-tailored TiO_2 PS composites. They showed a moderate increase in MFR, yielding only 10-40% higher values than unfilled PS. To confirm these results, we used a spiral mold tool to compare the final flow lengths of the melt-compounded nanocomposites. Spiral flow results (Fig. 23b) show that the ALD-tailored TiO_2 PA nanocomposites had a significantly longer spiral length than unfilled PA. This change was observed already at low ALD-created filler contents, as suggested by the MFR values. No such decrease in viscosity was observed in the other studied ALD-tailored PA or PS nanocomposites. Because temperature and shear rates remained virtually constant in the MFR test, the decrease in the viscosity of the PA TiO_2 nanocomposites may be traced to two factors: (1) wall slippage and PA polymer chain slippage over poorly bonded ALD-created TiO_2 fillers, and/or (2) reduced molecular weight following the degradation and chain scission of the polymer matrix during melt-compounding, as, e.g., McNally et al. (2003) and Xu et al. (2008) implied for nanoclay-filled composites.
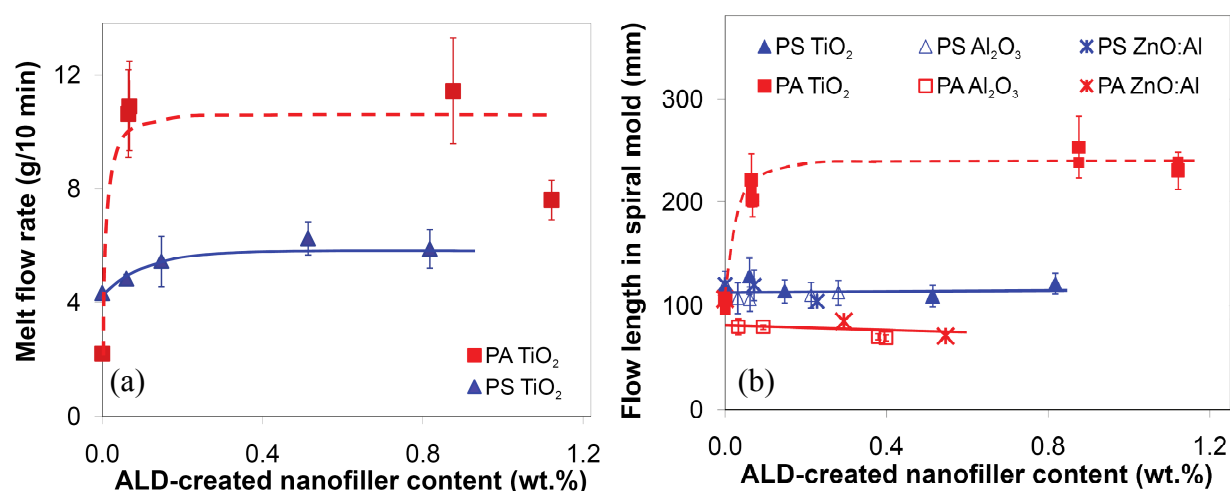
Fig. 23: (a) Melt-mass flow rates for uncoated and ALD-coated polymer particles measured at 191°C and (b) flow length of a spiral mold for melt-compounded unfilled matrixes and ALD-tailored nanocomposites as a function of ALD-created nanofiller content at a melt temperature of 220°C and a mold temperature of 80°C for PA, whereas for PS the corresponding temperatures were 190°C and 30°C, respectively (modified from *publications V-VI* with some unpublished results). Vertical bars show standard deviation values. The data is based on samples prepared from the second ALD-coating trial.

6.3.3 Viscosity and wall slip

In a wall slip, the melt flows by slipping along the walls of the molding system without sticking. Wall slip occurs generally because a lubricated layer forms along the wall. The most common is the apparent wall slip owing to, e.g., particle migration (generally away from this region or because of a high concentration of low molecular weight species near the wall) and the alignment of polymer molecules (Rides et al. 2008). The wall slip of entangled molten polymers is a surface-to-volume-dependent phenomenon. Therefore, steady shear experiments were run

with two different gap sizes. During a wall slip, a small gap (where material plate contact dominates over material property) should yield low viscosity values.

The shear viscosity results (Fig. 24) on ALD-tailored TiO_2 nanocomposites and reference matrixes show that a decrease in viscosity was evident only in PA composites, whereas that of PS remained unchanged after ALD-nanocomposite formation, as suggested by the spiral melt flow results (Fig. 23b). Furthermore, within experimental uncertainty, variation in gap size has no significant effect on viscosity. The results thus imply that the ALD-created decrease in viscosity is a material-dependent property and not only a near-wall phenomenon.
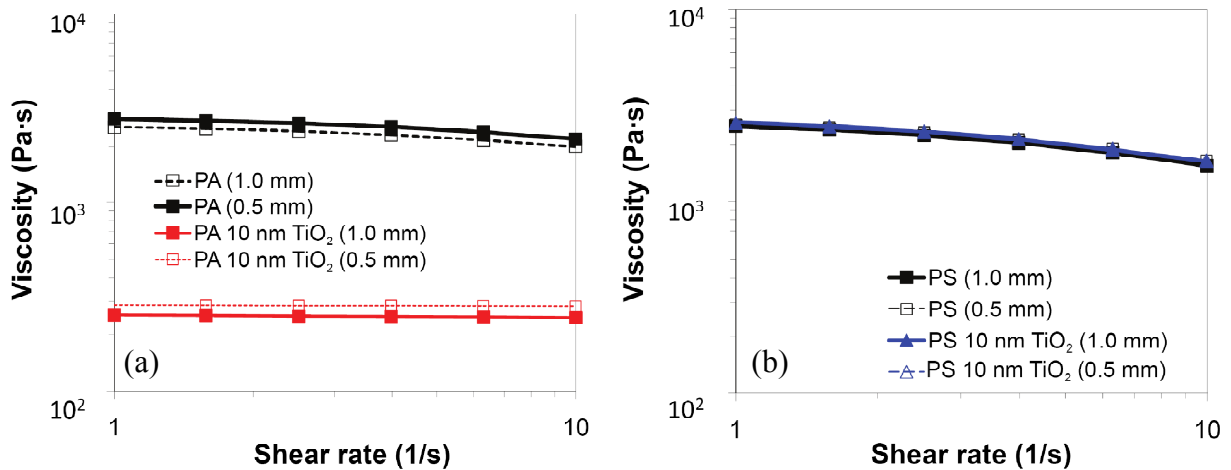
Fig. 24: Viscosity as a function of shear rate for (a) unfilled PA and PA 10-nm TiO_2 ALD-tailored nanocomposite measured at 200°C and for (b) unfilled PS and PS 10-nm TiO_2 ALD-tailored nanocomposite measured at 190°C. The value in parentheses is the gap distance (modified from *publication V*). The data is based on samples prepared from the second ALD-coating trial.

6.3.4 Molecular weight distribution

The rheological properties of entangled polymer melts depend strongly on the polymer molecular weight (Kemblowski & Torzecki 1983). To study the molecular weight, GPC measurements were run for PA and PS TiO_2 composites. Results (Table 5) show that the average molecular weights (M_n and M_w) and the molecular weight distribution (MWD) of PS were not affected by the presence of ALD-created TiO_2 nanofillers. However, contrary to our previous conclusions drawn from thermal studies (*publication III*), the molecular weight of the PA ALD nanocomposites decreased by 50%. In addition to decreased molecular weight, PA 10-nm TiO_2 ALD specimen also had a slightly boarder MWD than unfilled PA.

Table 5: GPC results for unfilled PA and PS matrixes and for their ALD-tailored TiO_2 nanocomposite samples prepared from the second ALD-coating trial (*publication V*).

Material	M_w[a]	M_n[a]	MWD
	(10^3 g/mol)	(10^3 g/mol)	M_w/M_n
PA	34	9.4	3.6
PA 10 nm TiO_2	17	4.4	3.9
PS	129	37	3.5
PS 10 nm TiO_2	131	38	3.4

[a] Standard deviation values were ±1 and ±2 for PA and PS, respectively.

Even if the molecular weight distribution of Al_2O_3 and ZnO:Al nanocomposites was not determined, it was expected that their thin film precursors and possible by-products did not significantly degrade the studied polymer matrixes, as suggested by their melt-flow results (Fig. 23). If such high PA matrix degradation occurred, why did the DSC results (section 5.2.3) on PA TiO_2 nanocomposites prepared from our first ALD-coating trial not reveal this? Examined closely, Fox and Flory's equation and experimental DSC results on, e.g., PS matrixes of different molecular weights (Fig. 25) reveal that T_g began to drop only at low molecular weight values (Santangelo & Roland 1998). For the PS matrix, T_g remained constant when M_n ranged from 10^2 to 10^4 kg/mol. Apparently, the molecular weight of the ALD-tailored PA TiO_2 nanocomposite was not low enough to alter the composite's T_g value compared to undegraded PA.
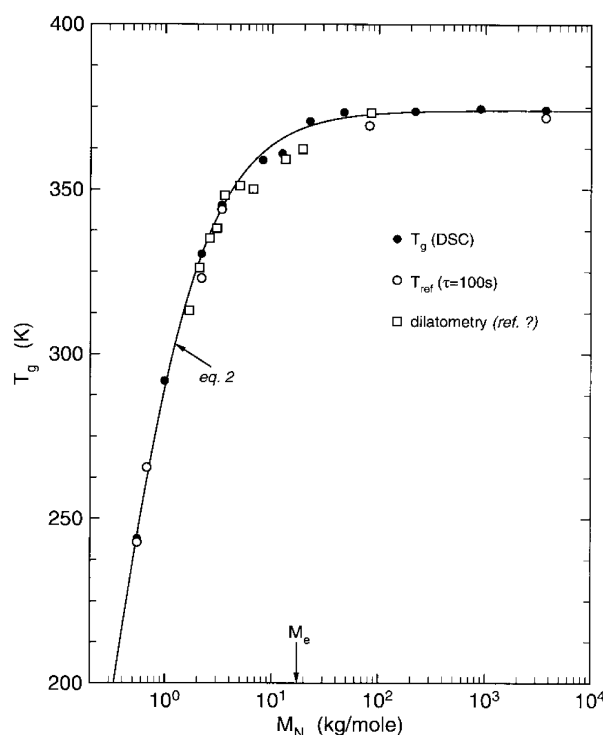
Fig. 25: Glass transition temperatures (T_g) for polystyrene of different molecular weights measured using DSC (●) as a function of number average molecular weight (M_n). Fox and Flory's T_g data for PS are shown for comparison (□). Further information is available from the original source. Reprinted from Santangelo & Roland (1998), Copyright (1998), with permission from the American Chemical Society.

Because the molecular weight of the ALD-tailored PA TiO_2 nanocomposites decreased uncontrollably and depended on the material combination, the phenomenon was considered an undesired property change. Concern was first felt over the polymers' molecular weight degradation after the compositional data of the ALD film on PA (*publication III,* section 6.2.1) had been tested with a SEM-EDS. Results suggested that the thin film contained a considerable amount of chlorine (0-14 wt.%). It was also confirmed in this work by SEM-EDS that the ALD-coating of PA and PS particles contained not only titanium but also chlorine. Their contents were high already at low ALD-coating thicknesses, though the build-up leveled off as the coating thickness increased. Typically, the chlorine content was higher on ALD-coated PA particles (0-12 wt.%) than on PS particles (0-4 wt.%).

Thin-film impurity content is thus seen a critical factor in PA matrix degradation. Clearly, if purging is not effective enough during ALD-coating, some precursor remnants and by-products

of chemical reactions remain in the coated material. The amount of impurities in the resulting ALD-film is often high at low processing temperatures (Aarik et al. 1997, Sammelselg et al. 1998). The precursors we used in ALD-coating, $TiCl_4$ and H_2O, produce hydrochloric acid (HCl) as a by-product in TiO_2 thin-film formation. Generally, PA 12 is not resistant or has limited resistance to Cl and HCl, whereas polystyrene may better withstand these chemicals (Plastics Design Library Staff 2001). This difference in their chemical resistance and chlorine content on powder particles may explain the varying molecular weight degradation behavior of the host polymers. Furthermore, the combination of moisture and photoactive TiO_2 may lead to uncontrollable polymer degradation. Consequently, long-term stability of all prepared ALD-tailored nanocomposites is a concern, but as the spiral-melt flow results repeated for TiO_2 PA and PS powders stored for 17-19 months after ALD-coating (see Fig. 4b in *publication V*) suggest, the studied materials did not significantly degrade in prolonged testing.

6.3.5 Filler dispersion

TEM observations of the composites show that ALD-created nanofillers dispersed well in both studied polymer matrixes (Fig. 26). The ALD-created nanofiller appeared in ribbons or plates with their thickness, length and surface area depending on, e.g., polymer particle size, created thin film, coating thickness, and thin film shell breaking mechanisms during melt-compounding.
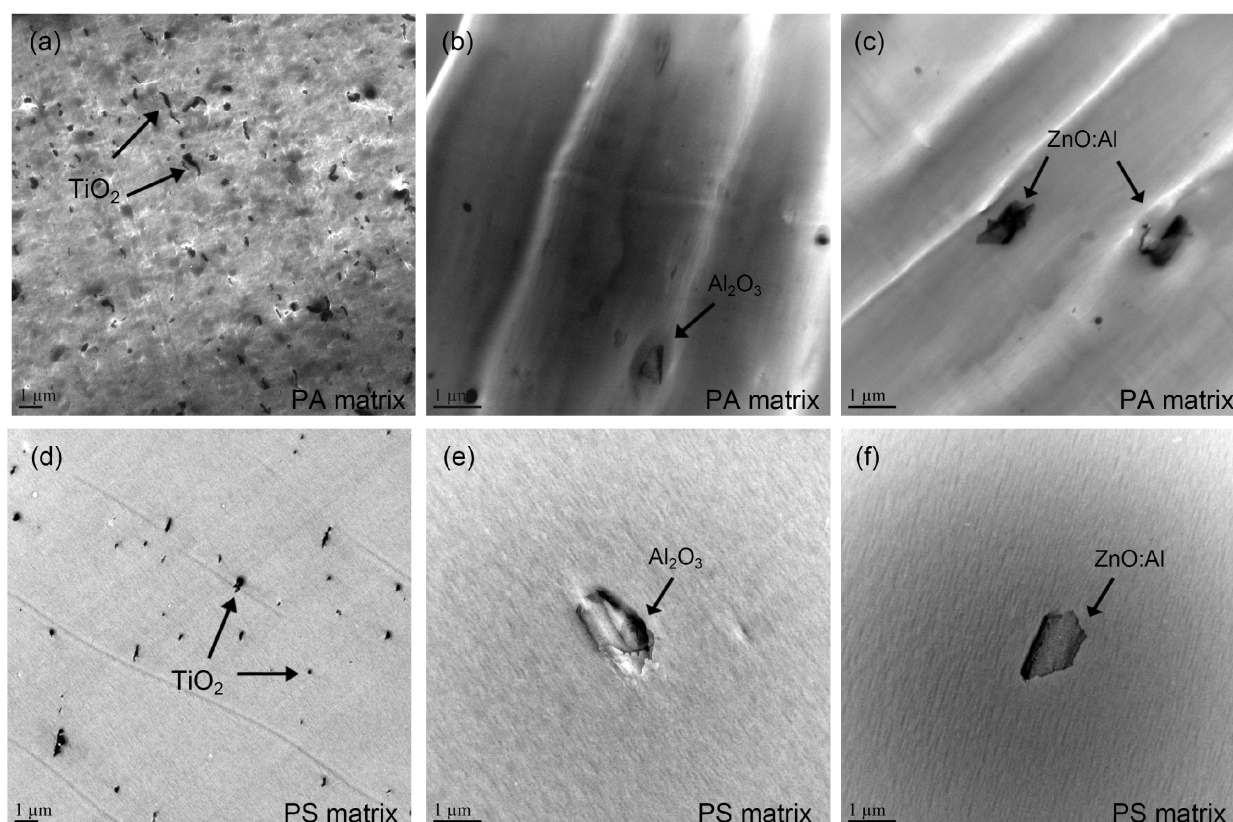
Fig. 26: TEM images of a) PA 25-nm TiO_2, (b) PA 25-nm Al_2O_3, (c) PA 25-nm ZnO:Al, (d) PA 25-nm TiO_2, (e) PS 25-nm Al_2O_3, and (f) PA 25-nm ZnO:Al ALD-tailored melt-compounded nanocomposites (modified from *publication VI*). The data is based on samples prepared from the second ALD-coating trial.

Typically, ALD-created ribbons were longer and/or larger in PS than in PA, but PS contained fewer individual nanofiller particles. This is partially explained by the smaller PA particle size.

Also the uniformity and ductility of thin film may have played a role. Typically, the largest plate-like nanofillers were found in Al_2O_3 nanocomposites, whereas the smallest ribbons were seen in TiO_2 composites. However, the structure and size distribution of the ALD-created nanofillers was significant within all studied samples, meaning that the smallest ALD-created nanoparticles are not visible in Fig. 26.

6.3.6 Mechanical properties

The effect of ALD-created nanofillers on ductile PA was evaluated especially in terms of TiO_2 filler, but also some studies were carried out on Al_2O_3 and ZnO:Al composites. The tensile test results for the ALD-tailored PA TiO_2 nanocomposites in Table 6 show that, apart from the PA 25 nm TiO_2 specimen, where the elongation at break decreased, both the yield strength and elongation at break increased 7-10% and 20-40%, respectively over unfilled PA, whereas the materials' Young's modulus did not change within the experimental error. The flexural studies on the TiO_2 nanocomposites agree well with their tensile test results, yielding a 3-16% increase in flexural strength (Table 6). The results on the TiO_2 nanocomposites suggest that the ALD-tailored nanocomposites maintained their ductility, though their molecular weight decreased significantly. Suh et al. (2007) observed a similar trend in the mechanical properties of consecutive melt-processed unfilled PA 6. Its elongation at break remained constant or increased until the 12th reprocessing cycle, when its molecular weight of PA 6 was decreased about 50%. Subsequent preprocessing cycles lowered both the elongation at break and molecular weight. In our work, the molecular weight degradation of PA presumably dominated over the effect of the TiO_2 nanofiller in mechanical properties, but their combined action modified PA from soft to harder material. In a preliminary study (*publication IV*), we also found that TiO_2 ALD-tailored nanocomposites may have a higher yield strength than unfilled PA. However, contrary to this work, a clear transition from ductile to brittle behavior was demonstrated in tensile strength experiments. This difference probably arose from different levels of molecular weight degradation and nanofiller content. In our second ALD-coating trial (*publications V-VI*), the PA 10-nm TiO_2 ALD specimen had 0.07 wt.% of TiO_2, whereas in our first ALD-coating trial (*publications III-IV*) it was as high as 1.1 wt.%. Furthermore, when the 10-nm ALD-coated material in our first ALD-coating trial was melt-compounded after ALD-coating, the average molecular weights M_w and M_n were $10 \cdot 10^3$ and $3.3 \cdot 10^3$ g/mol, respectively, thus even lower than in the second ALD-coating trial (Table 5). Suh et al. (2007) stated that when molecular weight degradation is high enough, the material turns brittle in a tensile test. Decrease in polymer chain length and broadening of the chain length distribution will eventually result in poor chain entanglements owing to decreased toughness. After chain scission, a crosslinking may also occur between the chains, often yielding high Young's modulus values (Suh et al. 2007).

For some unknown reason, tensile tests of Al_2O_3 and ZnO:Al ALD-tailored PA nanocomposites failed, and the mechanical test results on the reference PA matrix differed significantly from our previous studies. Due to a limited amount of material, the test could not be repeated, and no results are provided here. The flexural results on these nanocomposites (Table 6, Fig. 26c-d), however, were successful and suggest a minor increase (less than 3%) in flexural strength for the studied nanocomposites in comparison to unfilled matrixes.

Table 6: Measured filler contents and mechanical properties of unfilled polymer matrixes and ALD-tailored PS and PA nanocomposites (*publications V-VI* and some unpublished results). The data is based on samples prepared from the second ALD-coating trial.

Material	Inorganic weight content[a] (wt.%)	Nano-filler content (wt.%)	Young's Modulus (GPa)	Yield/Tensile strength[b] (MPa)	Elongation at break (%)	Flexural strength[c] (MPa)	Deflection at break (mm)
PA	1.47 ± 0.01	0	1.7 ± 0.1	45 ± 1	178 ± 3	51 ± 1	-
PA 5 nm TiO_2	1.53 ± 0.05	0.07	1.6 ± 0.1	49 ± 1	213 ± 93	53 ± 1	-
PA 10 nm TiO_2	1.53 ± 0.05	0.07	1.7 ± 0.1	49 ± 2	249 ± 11	52 ± 1	-
PA 25 nm TiO_2	2.34 ± 0.04	0.88	1.7 ± 0.1	48 ± 1	131 ± 61	54 ± 1	-
PA 40 nm TiO_2	2.34 ± 0.09	1.12	1.7 ± 0.1	49 ± 1	211 ± 34	59 ± 1	-
PA 5 nm Al_2O_3	1.52 ± 0.05	0.03	-	-	-	52 ± 1	-
PA 10 nm Al_2O_3	1.58 ± 0.11	0.09	-	-	-	51 ± 1	-
PA 25 nm Al_2O_3	1.87 ± 0.01	0.38	-	-	-	52 ± 1	-
PA 40 nm Al_2O_3	1.89 ± 0.06	0.40	-	-	-	54 ± 1	-
PA 10 nm ZnO:Al	1.78 ± 0.05	0.29	-	-	-	52 ± 1	-
PA 25 nm ZnO:Al	2.04 ± 0.05	0.55	-	-	-	52 ± 1	-
PS	0.07 ± 0.04	0	3.1 ± 0.1	39 ± 2	1.3 ± 0.1	106 ± 1	5 ± 1
PS 5 nm TiO_2	0.12 ± 0.04	0.06	3.1 ± 0.1	38 ± 2	1.3 ± 0.1	107 ± 1	5 ± 1
PS 10 nm TiO_2	0.21 ± 0.03	0.15	3.2 ± 0.1	39 ± 2	1.3 ± 0.1	107 ± 1	5 ± 1
PS 25 nm TiO_2	0.58 ± 0.08	0.51	3.0 ± 0.1	40 ± 1	1.4 ± 0.1	108 ± 1	5 ± 1
PS 40 nm TiO_2	0.88 ± 0.06	0.82	3.1 ± 0.2	40 ± 1	1.3 ± 0.1	108 ± 1	5 ± 1
PS 5 nm Al_2O_3	0.07 ± 0.04	0.03	3.1 ± 0.1	41 ± 1	1.3 ± 0.1	107 ± 2	7 ± 2
PS 10 nm Al_2O_3	0.10 ± 0.04	0.06	3.1 ± 0.1	41 ± 2	1.4 ± 0.1	107 ± 1	9 ± 3
PS 25 nm Al_2O_3	0.13 ± 0.05	0.21	3.1 ± 0.1	41 ± 1	1.4 ± 0.1	108 ± 1	7 ± 2
PS 40 nm Al_2O_3	0.28 ± 0.04	0.28	3.0 ± 0.1	39 ± 2	1.4 ± 0.1	108 ± 1	9 ± 2
PS 10 nm ZnO:Al	0.14 ± 0.01	0.07	2.9 ± 0.1	41 ± 1	1.4 ± 0.1	108 ± 1	9 ± 3
PS 25 nm ZnO:Al	0.30 ± 0.03	0.23	3.1 ± 0.1	40 ± 1	1.3 ± 0.2	107 ± 2	7 ± 2

[a] Determined by residual ash test.
[b] Yield strength for PA and tensile strength for PS.
[c] Flexural strength at yield on the tension side (see *publication V*).

The effect of ALD-created nanofillers on a hard and brittle polymer PS matrix was also evaluated. Despite the nanofiller's high aspect ratio, the tensile and flexural test results on PS nanocomposites suggest (Table 6) only minor changes in mechanical behavior compared to unfilled PS. Their tensile and flexural strength increased by less than 3% at the highest nanofiller content studied in this work, whereas Young's modulus and elongation at break remained virtually unchanged. Deflection at break increased about 3-8% due to the TiO_2 filler and about 20-70% due to Al_2O_3 or ZnO:Al fillers, though the results varied, as shown by the high standard deviation values.

The results imply that because of added ALD-created nanofiller, PS gained somewhat in strength and ductility, though the changes were generally small compared to, e.g., studies by Thomas et al. (2009), where a 5-wt.% TiO_2-filled (spherical particle, Ø 190 nm) isotactic PS composite yielded 5-20% increased Young's modulus, tensile strength, elongation at break, and flexural strength. Perhaps by using higher ALD-created filler contents (currently < 1.5 wt.%) along with a stronger thin film and adhesion between thin film and matrix, more significant changes can be obtained in the mechanical properties of ALD-tailored polymer nanocomposites.

7 Concluding remarks

This thesis work is part of a larger effort towards a fundamental understanding of polymer nanocomposites. The target was to explore the effect of different processing approaches including direct melt-compounding (*publication I*), masterbatch dilution (*publication II*), and ALD-tailored melt-compounding (*publications III-VI* and some unpublished data) on inorganic nanofiller dispersion within the polymer and to assess the performance of prepared composites. The principal conclusions of this thesis work are summarized as follows:

- Conventionally melt-compounded composites of low filler content ($\leq$ 5 wt.%) showed enhanced Young's modulus and heat release rate values compared to their unfilled counterpart, especially for PC/nanoclay composites and PP/PPgMA/MWCNT composites, respectively. The potential of nanofillers with a very large surface area to improve composite properties was not, however, fully realized. Both direct melt-compounding of PC composites and the two-step masterbatch dilution approach to PP composites yielded lower mechanical property enhancements than, e.g, obtained by other authors for nanoclay-filled polyamide prepared by in-situ polymerization. In addition to individual nanofillers, micron-sized filler clusters, stacks, or bundles were found in our composites depending on the incorporated filler. Furthermore, in the PC matrix, nanoclay surface treatment did not withstand the melt-compounding temperature and thus confined nanoclay morphology was also observed (*publications I-II*).

- Highly-dispersed and agglomerate-free PA TiO$_2$ nanocomposites were obtained by melt-compounding ALD-coated polymer particles in a microcompounder. Application of ALD-tailored melt-compounding enables formation of ribbon- or plate-like nanofillers with a high aspect ratio. Such filler morphology was considered useful, because filler particles with a high aspect ratio and surface area typically reinforce the polymer matrix more effectively than their spherical counterparts (*publications III-VI*).

- Incorporation of individually dispersed nanofillers with a high aspect ratio in a polymer matrix does not necessarily guarantee enhanced composite properties The effect of ALD-created metal oxide nanofillers including TiO$_2$, Al$_2$O$_3$ and ZnO:Al on the melt flow, tensile, and flexural properties of the PA and PS matrix was small if significant polymer degradation due to ALD-thin film coating could be avoided. This was mainly attributed to low filler content (< 1.5 wt.%) and possible insufficient interaction between filler and polymer (*publications V-VI* and some unpublished results).

A close look at the results reveals that the mechanical properties of composites prepared by direct- and masterbatch melt-compounding followed rather well the property trends already reported on similar material combinations. As was shown, PC's Young's modulus and yield strength increased with addition of small amounts of plate-like nanoclay, but the advantage was offset by decreased ductility. Suitable nanoclay surface modification is important for enhancing the mechanical properties. The masterbatch dilution approach with PP/PPgMA composites filled with spherical, plate-like, and tubular fillers, on the other hand, suggested no or only minor enhancements in Young's modulus and yield strength accompanied also with decreased elongation break compared to the PPgMA-modified PP matrix. The overall filler dispersion appeared to be somewhat better in PC than in PP/PPgMA, when the separation level of nanoclay silicate layers was compared. Limited shear force exerted by the melt-compounding unit and insufficient interaction between filler and matrix are some of the main reasons for agglomerates

found in the samples. The differences in the polymer matrix properties such as crystallinity and polarity parameters partially explain the differences in nanoclay dispersion results between the PC and PP composite. Even if poor filler dispersion typically entails poor fire performance, the flammability of PP composites decreased compared to their unfilled matrix counterpart. The highest PHRR reduction was obtained in the MWCNT-filled composite, whereas reduction was more moderate in nanoclay-, nano-TiO_2, nano-$CaCO_3$, and micro-$CaCO_3$-filled composites. The good performance of this tubular filler over spherical and plate-like fillers was attributed mainly to the higher volume content of MWCNTs, but also other factors such as the composite's lower oxygen permeability and higher thermal stability over the other PP composites contributed to the cone calorimeter results. The results as a whole showed that for any property improvements in the host matrix, it is important to choose the right filler type. Although filler agglomerates were found, it seems that if sufficient polymer-filler interaction as well as adequate nanofiller dispersion are achieved on a sufficiently small scale, enhanced nanocomposite properties can be obtained at low filler contents. However, due to partially agglomerated composites and several other factors affecting, e.g., the mechanical properties of composites, it was difficult to compare the different compositions, surface modifications and melt-compounding approaches.

ALD is a relatively new method for producing nanofiller coatings on polymer substrates, and only a few published studies exist in the field ALD-tailored polymer nanocomposites and none on their mechanical properties. This work showed that the ALD-tailored nanocomposite formation approach is sensitive to ALD process precursor remnants, by-products, and/or successive thermal treatments. The results suggest that if the matrix has poor chemical resistance, and if a significant amount of ALD-processing chemicals remain on ALD-coated powder particles, then the molecular weight of the polymer matrix decreased abruptly. Though only minor changes were detected in the mechanical properties of composites that could avoid host matrix degradation, ALD-tailored melt-compounding is considered an attractive technology to fabricate agglomerate-free nanocomposites. The novelty of the ALD-tailored approach is its ability to produce fine nanofiller dispersion with a high aspect ratio, versatile material combinations, and hence new material properties. Impurities in ALD-coatings can be minimized by optimizing the ALD process, and nanofiller content can be increased by, e.g., decreasing the polymer particle size. The strength of the thin film and the load transfer between ALD-nanofiller and surrounding matrix can be increased by selecting the correct type of thin film and processing conditions and by introducing ALD-created adhesive layers between ALD-created nanofiller and matrix. Another route is to perform additional surface coating step as with conventional fillers. Of interest would also be further studies on the effect on mechanical and electrical properties of oriented ALD-created nanofillers on the polymer matrix. Consequently, a further understanding and fine-tuning of the ALD process is required to realize the possibilities of this processing approach. Because of the current slow and expensive ALD-polymer powder coating technology, the ALD process is considered applicable only to high value products. Intensive work has been done on a scalable, cost-effective ALD reactor solution, but any results for wider than mere laboratory use lie still, to our knowledge, several years ahead.

On the whole, it remains a considerable challenge to develop an efficient process to uniformly disperse nanofillers that would adhere well to polymers throughout the matrix and to manufacture parts from such composites at a reasonable cost. Because the performance of a nanofilled composite appears to be specific to each material combination and affected by the final dispersion and mixing approaches, it is also difficult to predict the properties obtained. Thus, finding the optimal combination of polymer, filler material, and filler content requires intensive work and depends largely on the application.

References

Aarik, J., Aidla, A., Kiisler, A.-A., Uustare, T. & Sammelselg, V. 1997. Morphology and structure of TiO$_2$ thin films grown by atomic layer deposition. *Thin Solid Films* 148, pp. 268-275.

Ahn, S.H., Kim, S.H. & Kim, B.C. 2004. Mechanical properties of silica nanoparticle reinforced poly (ethylene 2, 6-naphthalate). *Macromolecular Research* 12, pp. 293-302.

Alexandre, M. & Dubois, P. 2000. Polymer-layered silicate nanocomposites: preparation, properties and uses of a new class of materials. *Materials Science and Engineering* 28, pp. 1-63.

Avella, M., Cosco, S., Lorenzo, M.L.D., Pace, E.D., Errico, M.E. & Gentile, G. 2006. iPP based nanocomposites filled with calcium carbonate nanoparticles: structure/properties relationships. *Macromolecular Symposia* 234, pp. 156-162.

Baniasadi, H., Ramazani, A.S.A. & Javan Nikkhah, S. 2010. Investigation of in situ prepared polypropylene/clay nanocomposites properties and comparing to melt blending method. *Materials & Design* 31, pp. 76-84.

Bikiaris, D., Vassiliou, A., Chrissafis, K., Paraskevopoulos, K.M., Jannakoudakis, A. & Docoslis, A. 2008. Effect of acid treated multi-walled carbon nanotubes on the mechanical, permeability, thermal properties and thermo-oxidative stability of isotactic polypropylene. *Polymer Degradation and Stability* 93, pp. 952-967.

Bosund, M. 2007. Passivation of GaAs surface using atomic layer deposition, Master of Science Thesis, Helsinki University of Technology. 71 p. (In Finnish)

Carrión, F.J., Arribas, A., Bermúdez, M.-D. & Guillamon, A. 2008. Physical and tribological properties of a new polycarbonate-organoclay nanocomposite. *European Polymer Journal* 44, pp. 968-977.

Carvalho, J.W.C., Sarantópoulos, C. & Innocentini-Mei, L.H. 2010. Nanocomposites-based polyolefins as alternative to improve barrier properties. *Journal of Applied Polymer Science* 118, pp. 3695-3700.

Chan, C.-M., Wu, J., Li, J.-X. & Cheung, Y.-K. 2002. Polypropylene/calcium carbonate nanocomposites. *Polymer* 43, pp. 2981-2992.

Chavarria, F., Shah, R.K., Hunter, D.L. & Paul, D.R. 2007. Effect of melt processing conditions on the morphology and properties of nylon 6 nanocomposites. *Polymer Engineering and Science* 47, pp. 1847-1864.

Cho, J.W. & Paul, D.R. 2001. Nylon 6 nanocomposites by melt compounding. *Polymer* 42, pp. 1083-1094.

Choi, D.-W., Kim, S.-J., Lee, J.H., Chung, K.-B. & Park, J.-S. 2012. A study of thin film encapsulation on polymer substrate using low temperature hybrid ZnO/Al$_2$O$_3$ layers atomic layer deposition. *Current Applied Physics* 12, pp. S19-S23.

Cipiriano, B.H., Kashiwagi, T., Raghavan, S.R., Yang, Y., Grulke, E.A., Yamamoto, K., Shields, J.R. & Douglas, J.F. 2007. Effects of aspect ratio of MWNT on the flammability properties of polymer nanocomposites. *Polymer* 48, pp. 6086-6096.

Dennis, H.R., Hunter, D.L., Chang, D., Kim, S., White, J.L., Cho, J.W. & Paul, D.R. 2001. Effect of melt processing conditions on the extent of exfoliation in organoclay-based nanocomposites. *Polymer* 42, pp. 9513-9522.

Dhibar, S., Kar, P. & Khatua, B.B. 2012. Preparation of highly exfoliated and transparent polycarbonate/clay nanocomposites by melt blending of polycarbonate and poly(methyl methacrylate)/clay nanocomposites. *Journal of Applied Polymer Science* 125, pp. E601-E609.

Dumont, M.-J., Reyna-Valencia, A., Emond, J.-P. & Bousmina, M. 2007. Barrier properties of polypropylene/organoclay nanocomposites. *Journal of Applied Polymer Science* 103, pp. 618-625.

Ehrenstein, G.W, Riedel, G. & Trawiel, P. (Eds.) 2004. Thermal analysis of plastics, theory and practice, Hanser Publishers, Munich.

Eteläaho, P., Nevalainen, K., Suihkonen, R., Vuorinen, J. & Järvelä, P. 2009a. Effects of two different maleic anhydride-modified adhesion promoters (PP-g-MA) on the structure and mechanical properties of nanofilled polyolefins. *Journal of Applied Polymer Science* 114, pp. 978-992.

Eteläaho, P., Nevalainen, K., Suihkonen, R., Vuorinen, J., Hanhi, K. & Järvelä, P. 2009b. Effects of direct melt compounding and masterbatch dilution on the structure and properties of nanoclay-filled polyolefins. *Polymer Engineering and Science* 49, pp. 1438-1446.

Feng, J., Hao, J., Du, J. & Yang, R. 2012. Effects of organoclay modifiers on the flammability, thermal and mechanical properties of polycarbonate nanocomposites filled with a phosphate and organoclays. *Polymer Degradation and Stability* 97, pp. 108-117.

Fina, A., Cuttica, F. & Camino, G. 2012. Ignition of polypropylene/montmorillonite nanocomposites. *Polymer Degradation and Stability* 97, pp. 2619-2626.

Fornes, T.D., Yoon, P.J., Keskkula, H. & Paul, D.R. 2002. Nylon 6 nanocomposites: the effect of matrix molecular weight. *Polymer* 43, pp. 2121-2122.

Furlan, L.G., Ferreira, C.I., Dal Castel, C., Santos, K.S., Mello, A.C.E., Liberman, S.A., Oviedo, M.A.S. & Mauler, R.S. 2011. Effect of processing conditions on the mechanical and thermal properties of high-impact polypropylene nanocomposites. *Materials Science and Engineering: A* 528, pp. 6715-6718.

Gahleitner, M., Jääskeläinen, P., Ratajski, E., Paulik, C., Reussner, J., Wolfschwenger, J. & Neißl, W. 2005. Propylene–ethylene random copolymers: Comonomer effects on crystallinity and application properties. *Journal of Applied Polymer Science* 95, pp. 1073-1081.

Gao, Y., Liu, L. & Zhang, Z. 2009. Mechanical performance of nano-$CaCO_3$ filled polystyrene composites. *Acta Mechanica Solida Sinica* 22, pp. 555-562.

Gelfer, M., Burger, C., Fadeev, A., Sics, I., Chu, B., Hsiao, B.S., Heintz, A., Kojo, K., Hsu, S-L., Si, M. & Rafailovich, M. 2004. Thermally induced phase transitions and morphological changes in organoclays. *Langmuir* 20, pp. 3746-3758.

Gianelli, W., Camino, G., Dintcheva, N.T., Verso, S.L. & Mantia, F.P.L. 2004. EVA-montmorillonite nanocomposites: Effect of processing conditions. *Macromolecular Materials and Engineering* 289, pp. 238-244.

Groner, M.D., Fabreguette, F.H., Elam, J.W. & George, S.M. 2004. Low-temperature Al_2O_3 atomic layer deposition. *Chemistry of Materials* 16, pp. 639-645.

Gupta, R.K., Kennel, E. & Kim, K-J. (eds.) 2010. Polymer nanocomposites handbook, CRC press, Boca Raton.

Hasegawa, N., Kawasumi, M., Kato, M., Usuki, A. & Okada, A. 1998. Preparation and mechanical properties of polypropylene–clay hybrids using a maleic anhydride-modified polypropylene oligomer. *Journal of Applied Polymer Science* 67, pp. 87-92.

Hassinger, I. & Burkhart, T. 2012. Multiple extrusion and dilution of nanocomposites and their effect on the mechanical properties. *Journal of Thermoplastic Composite Materials* 25, pp. 573-590.

Heller, C.M.A, Erlat, A.G. & Breitung, E.M. 2008. Systems and methods for roll-to-roll atomic layer deposition on continuously fed objects. *International Patent Application* PCT/US2007/066029, WO/2008/057625. 30 p.

Hinsken, H., Moss, S., Pauquet, J.-R. & Zweifel, H. 1991. Degradation of polyolefins during melt processing. *Polymer Degradation and Stability* 34, pp. 279-293.

Hopmann, C., Michaeli, W. & Puch, F. 2012. Experimental investigation on the influence of the composition on the morphology and the mechanical properties of short glass fiber-reinforced polypropylene nanocomposites. *Polymer Composites* 33, pp. 2228-2235.

Housmans, J.-W., Peters, G.W.M. & Meijer, H.E.H. 2009. Flow-Induced crystallization of propylene/ethylene random copolymers. *Journal of Thermal Analysis & Calorimetry* 98, pp. 693-705.

Hsieh, A.J., Moy, P., Beyer, F.L., Madison, P., Napadensky, E., Ren, J. & Krishnamoorti, R. 2004. Mechanical response and rheological properties of polycarbonate layered-silicate nanocomposites. *Polymer Engineering and Science* 44, pp. 825-837.

Hull, R.T., Witkowski, A. & Hollingbery, L. 2011. Fire retardant action of mineral fillers. *Polymer Degradation and Stability* 96, pp. 1462-1469.

Hussain, F., Hojjati, M., Okamoto, M. & Gorga, R.E. 2006. Review article: Polymer-matrix nanocomposites, processing, manufacturing, and application: An overview. *Journal of Composite Materials* 40, pp. 1511-1575.

Jancar, J. (ed.) 1999. Advances in polymer science. Mineral fillers in thermoplastics I. Raw materials and processing. Springer-Verlag Berlin Heidelberg, Germany.

Jensen, J.M., Oelkers, A.B., Toivola, R. & Johnson, D.C. 2002. X-ray reflectivity characterization of ZnO/Al_2O_3 multilayers prepared by atomic layer deposition. *Chemistry of Materials* 14, pp. 2276-2282.

Jordan, J., Jacob, K.I., Tannenbaum, R., Sharaf, M.A. & Jasiuk, I. 2005. Experimental trends in polymer nanocomposites—a review. *Materials Science and Engineering: A* 393, pp. 1-11.

Kashiwagi, T., Grulke, E., Hilding, J., Groth, K., Harris, R., Butler, K., Shields, J., Kharchenko, S. & Douglas, J. 2004. Thermal and flammability properties of polypropylene/carbon nanotube nanocomposites. *Polymer* 45, pp. 4227-4239.

Kemblowski, Z. & Torzecki, J. 1983. Determination of the weight-average molecular weight of polyamide-6 on the basis of melt viscosity. *Rheologica Acta* 22, pp. 186-196.

Kim, D., Lee, J.S., Barry, C.F. & Mead, J.L. 2008. Evaluation and prediction of the effects of melt-processing conditions on the degree of mixing in alumina/poly(ethylene terephthalate) nanocomposites. *Journal of Applied Polymer Science* 109, pp. 2924-2934.

Kim, S., Do, I. & Drzal, L.T. 2009. Multifunctional xGnP/LLDPE nanocomposites prepared by solution compounding using various screw rotating systems. *Macromolecular Materials and Engineering* 294, pp. 196-205.

Kim, Y.W., Park, J.T., Koh, J.H., Min, B.R. & Kim, J.H. 2008. Molecular thermodynamic model of the glass transition temperature: dependence on molecular weight. *Polymers for Advanced Technologies* 19, pp. 944-946.

King, D.M., Spencer, J.A., Liang, X., Hakim, L.F. & Weimer, A.W. 2007. Atomic layer deposition on particles using a fluidized bed reactor with in situ mass spectrometry. *Surface and Coatings Technology* 201, pp. 9163-9171.

Kojima, Y., Usuki, A., Kawasumi, M., Okada, A., Fukushima, Y., Kurauchi, T. & Kamigaito, O. 1993. Mechanical properties of nylon 6-clay hybrid. *Journal of Materials Research* 8, pp. 1185-1189.

Kääriäinen, T.O., Maydannik, P., Cameron, D.C., Lahtinen, K., Johansson, P. & Kuusipalo, J. 2011. Atomic layer deposition on polymer based flexible packaging materials: Growth characteristics and diffusion barrier properties. *Thin Solid Films* 519, pp. 3146-3154.

Laachachi, A., Leroy, E., Cochez, M., Ferriol, M. & Lopez Cuesta, J.M. 2005. Use of oxide nanoparticles and organoclays to improve thermal stability and fire retardancy of poly(methyl methacrylate). *Polymer Degradation and Stability* 89, pp. 344-352.

Laoutid, F., Bonnaud, L., Alexandre, M., Lopez-Cuesta, J.-M. & Dubois, Ph. 2009. New prospects in flame retardant polymer materials: From fundamentals to nanocomposites. *Materials Science and Engineering: R: Reports* 63, pp. 100-125.

Lee, K.M. & Han, C.D. 2003. Effect of hydrogen bonding on the rheology of polycarbonate/organoclay nanocomposites. *Polymer* 44, pp. 4573-4588.

Leskelä, M. & Ritala, M. 2002. Atomic layer deposition (ALD): from precursors to thin film structures. *Thin Solid Films* 1, pp. 138-146.

Liang, X., Hakim, L.F., Zhan, G-D., McCormick, J.A., George, S.M., Weimer, A.W., Spencer, J.A., Buechler, K.J., Blackson, J. & Wood, C.J. 2007. Novel processing to produce polymer/ceramic nanocomposites by atomic layer deposition. *Journal of the American Ceramic Society* 90, pp. 57-63.

Liang, X. 2008 Novel processing to produce polymer/ceramic nanocomposites by atomic layer deposition. Doctor of Science Thesis. University of Colorado, 240 p.

Liang, X., King, D.M., Groner, M.D., Blackson, J.H., Harris, J.D., George, S.M. & Weimer, A.W. 2008. Barrier properties of polymer/alumina nanocomposite membranes fabricated by atomic layer deposition. *Journal of Membrane Science* 322, pp. 105-112.

Marić, M. & Macosko, C.W. 2001. Improving polymer blend dispersion in mini-mixers. *Polymer Engineering and Science* 41, pp. 118-130.

McNally, T., Murphy, W.R., Lew, C.Y., Turner, R.J. & Brennan, G.P. 2003. Polyamide-12 layered silicate nanocomposites by melt blending. *Polymer* 44, pp. 2761-2722.

Mehrabzadeh, M. & Kamal, M.R. 2004. Melt processing of PA-66/clay, HDPE/clay and HDPE/PA-66/clay nanocomposites. *Polymer Engineering and Science* 44, pp. 1152-1161.

Miikkulainen, V., Leskelä, M., Ritala, M. & Puurunen, R.L. 2013. Crystallinity of inorganic films grown by atomic layer deposition: Overview and general trends. *Journal of Applied Physics* 113, 101 p.

Modesti, M., Lorenzetti, A., Bon, D. & Besco, S. 2005. Effect of processing conditions on morphology and mechanical properties of compatibilized polypropylene nanocomposites. *Polymer* 46, pp. 10237-10245.

Nevalainen, K., Hintze, C., Suihkonen, R., Eteläaho, P., Vuorinen, J., Järvelä, P. & Isomäki, N. 2008. Rheological properties of melt-compounded and diluted nanocomposites of atomic-layer-deposition-coated polyamide particles. *Annual Transactions the Nordic Rheology Society* 16, pp. 125-133.

NIOSH, National Institute for Occupational Safety and Health. 2009. Approaches to safe nanotechnology: managing the health and safety concerns associated with engineered nanomaterials, DHHS, Publication no. 2009-125, March 2009.

Osman, M.A., Atallah, A., Schweizer, T. & Öttinger, H.C. 2004. Particle–particle and particle-matrix interactions in calcite filled high-density polyethylene—steady shear. *Journal of rheology* 48, pp. 1167-1184.

Paul, D.R. & Robeson, L.M. 2008. Polymer nanotechnology: Nanocomposites. *Polymer* 49, pp. 3187-3204.

Pavlidou, S. & Papaspyrides, C.D. 2008. A review on polymer–layered silicate nanocomposites. *Progress in Polymer Science* 33, pp. 1119-1198.

Plastics Design Library Staff. 2001. Chemical resistance of plastics and elastomers (3rd Electronic edn.), William Andrew Publishing/Plastics Design Library.

Pluart, L.Le, Duchet, J., Sautereau, H. & Gérard, J.F. 2003. Tailored interfaces in nanocomposites. *Macromolecular Symposia* 194, pp. 155-160.

Pore, V. 2010. Atomic layer deposition and photocatalytic properties of titanium dioxide thin films, Doctor of Science Thesis, University of Helsinki, Yliopistopaino Helsinki, 89 p.

Prashantha, K., Soulestin, J., Lacrampe, M.F., Krawczak, P., Dupin, G. & Claes, M. 2009. Masterbatch-based multi-walled carbon nanotube filled polypropylene nanocomposites: Assessment of rheological and mechanical properties. *Composites Science and Technology* 69, pp. 1756-1763.

Puurunen, R.L. 2005. Surface chemistry of atomic layer deposition: A case study for the trimethylaluminum/water process. *Journal of Applied Physics* 97, pp. 121301-12130.

Rakhimkulov, A.D., Lomakin, S.M., Dubnikova, I.L., Shchegolikhin, A.N., Davidov, E.Y. & Kozlowski, R. 2010. The effect of multi-walled carbon nanotubes addition on the thermo-oxidative decomposition and flammability of PP/MWCNT nanocomposites. *Journal of Materials Science* 45, pp. 633-640.

Rault, F., Pleyber, E., Campagne, C., Rochery, M., Giraud, S., Bourbigot, S. & Devaux, E. 2009. Effect of manganese nanoparticles on the mechanical, thermal and fire properties of polypropylene multifilament yarn. *Polymer Degradation and Stability* 94, pp. 955-964.

Ray, S.S. & Okamoto, M. 2003. Polymer/layered silicate nanocomposites: a review from preparation to processing. *Progress in Polymer Science* 28, pp. 1539-1641.

Rides, M., Allen, C., Fleming, D., Haworth, B. & Kelly, A. 2008. Intercomparison of slip flow velocity measurements of filled polymers by capillary extrusion rheometry. *Polymer Testing* 27, pp. 308-320.

Ritala, M. & Leskelä, M. 2002. Atomic layer deposition, in Handbook of thin film materials, (Ed. Nalwa, H.S.), Vol. 1, Academic Press, San Diego, CA, pp. 103-159.

Rothon, R.N. 2003. Particulate-filled polymer composites (2nd Edition). Smithers Rapra Technology.

Rumiana, K (ed.). 2007. Thermoset nanocomposites for engineering applications. Smithers Rapra Technology. Shropshire, UK. 344 p.

Sammelselg, V., Rosental, A., Tarre, A., Niinistö, L., Heiskanen, K., Ilmonen, K., Johansson, L.-S. & Uustare, T. 1998. TiO$_2$ thin films by atomic layer deposition: a case of uneven growth at low temperature. *Applied Surface Science* 134, pp. 78-86.

Santangelo, P.G. & Roland, C.M. 1998. Molecular weight dependence of fragility in polystyrene. *Macromolecules* 31, pp. 4581-4585.

Sarwar, M.I., Zulfiqar, S. & Ahmad, Z. 2007. Preparation and properties of polyamide–titania nanocomposites. *Journal of Sol-Gel Science and Technology* 44, pp. 41-46.

SFE. 2007. Solid surface energy data (SFE) for common polymers. Available on site: www.surface-tension.de/solid-surface-energy.htm (referred on 1.1.2013).

Song, R., Wang, Z., Meng, X., Zhang, B. & Tang, T. 2007. Influences of catalysis and dispersion of organically modified montmorillonite on flame retardancy of polypropylene nanocomposites. *Journal of Applied Polymer Science* 106, pp. 3488-3494.

Spencer, J.A., Liang, X., George, S.M., Buechler, K.J., Blackson, J., Wood, C.J., Dorgan, J.R. & Weimer, A.W. 2007. Fluidized bed polymer particle ALD process for producing HDPE/Alumina nanocomposites. *The 12th International Conference on Fluidization—New Horizons in Fluidization Engineering* RP4, pp. 417-424.

Su, K-H., Lin, J-H. & Lin, C-C.J. 2007. Influence of reprocessing on the mechanical properties and structure of polyamide 6. *Journal of Materials Processing Technology* 192-193, pp. 532-538.

Suin, S., Shrivastava, N.K., Maiti, S. & Khatua, B.B. 2013. Phosphonium modified organoclay as potential nanofiller for the development of exfoliated and optically transparent polycarbonate/clay nanocomposites: Preparation and characterizations. *European Polymer Journal* 49, pp. 49-60.

Sumita, M., Tsukumo, Y., Miyasaka, K. & Ishikawa, K. 1983.Tensile yield stress of polypropylene composites filled with ultrafine particles. *Journal of Materials Science* 18, pp. 1758-1764.

Szustakiewicz, K., Kiersnowski, A., Gazińska, M., Bujnowicz, K. & Pigłowski, J. 2011. Flammability, structure and mechanical properties of PP/OMMT nanocomposites. *Polymer Degradation and Stability* 96, pp. 291-294.

Tan, J., Jia, Z., Sheng, D., Liu, X. & Yang, Y. 2012. Effect of the molecular structure of polyurethane elastomers on the thermomechanical properties of PUE/PC blends. *Journal of Applied Polymer Science* 124, pp. 412-420.

Thomas, S.P., Thomas, S. & Bandyopadhyay, S. 2009. Mechanical, atomic force microscopy and focussed ion beam studies of isotactic polystyrene/titanium dioxide composites. *Composites Part A: Applied Science and Manufacturing* 40, pp. 36-44.

Tsai, S-J., Ashter, A., Ada, E., Mead, J.L., Barry, C. & Ellenbecker, M.J. 2008. Control of airborne nanoparticles release during compounding of polymer nanocomposites. *NANO: Brief Reports and Reviews* 3, pp. 301-309.

Varghese, S. & Karger-Kocsis, J. 2004. Melt-compounded natural rubber nanocomposites with pristine and organophilic layered silicates of natural and synthetic origin. *Journal of Applied Polymer Science* 91, pp. 813-819.

Vermogen, A., Masenelli-Varlot, K., Séguéla, R., Duchet-Rumeau, J., Boucard, S. & Prele, P. 2005. Evaluation of the structure and dispersion in polymer-layered silicate nanocomposites. *Macromolecules* 38, pp. 9661-9669.

Wang, Y. 2000. Compounding in Co-rotating twin-screw extruders. Vol. 10, No. 8, Report 116, Rapra Publishing. 136 p.

Wang, Z., Xie, G., Wang, X., Li, G. & Zhang, Z. 2006. Rheology enhancement of polycarbonate/calcium carbonate nanocomposites prepared by melt-compounding. *Materials Letters* 60, pp. 1035-1038.

White, J.L. 1991.Twin screw extrusion technology and principles, Hanser Publishers, New York.

Wilson, C.A., McCormick, J.A., Cavanagh, A.S., Goldstein, D.N., Weimer, A.W. & George, S.M. 2008. Tungsten atomic layer deposition on polymers. *Thin Solid Films* 516, pp. 6175-6185.

Wu, C.L., Zhang, M.Q., Rong, M.Z. & Friedrich, K. 2002. Tensile performance improvement of low nanoparticles filled-polypropylene composites. *Composites Science and Technology* 62, pp. 1327-1340.

Wypych, G. 2010. Handbook of Fillers, 3rd Edition. ChemTec Publishing.

Xu, G., Chen, G., Ma, Y., Ke, Y. & Han, M. 2008. Rheology of a low-filled polyamide 6/montmorillonite nanocomposite. *Journal of Applied Polymer Science* 108, pp. 1501-1505.

Yoon, P.J., Hunter, D.L. & Paul, D.R. 2003a. Polycarbonate nanocomposites. Part 1. Effect of organoclay structure on morphology and properties. *Polymer* 44, pp. 5323-5339.

Yoon, P.J., Hunter, D.L. & Paul, D.R. 2003b. Polycarbonate nanocomposites: Part 2. Degradation and color formation. *Polymer* 44, pp. 5341-5354.

Zhang, H., Zhang, Z., Yang, J.-L. & Friedrich, K. 2006. Temperature dependence of crack initiation fracture toughness of various nanoparticles filled polyamide 66. *Polymer* 47, pp. 679-689.

Zhu, L. & Xanthos, M. 2004. Effects of process conditions and mixing protocols on structure of extruded polypropylene nanocomposites. *Journal of Applied Polymer Science* 93, pp. 1891-1899.

"All truths are easy to understand once they are discovered;
the point is to discover them"
– Galileo Galilei